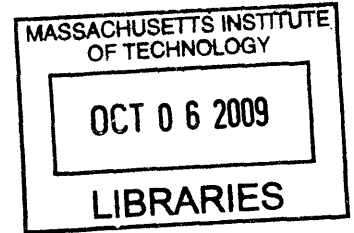


Identification and functional characterization of two patterning genes, *Zic4* and *Ten_m3*, in topographic map formation of the visual pathway

by

Sam H. Horng

BA Biology, Columbia University, 2000



Submitted to the Department of Brain and Cognitive Sciences in partial fulfillment of the requirements for the degree of

Doctor of Philosophy in Neuroscience
at the
Massachusetts Institute of Technology

ARCHIVES

September, 2009

[February 2010]

© Massachusetts Institute of Technology 2009. All rights reserved

Signature of Author: _____
Department of Brain and Cognitive Sciences
July 21, 2009

Certified by: _____
Mriganka Sur
Sherman Fairchild Professor Neuroscience
Head, Department of Brain and Cognitive Sciences
Faculty Advisor

Accepted by: _____
Matt Wilson
Professor of Neuroscience
Chairman, Committee for Graduate Studies

Identification and functional characterization of two patterning genes, *Zic4* and *Ten_m3*, in topographic map formation of the visual pathway

by

Sam Horng

Submitted to the Department of Brain and Cognitive Sciences in partial fulfillment of the requirements for the degree of Doctor of Philosophy in Neuroscience

ABSTRACT

A central feature of visual pathway development is its organization into retinotopic maps. The developmental process by which these maps form involves a transition from early patterning cues to arrays of axonal guidance factors allowing the relative order of retinotopic axons to be preserved. Mechanisms linking patterning molecules of early development to topographic wiring and subsequent functional responses are not well understood. In this thesis, I performed a microarray screen comparing gene expression in early visual and auditory regions of the thalamus in order to identify early patterning candidates with a potential role in visual pathway differentiation. Among the candidates enriched in the visual thalamus, the transcription factor, *Zic4*, was found to be expressed in gradients of the developing retina, lateral geniculate nucleus (LGN) and primary visual cortex (V1). Mice lacking *Zic4* exhibited a deficit in eye-specific patterning to the thalamus that was complementary to the phenotype seen in mice lacking *Ten_m3*, a type II homophilic transmembrane receptor and transcriptional regulator. Using intrinsic signal optical imaging techniques, I characterized the functional properties of primary visual cortical retinotopic maps in *Zic4* and *Ten_m3* null mice and identified complementary changes in the ipsilateral representation of V1, as well as evidence for eye-specific mismatch in the cortical binocular zone. Additionally, complementary positional shifts in V1 were found in these mutants identifying a bidirectional modulation of mapping mechanisms in the visual pathway. In order to test whether *Zic4* and *Ten_m3* interact in serial or parallel pathways, I analyzed the retinogeniculate and cortical maps in the combination mutant. The *Ten_m3/Zic4* double null mouse exhibited a partial rescue of retinogeniculate mapping and a complete reversal of the cortical changes found in either mutant alone, suggesting that the two genes interact to modulate common downstream effectors in opposite directions. In sum, this thesis presents a gene microarray screen used to identify *Zic4* as a novel visual patterning gene, characterizes its loss-of-function phenotype on retinotopic mapping in the thalamus and cortex, and studies its antagonistic interaction with *Ten_m3*, another visual pathway patterning gene with a complementary loss-of-function phenotype.

Thesis supervisor: Mriganka Sur

Title: Sherman Fairchild Professor of Neuroscience

ACKNOWLEDGEMENTS

Many thanks to Mriganka Sur for his support, enthusiasm and scientific mentorship. He provided so many learning opportunities and really encouraged me to think both creatively and critically and to push for my personal best.

I want to thank my thesis committee members, Morgan Sheng, Yasonuri Hayashi, Li-Huei Tsai and Cathy Leamey, who provided great advice on the projects and unwavering support at every stage of my graduate work.

Thanks to members of the Sur lab for providing a rigorously intellectual and creative environment in which to work. Colleagues to whom I'm especially indebted for their support, guidance and kindness are Charlene Ellsworth and Serkan Oray. Thanks to Christine Waite and Monique Brouillette for support in the early days. Thanks to Hongbo Yu for optical imaging guidance, and Amanda Mower, Audra Van Wart, Rong Mao, Caroline Runyan and Jitendra Sharma for useful project discussions. Thanks to Alvin Lyckman, Gabriel Kreiman, and Cathy Leamey for showing me the ropes and providing vital collaborations. Special thanks to Damon Page for all of the advice, our many interesting conversations and for reinforcing my appreciation for the intrinsic rewards of scientific inquiry. Thanks to Orsi Kuti, Chrysa Prestia and Bibek Karki for indispensable technical support. Thanks to Travis Emery for his outstanding management of the lab and unwavering good cheer. A big thank you to Cortina Mccurry, a colleague and good friend.

Thanks to Seema Shah, Melva James, Kit Lo, Gloria Chiang, Pete Lokken, and Gishnu Das for grounding me and providing unconditional support. Tremendous thanks

to Jason, Susanna, Sharon, Frank, Jeff, George, Callan, Jocelyn, Thisbe and Ma for everything.

COLLABORATIONS

Work presented in Chapter 2 of this thesis was performed in collaboration with Charlene Ellsworth, who conceived the project, Gabriel Kreiman, who performed the gene set enrichment analysis and provided computational guidance, Marissa Blank and Kathleen Millen, who provided the *Zic4* null mice, and Damon Page, who taught me to run the behavioral tests. All of these collaborators additionally provided intellectual contributions to the formulation and execution of experiments. Work presented in Chapter 3 was performed in collaboration with Cathy Leamey, who characterized the *Ten_m3* null anatomical phenotype and brought an interest in this gene to my project, Caroline Runyan, who helped formulate experiments, Kathleen Millen, Takashi Inoue and Jun Aruga, who provided in situ hybridization data and their expertise in all things *Zic*.

TABLE OF CONTENTS

Abstract.....	3
Table of Contents.....	6
Chapter 1: Introduction.....	7
Chapter 2: Differential Gene Expression in the Developing Lateral Geniculate Nucleus and Medial Geniculate Nucleus in Normal and Visually Rewired Mice Reveals Novel Roles for <i>Zic4</i> and <i>Foxp2</i> in Visual and Auditory Pathway Development.....	10
Summary.....	10
Introduction.....	12
Methods.....	14
Results.....	21
Discussion.....	31
Figures.....	39
Chapter 3: <i>Zic4</i> and <i>Ten_m3</i> Exert Complementary Effects on Retinotopic Map Formation and Position of the Visual Cortex.....	69
Summary.....	69
Introduction.....	71
Methods.....	74
Results.....	77
Discussion.....	85
Figures.....	94
Chapter 4: Summary and Conclusions.....	112
References.....	114

CHAPTER 1

INTRODUCTION

A critical function of the brain is to provide an orderly and efficient neural representation of important sensory stimuli from the outside world. In the mammalian visual pathway, representations of light reflectance in visual space are relayed from the retina as a topographic map to the thalamus and superior colliculus. Along this pathway projections from the two eyes are kept in parallel. Retinotopic and eye-specific information from the thalamus are transferred to the primary visual cortex (V1), where additional stimulus features are extracted. The mechanisms by which visual stimulus feature maps are established and modified in response to experience are an active area of investigation. A number of genetically encoded axonal guidance systems have been implicated in the establishment of retinotopic maps, including the EphA-ephrinA signaling pathway. However, connections between early genetic programs of development, which arise out of local signaling cascades that establish molecular gradients contributing to the differentiation of regions into functional areas, and later processes of circuit formation are not well understood.

THESIS OUTLINE

This thesis is presented as two studies exploring the link between early sensory specific patterning events and subsequent pathways of structural and functional differentiation. The first study, reported in chapter two, presents a gene microarray

approach to discovering molecular candidates for sensory pathway development. In order to identify novel candidates for visual and auditory pathway differentiation, tissue from the neonatal and perinatal visual and auditory thalamic nuclei were dissected, pooled and subjected to gene expression analysis. Significant enriched genes for the visual and auditory pathway were isolated and confirmed as candidates using quantitative real-time polymerase chain reaction and in situ hybridization techniques. Two transcription factors, *Zic4* and *Foxp2*, which were strongly enriched in the visual and auditory thalamus, respectively, were functionally characterized. Retinogeniculate mapping defects were discovered in *Zic4* null mice, identifying a novel role for this patterning gene in topographic organization of the visual pathway. *Foxp2* levels were found to be regulated by activity in the auditory thalamus, the first demonstration in mammals of an activity-dependent role in the auditory pathway for this transcriptional repressor. In order to test how novel sensory inputs change patterns of gene expression in the auditory thalamus, an additional microarray screen was performed comparing the normal auditory thalamus to that in which retinal axons were surgically rerouted to innervate it. These experiments revealed that both patterns of the visual thalamus and novel genes of plasticity were induced in the visually “rewired” auditory thalamus.

The second study, presented in chapter three, explores the role of *Zic4* in cortical retinotopic map formation. Additionally, its interaction with *Ten_m3*, a previously identified patterning gene of the visual pathway with a complimentary retinogeniculate loss-of-function phenotype, was examined. Using intrinsic signal optical imaging techniques, binocularly, contralaterally and ipsilaterally driven maps were obtained in the *Zic4* null, *Ten_m3* null and combination null mice. Complementary deficits in the

ipsilateral representation and cortical position of V1 were found in the single null mice, with a rescue in the double null mouse, suggesting that the two genes interact to regulate common downstream pathways in opposite directions. The *Zic4* and *Ten_m3* null mice also exhibited signs of cortical suppression in areas of ipsilateral and contralateral drive, evidence for an intraocular mismatch. The combination mutant did not show cortical suppression, further supporting the counteracting effects of the two genes. Finally, the de-novo presence of ocular dominance columns was observed in *Ten_m3* null mice, but not *Zic4* null mice, raising interesting implications for the creation of novel cortical feature maps in higher mammals.

The final chapter summarizes the findings of these two chapters and provides some general conclusions and discussion of the significance of the results.

PUBLICATIONS

The work presented in this thesis has been reported in four abstracts at the Society of Neuroscience meetings (2005-2008) and in two journal articles, both of which are in the process of submission.

CHAPTER 2

Differential Gene Expression in the Developing Lateral Geniculate Nucleus and Medial Geniculate Nucleus in Normal and Visually Rewired Mice Reveals Novel Roles for *Zic4* and *Foxp2* in Visual and Auditory Pathway Development

SUMMARY

Primary sensory nuclei of the thalamus process and relay parallel channels of sensory input into the cortex. The developmental processes by which these nuclei acquire distinct functional roles are not well understood. To identify novel groups of genes with a potential role in differentiating two adjacent sensory nuclei, we performed a microarray screen comparing perinatal gene expression in the principal auditory relay nucleus, the medial geniculate nucleus (MGN), and principal visual relay nucleus, the lateral geniculate nucleus (LGN). We discovered and confirmed groups of highly ranked, differentially expressed genes with qRT-PCR and *in situ* hybridization. A functional role for *Zic4*, a transcription factor highly enriched in the LGN, was investigated using *Zic4* null mice, which were found to have changes in topographic patterning of retinogeniculate projections. *Foxp2*, a transcriptional repressor expressed strongly in the MGN, was found to be positively regulated by activity in the MGN. These findings identify roles for two differentially expressed genes, *Zic4* and *Foxp2*, in visual and auditory pathway development. Finally, to test whether modality-specific patterns of gene expression are influenced by extrinsic patterns of input, we performed an additional

microarray screen comparing the normal MGN to “rewired” MGN, in which normal auditory afferents are ablated and novel retinal inputs innervate the MGN. Data from this screen indicate that rewired MGN acquires some patterns of gene expression that are present in the developing LGN, including an upregulation of *Zic4* expression, as well as novel patterns of expression which may represent unique processes of cross-modal plasticity.

INTRODUCTION

Sensory information is processed along pathways comprised of modality specific brain regions (Sur and Rubenstein, 2005; Kiecker and Lumsden, 2005; Lim and Golden, 2006). These regions arise during embryogenesis, when signaling centers induce graded patterns of gene expression to instruct local differentiation programs (Figdor and Stern, 1993, Ragsdale and Grove, 2001; Nakagawa and O'Leary, 2002; Grove and Fukuchi-Shimogori, 2003, Shimogori et al., 2004). The mechanisms linking early patterning events and later processes of functional differentiation are not well understood in the dorsal thalamus, the principal relay and processing center for all incoming sensory information to the cortex except for olfaction (Jones, 2007).

The lateral geniculate nucleus (LGN) and medial geniculate nucleus (MGN) are primary sensory thalamic nuclei, receiving visual and auditory afferents from the retina and inferior colliculus (IC), respectively, which in turn send respective projections to the primary visual cortex (V1) and primary auditory cortex (A1) (Fig. 1A). They parcellate as neighbors in relative dorsocaudal and ventroanterior positions (Kiecker and Lumsden, 2004), which likely affect their exposure to molecular signals during development and subsequent patterns of gene expression (Kataoka and Shimogori, 2008; Vue et al, 2009).

In order to identify genetic programs that contribute to the functional specification of the LGN and MGN, we performed a gene microarray screen comparing LGN and MGN at postnatal day 0 (P0) and 5 (P5), a time after structural parcellation has occurred but during afferent ingrowth and continued cellular differentiation and synapse formation (Jones, 2007). To test the sensitivity of our screen in isolating genes with a sensory-

specific role in thalamic differentiation, we characterized functional roles of two novel candidates, the zinc-finger transcription factor, *Zic4*, and the transcriptional repressor, *Foxp2*, in visual and auditory pathway development, respectively.

A persistent question in developmental neurobiology is the extent to which intrinsic lineage derived programs and extrinsic factors from inputs instruct the differentiation of functional regions (Miyashita-Lin et al., 1999; Dehay, et al, 1993, 2001). We tested whether specific sensory inputs contribute to the genetic differences between the LGN and MGN by comparing gene expression between normal MGN and “rewired MGN” (rwMGN), which has surgically been induced to receive visual input. In mice, hamsters and ferrets, ablating the inferior colliculus (IC) early in development is sufficient to induce retinal afferents to innervate the MGN and drive the auditory pathway to process visual information (Schneider, 1973; Sur et al., 1988; Lyckman et al., 2001; Newton et al., 2004). Although structural features of the MGN and A1 persist, functional features of visual processing occur (Sharma et al., 2000; von Melchner et al., 2000). We compared normal MGN and rwMGN at P5, the earliest age at which retinal afferents are detected in MGN after IC ablation. Finally, we tested whether loss of a downregulated gene, *Slc6a4*, was sufficient for rewiring in the absence of IC ablation.

MATERIALS AND METHODS

Animals

Wild-type mice of background strain 129/SvEv were used for the microarray analysis. *Zic4* null mice had been generated previously and obtained as a gift from the Millen lab (Grinberg and Millen, 2004). These mice were maintained on a 129/SvIMJ background and were viable and fertile. *Slc6a4* null mice were generated previously and obtained from Taconic (*B6.129-Slc6a4^{tm1Kpl}*, Bengel et al, 1998). This line was maintained on a C57/Bl6 background. All experiments were approved by MIT's IACUC and performed in compliance with NIH guidelines.

Dissection of Thalamic Nuclei and RNA Preparation

Fifteen to twenty neonatal (P0) and perinatal (P5) 129/Svev mice were used for each of three (P5) to four (P0) biological replicates of LGN and MGN (14 groups total, n=45-60 mice per group). Brains were dissected and submerged under RNase-free conditions in RNeasy (Qiagen, Valencia, CA). Under light microscopy, the cortex was peeled off exposing the thalamus. The LGN and MGN were removed bilaterally with micro-dissection spring scissors and stored in 1ml Trizol (Invitrogen, Carlsbad, CA). Dissection of appropriate nuclei was confirmed with coronal sections of dissected thalami. Approximately 0.5 mg of nucleus-specific tissue was acquired from each animal. Anatomical localization of the LGN relative to the MGN was inferred from thalamus specimens of representative animals subjected to intraocular WGA-HRP injections and tetra-methyl benzadine reaction. Tissue was homogenized by sequential

pulverization through an 18, 22 and 26 gauge needle and 1 cc syringe. RNA was tissue extracted using a Qiagen RNAeasy kit, and a cDNA copy of the RNA was made using an Invitrogen Superscript T7 in vitro reverse transcription kit and T7 oligo-dT primers. Labeled cRNA was synthesized using biotinylated nucleotides with an Enzo Biolabeling Kit.

Gene Microarray Hybridization and Analysis

15-20 µg of labeled cRNA from each of three (P5) to four (P0) replicates for P0 and P5 LGN and MGN was applied to Affymetrix murine U74v2 or 430 2.0 microarray chips by the Massachusetts Institute of Technology Biopolymers lab.

Microarray cel files were normalized and subjected to Robust Multichip Average (RMA) pre-processing using RMAexpress software (Irizarry et al, 2003; Bolstad et al, 2003). Significance Analysis of Microarrays (SAM) was used to identify enriched genes by setting a minimum fold change at 1.5 and adjusting the delta value (a threshold value for the difference between the observed relative difference vs. the expected relative difference, as an average over n permutations) to present <0.01% False Discovery Rate (FDR) (Tusher et al., 2001). Many genes are represented on the Affymetrix chips by multiple probes. All probes mapping onto the same gene identified through this screen showed consistent patterns of differential expression between LGN and MGN.

Quantitative Real-Time PCR

LGN and MGN RNA samples were harvested as described above and used for single strand cDNA synthesis from oligoDT primers. Primers amplifying a 150-200 bp

amplicon of each gene in enriched sets were designed by using the Whitehead Institute Primer3 program (see Suppl. Table 1 for primer sequences). Primer efficiencies were calculated using a standard Ct curve on serial dilutions of cDNA template amplified with SYBR Green PCR mix (Qiagen, Valencia, CA) in the DNA Engine Opticon 2 System. PCR reactions were performed in triplicate for each sample and relative quantitation was calculated using the Pfaffl formula with Gapdh as reference:

$$E(\text{efficiency})=10^{(-1/\text{slope})}, \text{ fold change}=[E_{\text{target}}^{\Delta\text{Ct target (sample1-sample2)}} / E_{\text{reference}}^{\Delta\text{Ct reference (sample1-sample2)}}]$$

***In Situ* Hybridization**

Five hundred-600 bp digoxigenin (DIG)-labeled antisense and sense riboprobes (see Suppl. Table 2 for primer sequences) were synthesized from sample cDNA using a T7 reverse transcriptase in vitro kit with DIG labeled ribonucleotides (Invitrogen, Carlsbad, CA). Riboprobes were purified on Micro Bio-spin Columns (Biorad, Hercules, CA) and quantified by UV spectrophotometry. Brains at P0 and P5 were flash frozen in isopentane, stored at -80° C and sectioned at 18 μm at -20° C on a cryostat (n=3 per gene of interest at P0, n=2 at P5). Sections were processed using the *in situ* hybridization protocol of Braissant and Wahli, 1998 and analyzed using a Zeiss Axioskop 2 microscope. *Zic4* gradients were measured using a line capture tool along the nasal-temporal axis of the retina (4 sections of 1 animal) and the dorsolateral-ventromedial axis (n=5 sections of 1 animal) of the LGN in ImageJ. Signal was normalized to the maximum value and averaged across 10 bins.

Gene Set Enrichment Analysis

Gene set enrichment analysis (GSEA) was performed on the following comparisons: P0 LGN vs. P0 MGN, P5 LGN vs. P5 MGN, and P5 MGN vs. rwP5 MGN. Gene sets from the c2 (curated gene sets) collection of the Broad Institute Molecular Signatures Database (<http://www.broad.mit.edu/gsea/index.jsp>) were used. For a given probe i , the signal to noise ratio (SNR) between the mean expression level ($s\mu_i$) across samples of two conditions ($s = \text{P0 LGN, P0 MGN, etc.}$) was defined as:

$SNR_i = (\text{LGN}\mu_i - \text{MGN}\mu_i) / (\text{LGN}\sigma_i + \text{MGN}\sigma_i)$, where $s\sigma_i$ = standard deviation across samples.

The probes were then ranked by SNR in an ordered list L . Given a set G containing N_G probes, two cumulative distribution functions were compared: $\text{Phit}(i)$ = proportion of genes in G with $\text{rank} < i$ and $\text{P}_{\text{miss}}(i)$ = proportion of genes outside G that show a $\text{rank} < i$ with the running enrichment score defined as $\text{RES}(i) = \text{Phit}(i) - \text{P}_{\text{miss}}(i)$. The peak enrichment score, ES , refers to the maximum deviation of $\text{RES}(i)$ from 0. Statistical significance of ES was evaluated in comparison to a null distribution from 1,000 permutations obtained by randomly shuffling the condition labels for each probe. Multiple comparisons were controlled for using the Family Wise Error Rate and enrichment scores were normalized across gene sets by centering and scaling:

$$\text{Phit}(i) = \#[g_{(j \leq i)} \in G] / N_G, \text{P}_{\text{miss}}(i) = \#[g_{(j \leq i)} \notin G] / [N - N_G], L = \{g_1 \dots g_N\}$$

Anatomical Tracing and Retinogeniculate Projection Analysis

Retinogeniculate projections were traced using intraocular injections of Alexa fluor 488- and 594-conjugated cholera toxin-B (CTB, Invitrogen Molecular Probes, Carlsbad, CA). Paired littermates of wild-type and *Zic4* null mice (P30-48) were injected using a Hamilton syringe with 1-2 μ l of 488-CTB and 594-CTB in each eye. Mice were allowed to recover for 48 hours to complete tracing and sacrificed.

Retinogeniculate tracings were imaged from 50 μ m brain sections using a Zeiss Axioskop 2 microscope. LGN images were divided into anterior, middle and posterior groups. For each animal, 2 sections from each hemisphere in anterior, middle and posterior groups were imaged and analyzed (n=4 WT, n=4 KO). Axiovision LE Rel. 4.4 software was used to measure the dorsomedial and dorsoventral length of the LGN and ipsilateral projection, as well as to count the number of ipsilateral clusters in each section. A Matlab script was used to measure the overlap between contralateral and ipsilateral terminals, the total number of LGN pixels, and the scatter of ipsilateral terminals (measured as the difference in intensity between a pixel and the average of its 5 nearest neighbors).

Activity-Dependent Induction of Gene Expression

Littermate C57/B16 mice at age P18 were placed in a dark, sound-proof room for 48 hours and then either sacrificed in the control group or treated with ramped exposure to 90 dB of white noise for 90 minutes and then sacrificed. The white noise generator was an ASR- PRO1 acoustic startle reflex test apparatus (Med Associates, St. Albans, VT), with intensity controlled using Startle Reflex Software (Med Associates, St. Albans,

VT). The background noise of the room in which we carried out acoustic stimulation was 55dB. Mice were held in the apparatus in an acrylic cage that contained numerous holes to allow for the passage of sound. To minimize the risk of audiogenic seizures, mice were placed in the apparatus and exposed to background noise for 10 minutes and then to white noise at 60dB for 10 min, 70 dB for 10 min, 80 dB for 10 min and finally 90 dB for 90 minutes. Thalamic and cortical tissue was dissected bilaterally from n=4 animals for both the experimental and control groups, flash frozen and then homogenized with a RIPA buffer/proteinase inhibitor cocktail (Roche) with sodium orthovanadate (1mM final concentration) and centrifuged. After supernatant protein concentration was quantified with a Bradford 595 Assay, 15ug of cortical samples and 30ug of thalamic samples were run at 200V for 35 minutes on NuPAGE 4-12% Bis-Tris Gel (Invitrogen, Carlsbad, CA), transferred at 35 mV for 70 min to a PVDF membrane (Invitrogen, Carlsbad, CA), and stained with Foxp2 (1:500, Abcam, Cambridge, MA), cFos (1:500, Santa Cruz, Santa Cruz, CA) and GAPDH (1:500, Abcam, Cambridge, MA) antibodies followed by 1:500 peroxidase-conjugated anti-rabbit secondary antibody (Jackson Labs, Bar Harbor, MA) and development with ECL Western blotting detection reagents (Amersham, Pittsburgh, PA) on Kodak film. Foxp2 and cFos signal was quantified and normalized to GAPDH signal in ImageJ. Data from three technical replicates was averaged and used for statistical analysis.

Visual Rewiring of the MGN

Neonatal P0 mice were anesthetized on ice (hypothermia) for 20 minutes. The scalp was opened and IC ablated bilaterally using a Bovie Cautery High Temperature

Loop Tip (Aaron Medical; Ferndale, MI). The incision was glued with Vetbond and animals were allowed to recover. At P5, thalamic tissue was dissected as described above. Intraocular CTB injections were also performed as described above.

RESULTS

Gene microarrays identify patterns of differential gene expression between the perinatal LGN and MGN

The positions of LGN and MGN are exposed at the lateral edges of the thalamus after cortex removal and were dissected under a light microscope (Fig. 1A-D). Of approximately 45,000 probes screened on the Affymetrix 430 2.0 microarray chip, a Significance Analysis of Microarrays (SAM) analysis identified 23 probes, corresponding to 20 unique genes, as enriched in the P0 LGN relative to the P0 MGN with a fold-change (FC) >2 and false discovery rate (FDR) $<0.01\%$ ($n=15-20$ per replicate, 4 replicates per group, $\text{delta-value}=0.831$, Fig. 2A). Nineteen probes, corresponding to 13 genes, were enriched in P0 MGN relative to the P0 LGN (Fig. 2B). In the P5 LGN vs. MGN screen, 125 probes, corresponding to 90 unique genes, were enriched in P5 LGN and 128 probes, corresponding to 74 unique genes, in P5 MGN using $\text{FC}>2$ and $\text{FDR}<0.01\%$ ($n=15-20$ per replicate, 3 replicates per group, $\text{delta value}=1.441$). Seventeen/20 (85%) of the P0 LGN genes (Fig 2A, red type) were present in the P5 LGN group and 12/13 (92%) of the P0 MGN genes (Fig. 2B, blue type) were present in the P5 MGN group, demonstrating the presence of genes that are always different between LGN and MGN during a perinatal window (P0-P5). In order to reduce the P5 candidate genes to a more manageable number, we screened further using $\text{FC}>3$, yielding 41 probes, representing 31 unique genes, as enriched in P5 LGN (Fig. 2C) and 43 probes, representing 30 unique genes, in P5 MGN (Fig 2D). Thirteen/30 (43%) of these P5 LGN

enriched genes were present in the P0 LGN group (Fig. 2C, red type) and 10/30 (33.3%) P5 MGN enriched genes in the P0 MGN group (Fig. 2D, blue type).

In order to control for potential differences in maturational state, we tested whether LGN and MGN undergo similar global processes of differentiation from P0 to P5 by using SAM analysis to compare LGN at P0 vs. P5 and MGN at P0 vs. P5 (Suppl. Fig 1). In the LGN comparison, 12,712 probes were upregulated at P5 and 1,655 were downregulated using $FC > 2$ and $FDR < 0.01\%$ (Δ value=0.596), while in the MGN comparison, using the same criteria, 13,266 were upregulated at P5 and 2,846 were downregulated (Δ value=0.604). Since nearly a third of all the probes screened showed significant change between P0 and P5, we compared the most highly ranked genes. Among the top 115 probes for both the LGN and MGN age-enriched groups, 91/115 (79%) were identical, suggesting that LGN and MGN undergo common processes of maturation between P0 and P5 (Suppl. Fig. 1, green type).

Of the genes enriched in the LGN with respect to MGN, many were transcription factors, including those implicated in neuronal migration (*Arx* and *Dlx1*), cellular differentiation (*Zic1*, *Zic3*, *Zic4* and *Zic5*), and areal patterning (*Pax6*). Non-transcription factor genes in LGN included cell-adhesion molecules (*Cad8*), neurotransmitter synthesis enzymes (*Gad1*), and cellular signals (*Sst*, *Cck*, *Npy*). Transcription factors were also overwhelmingly present in the genes enriched in the MGN with respect to LGN, including a previously identified dorsal thalamic marker, *Gbx2*. Another gene, *Foxp2*, a transcriptional repressor implicated in speech and language development in humans (Vargha-Khadem et al., 2005), was highly enriched in

MGN. Non-transcription factor genes included those involved in retinoic acid signaling (*Crabp2*), Wnt signaling (*Ck2-alpha*) and Ca²⁺ signaling (*Calb1*).

In order to isolate genes with a potential role in sensory-specific processes of neural circuit formation, we retrieved P5 LGN and P5 MGN expression data for a list of genes with a demonstrated role in axon guidance compiled from the literature. Screening 118 unique genes represented by 309 probes (Suppl. Table 3), we found the following factors enriched in P5 LGN with respect to P5 MGN: *EphA7*, *ephrinA5*, *Fgfr1*, *Wnt4/5a*, *Sema5b/6a/6d*, *Slit2*, *Unc5b*, *NCAM1*, *Sfrp2*, *Neuropilin1/2*, *Ntrk2/3*, and *Slitrk5* (Suppl. Fig. 2A). In turn, the following factors were enriched in P5 MGN with respect to P5 LGN: *Bdnf*, *EphA1*, *EphB2*, *ephrinA2/A3*, *Frizzled1/3*, *netrinG1*, and *Slitrk6* (Suppl. Fig. 2B), suggesting that distinct groups of axon guidance factors contribute to neural connectivity and circuit formation in the two nuclei.

Real-Time PCR and *in situ* hybridization confirm differential gene expression from LGN and MGN enriched sets

Differential gene expression levels between LGN and MGN were confirmed using quantitative real time PCR (qRT-PCR) on all genes of the P0 LGN and P0 MGN sets. All 20 of the P0 LGN enriched genes were confirmed with qRT-PCR, with significant upregulation ($p < 0.05$) and FC > 2 in LGN samples vs. MGN samples (Fig. 3A). All 13 of the P0 MGN enriched genes were also confirmed with qRT-PCR with significant upregulation ($p < 0.05$) and FC > 4 (Fig. 3B).

Top ranking genes for both the P0 and P5 LGN and MGN groups were selected for *in situ* hybridization in order to document anatomical expression patterns in more detail. At both P0 and P5, *Zic4* and *Zic1*, two members of the *Zic* family of transcription factors, exhibited stronger expression in neonatal LGN than MGN (Fig. 4A-B, A'-B'), with no signal from sense probes (data not shown). *Zic4* exhibited a graded expression pattern both in the dorsal subdivision of the LGN (LGd) with high levels dorsolaterally and in the retina with high levels on the temporal side (Fig. 4B, Suppl. Fig. 3), suggesting a possible role in retinotopic patterning of retinogeniculate projections. At both P0 and P5, *Crabp2*, *Foxp2* and *Sdccag33*, demonstrated stronger expression in neonatal MGN than LGN (Fig 4C-E, C'-E') and no signal with sense probes (data not shown). *Foxp2* showed strong expression in both dorsal and ventral subdivisions of the MGN (MGd, MGv), while *Crabp2* was localized primarily to the MGd and *Sdccag33* localized exclusively to the MGv.

Gene Set Enrichment Analysis identifies functional pathways within LGN and MGN enriched sets

The analyses above are based on the study of individual genes. It is possible to screen for groups of genes that share similar functions, structure, biochemical pathways, and chromosomal location. Even if individual genes within a gene group show only minor changes in expression, group analysis can uncover large changes for the group as a whole. In order to identify functionally related groups of genes with collective enrichment in the LGN or MGN, Gene Set Enrichment Analysis (GSEA) using the c2

(curated gene sets) collection of the Broad Institute Molecular Signatures Database (<http://www.broad.mit.edu/gsea/index.jsp>) was performed (Subramanian et al, 2005).

These pathways may represent developmental programs in the functional specification of the perinatal LGN and MGN. Eighteen/1892 screened gene sets were significantly enriched in P0 LGN at $p < 0.01$ (Suppl. Table 4). Among the top 18 pathways were the cardiac EGFP pathway, phosphatidylinositol signaling system, p53 upregulated genes, CD40 downregulated genes and the IL-2 receptor pathway, the last two suggesting a role for cytokine signaling in cellular differentiation within the LGN.

One hundred eleven/1892 gene sets had significant enrichment at $p < 0.01$ in P0 MGN (Suppl. Table 5). The top pathway was the Alzheimer's disease set; additional pathways in the top 20 included the GATA3 gene set, upregulation with loss of *Mecp2* set and the *Hoxc8* pathway.

GSEA performed on the P5 data revealed 193/ 1892 gene sets enriched in the P5 LGN at $p < 0.01$ (Suppl. Table 6). Pathways ranked in the top 20 included a gene set upregulated by TNF α signaling, both PI3K and mTOR signaling cascades, and the VEGF pathway. All four of these pathways have been previously suggested to play a role in the maintenance and plasticity of the developing and adult visual pathway (see Discussion), and their presence here suggests an additional role in early retinothalamic development. In the P5 MGN, 32 / 1892 gene sets were significantly enriched at $p < 0.01$ (Suppl. Table 7). The most significant set was the Wnt signaling pathway, which has been implicated in diencephalic patterning with a Wnt source emanating from the alar plate (Braun et al, 2003; Zhou et al, 2004). Other top pathways included the NFAT pathway, Hox patterning genes, an additional Wnt signaling set, and the CCR3 pathway.

Zic4 contributes to the patterning of retinogeniculate projections

The role of *Zic4* in visual pathway development was explored, because of its strong enrichment in the LGd and previous work identifying the role of gene family member, *Zic2*, in ipsilateral steering of retinal ganglion cell axons at the optic chiasm (Pak et al., 2004). While *Zic2* expression is not appreciably detected with *in situ* hybridization in the LGd, *Zic4* is strongly expressed in a gradient along the dorsolateral axis, as well as in a high temporal to low nasal gradient in retinal ganglion cells (Suppl. Fig. 3). In order to test whether *Zic4* is necessary for normal retinogeniculate patterning, intraocular injections of CTB were performed in littermate control and *Zic4* null mice at an age when retinogeniculate terminals have matured to their adult form (P30-P48) (Guido, 2008).

No changes in the size of LGd were observed (Fig. 5), suggesting that nuclear development and gross targeting were intact. However, a number of defects were detected in the rostral third portion of LGd, where *Zic4* null mice exhibited: 1) a marked dorsomedial expansion of the ipsilateral termination zone ($71.9 \pm 4.8\%$ of the dorsomedial axis in KOs vs. $48.2 \pm 3.3\%$ in wild-type, $p < 0.0005$, t-test, $n=4$ each group, Fig. 5A-F, A'-F', dotted line, Fig. 5G), 2) increases in the number of ipsilateral terminal clusters (mean no. of clusters = 1.62 ± 0.17 vs. 1.12 ± 0.08 , KO vs. control, $p < 0.05$, t-test, $n=4$ each group), and 3) an increase in the percentage of LGd filled by ipsilateral projections ($21.18 \pm 2.5\%$ KO vs. $14.49 \pm 1.7\%$ control, t-test, $p < 0.05$, $n=4$ each group). There was no statistically significant difference in the amount of overlap between

contralateral and ipsilateral terminals (number of overlap pixels/total LGN pixels), although the *Zic4* null mouse showed a trend of an increase in overlap ($1.74 \pm 0.26\%$ KO vs. $0.98 \pm 0.34\%$ control, $p=0.08$, t-test) suggesting that activity-dependent processes of eye-specific segregation were not largely disrupted, though may be slightly attenuated, in the absence of *Zic4*. Furthermore, no difference in ipsilateral spread along the dorsoventral axis was found, indicating that altered ipsilateral terminal spread occurs only along the dorsomedial axis in *Zic4* null mice (Fig. 5G). Finally, despite an increased number of clusters in the knock outs, there was no difference in the scatter of ipsilateral terminals, suggesting that ipsilateral zones are compact and segregated from contralateral terminals. Middle and posterior third portions of the LGd showed no difference between knock outs and wild-type (data not shown).

Foxp2 is regulated by activity in the auditory thalamus

Foxp2 is a transcriptional repressor necessary for proper human speech and language development (reviewed in Vargha-Khadem et al, 2005), but whose role in the auditory pathway has not yet been explored. Because *Foxp2* expression has been shown to be dynamically regulated in songbirds during periods of plasticity (Teramitsu and White, 2006), we tested whether *Foxp2* levels are modulated by auditory activity *in vivo*. Using Western blots, we found that Foxp2 protein was increased significantly in the MGN of P18 wild-type C57/Bl6 animals after 120 minutes of high volume (90 dB) white noise stimulation compared to untreated controls (1.04 ± 0.025 vs. 0.78 ± 0.037 , $p < 0.05$, t-test, $n=4$ pooled for each group, technical replicate $n=3$ for each group, Fig. 6A, B, D).

cFos expression was used as a positive control for early activity dependent regulation of gene expression in the auditory thalamus and cortex (MGN: 1.29 ± 0.02 vs. 0.78 ± 0.02 , $p < 0.05$, A1: 1.27 ± 0.025 vs. 0.76 ± 0.059 , $p < 0.05$, t-test, Fig. 6A,C,E). In the LGN and V1, neither Foxp2 nor cFos levels were changed in experimental animals compared to control, suggesting that activity dependent regulation is specific to the sensory pathway being stimulated (Foxp2 LGN: 1.09 ± 0.02 vs. 1.08 ± 0.07 , $p = 0.927$, t-test; cFos LGN: 0.96 ± 0.02 vs. 0.92 ± 0.12 , $p = 0.75$, t-test; Foxp2 V1: 1.01 ± 0.048 vs. 1.19 ± 0.232 , $p = 0.54$, t-test; cFos V1: 1.05 ± 0.108 vs. 0.85 ± 0.096 , $p = 0.786$, t-test; Fig. 6B,C). Furthermore, Foxp2 expression did not change with auditory stimulation in the primary auditory cortex (A1) indicating that Foxp2 acts in an activity dependent manner only in the thalamus (0.967 ± 0.14 vs. 0.977 ± 0.03 , $p = 0.585$, t-test).

Of note, we found that Foxp2 levels were higher in the normal LGN than the normal MGN at P18, a result consistent with expression results in the adult brain from the Allen Brain Atlas (<http://www.brain-map.org/>). This result suggests that dynamic levels of Foxp2 expression may be involved in later development of the visual pathway as well.

Visually rewired MGN exhibits LGN like patterns of gene expression as well as novel patterns of plasticity related genes

In order to clarify whether genetic programs of specification in the LGN and MGN are shaped by the identity of their inputs, we performed rewiring experiments in which retinal axons are rerouted to the MGN after ablation of the neonatal IC (Lyckman et al., 2001; Newton et al., 2004) and tested whether visual inputs to the MGN might

induce LGN-like patterns of gene expression and/or downregulate genes typically enriched in the MGN (Fig. 7A-C). Screening 45,000 probes on the Affymetrix 430 2.0 microarray chip, a Significance Analysis of Microarrays (SAM) analysis identified 14 probes, corresponding to 12 unique genes, as enriched and 1 probe representing 1 gene as downregulated in the P5 rwMGN with FC >2 and FDR <0.01% (n=15-20 per replicate, 3 replicates per group, delta-value=0.489). In order to expand the candidate list, we loosened our criteria to FC >1.5 and FDR <3.37% (delta-value=0.666), yielding 44 probes, corresponding to 41 unique genes, as enriched (Fig. 7D) and 5 probes, corresponding to 5 unique genes, as downregulated in the rwMGN (Fig. 7E). Ten/41 (24.4%) of these enriched genes were present in the P5 LGN enriched group, including *Zic4*, indicating that some LGN specific patterns of gene expression are upregulated in the MGN after visual “rewiring” (Fig.7D, red type). *Zic4* upregulation in rwMGN was confirmed with *in situ* hybridization, as was a lack of change in MGN marker, *Foxp2* (Suppl. Fig. 6). The remaining 31 enriched genes potentially represent novel processes of plasticity and/or response to injury (Fig. 7D, black type). Only one of those genes, *Pappa*, was a gene enriched in the P5 MGN group compared to P5 LGN (Fig. 7E, blue type); this gene encodes for pregnancy associated plasma protein A and has been implicated in positively regulating IGF-1 availability (Harrington et al., 2007).

Using the results of the SAM analysis of rwMGN and normal MGN, we searched for candidates with a potential role in guidance of retinal axons to their novel sensory target, rwMGN. In order to eliminate candidates with a non-specific role in responsiveness to injury, we performed a control microarray on the P5 MGN from mice in which only the superior colliculus (SC) had been ablated at P0 (scMGN; data not

shown). Ablating the SC, but not the IC, has been shown to induce ectopic targeting of retinal axons to the lateral posterior nucleus (LP) of the thalamus, but not the MGN, and therefore served as a control for changes in gene expression due to midbrain injury (Newton et al, 2004). One candidate, *Slc6a4*, a gene encoding a surface membrane serotonin transporter, was significantly downregulated in rwMGN and showed no difference between the normal MGN and scMGN (Suppl. Fig. 4). Because serotonin signaling has been shown to modulate target recognition of thalamocortical axons (Bonnin et al., 2007) and *Slc6a4* has been shown to modulate eye specific segregation of retinogeniculate terminals (Upton et al, 1999, 2001; Salichon et al., 2001), we hypothesized that this gene might play a role in axon targeting to the rwMGN. However, intraocular CTB injections of *Slc6a4* knock out mice revealed no ectopic projections to the MGN (n=3 KO, n=2 WT, Suppl. Fig. 4), suggesting that loss of *Slc6a4* is not sufficient to induce rewiring of retinal axons to the MGN.

In order to identify additional candidates with a potential role in visual rewiring, we screened the P5 MGN and rwMGN data with our list of known axon guidance genes (Suppl. Table 3). We found that *Epha7*, *plexin-C1*, *RGMb*, and *Ntrk2* were upregulated in rwMGN, while *semaphorin3a*, *Dcc*, *netrinG2*, *robo2*, *NCAM1*, and *slit2* were downregulated (Suppl. Fig. 5), suggesting that a suite of axon guidance factors modulates targeting and topographic mapping of retinal ganglion cell axons into the rwMGN. Two upregulated factors in rwMGN, *Epha7* and *Ntrk2*, were increased in P5 LGN compared to P5 MGN and possibly represent common mechanisms of retinogeniculate targeting and/or patterning in the LGN and rwMGN.

Finally, GSEA analysis identified 332 / 1892 gene sets significantly upregulated in the rwMGN relative to the P5 MGN at $p < 0.01$ (Suppl. Table 8). Gene sets in the top 20 included a set of genes downregulated in response to rapamycin, inhibitor of the mTOR pathway, and the TNF α pathway, potentially reflecting cell death in response to deafferentation. Six / 1892 gene sets were significantly downregulated at $p < 0.01$ (Suppl. Table 9). Among these sets were the NF- κ B pathway and Wnt signaling pathway, the latter of which was the most significantly enriched set of the P5 MGN.

DISCUSSION

Using gene microarrays, we identified groups of novel candidate genes with a potential role in LGN and MGN specification. Measuring differential gene expression from P0 to P5 allowed us to capture patterns of gene expression present during a postnatal period of thalamic afferentation, cellular differentiation and synapse formation. At P0, a relatively small number of genes distinguish the LGN (20) from the MGN (13), and a large proportion of these genes (85% and 92%, respectively) continue to show differential gene expression at P5, suggesting that there are a small number of programs which orchestrate the postnatal differentiation of LGN and MGN. The number of genes distinguishing the LGN and MGN increases dramatically at P5 (about 5-fold), reflecting a proliferation of secondary differentiation programs with age. At the two ages, the number of differentially enriched genes is similar for the LGN and MGN, suggesting that a comparable number of programs act to functionally differentiate each nucleus. Finally, between P0 and P5, changes in gene expression are remarkably similar in the LGN and

MGN (79% of the top differentially expressed probes are identical), suggesting that LGN and MGN undergo similar and independent processes of maturation during this time. These data strengthen the likelihood that LGN and MGN enriched genes are involved in sensory-specific processes of differentiation.

Among the candidates for LGN specification were four of the five members of the *Zic* family of transcription factors (*Zic4*, *Zic1*, *Zic3*, and *Zic5*). These genes have been implicated in various early patterning events and exhibit graded expression throughout the developing brain (Gaston-Massuet et al, 2005, Aruga, 2004). However, their role in visual pathway development was not yet unexplored. Family member, *Zic2*, which has been implicated in ipsilateral pathfinding of retinal axons to the thalamus (Pak et al, 2004), was notably absent from our screen, and is not detectably expressed in the LGd (data not shown).

Among the MGN candidates were three transcriptional modulators, *Foxp2*, a transcriptional repressor, *Crabp2*, a retinoic acid binding protein, and *Sdccag33* (aka. *Tshz1*), a zinc-finger transcription factor. *Crabp2* and *Sdccag33* showed exclusive expression in the MGd and MGv, respectively, making them potentially useful as MGN markers for future studies testing the functional disruption of local signals as well as for the creation of region specific transgenes (Kitamura et al., 1997, Nakagawa and O'Leary, 2001, Jones and Rubenstein, 2004, Vue et al., 2007, Szabo et al., 2009).

Functional significance of LGN and MGN enriched genes

Visual and auditory stimuli have distinct spatio-temporal characteristics and the brain regions processing these stimuli exhibit divergent representations of stimulus features, distinct patterns of firing, or frequency codes, and differences in intra-areal circuitry (Jones, 2007, Sharma et al., 2000). Candidate genes in LGN and MGN enriched groups potentially contribute to processes of specification during the first postnatal week, including axonal pathfinding, which in rodents, has been documented to occur for vision from E15 through P5 (Tuttle et al., 1998; Lyckman et al., 2001). Postnatal processes of cellular differentiation, synaptogenesis and circuit formation during this period are not well described, and the screen provides a framework of candidates from which to investigate these processes. Because the data captured a postnatal window of active afferentation (P0-P5), we additionally screened for known axon guidance factors, providing additional candidates for sensory-specific wiring, including the semaphorins and neuropilins in the P5 LGN and Wnt signaling in the P5 MGN.

Differences in gene expression originate in part from differences in the position of precursor cells of the MGN and LGN relative to local signaling centers, such as the zona limitans intrathalamica (ZLI) (Vue et al., 2007). Postmitotic cells may also be responsive, though it is not known to what extent cell fates are determined at this stage (Szabo et al, 2009). The nature and identity of these signals are newly being discovered, with cues from the ZLI (such as Shh), from the alar plate (such as Wnt) and from the p2/p3 border (i.e. the border between the thalamus and pretectum; such as FGF8) potentially playing a role (Kiecker and Lumsden, 2004; Kataoka and Shimogori, 2008; Vue et al., 2009). Our screen likely includes candidates that participate in these region or lineage specific programs of genetic differentiation.

Patterns of gene expression have been correlated with cell populations giving rise to specific nuclei and our study confirmed some previously published markers of the LGN, MGN and dorsal thalamus. *Dlx1* and *Arx* expression appears early in the lateral ZLI, and co-localizes with cells that later form the LGv (Kitamura et al., 1997). Selective expression of *Isl1*, *Pax6* and *Dlx1,2,5* in the LGN and *Gbx2* in the MGN has been observed (Nakagawa and O'Leary, 2001; Kawasaki et al., 2004). Our *in situ* hybridizations show that expression is typically not exclusive to the LGN or MGN but present in several nuclei, suggesting that these regional markers act in unique combinations to influence the differentiation of multiple nuclei.

In addition to our screen for individual candidates, we used a Gene Set Enrichment Analysis (GSEA) approach to search for groups of genes annotated into functionally related pathways that exhibited collective patterns of differential expression between LGN and MGN (Tilford and Seimers, 2009; Lyckman et al, 2008). Large-scale methods, like unsupervised clustering, were not performed, as it would be ambiguous to interpret groups of genes that show similar expression patterns but are not clearly linked from a functional viewpoint. The GSEA approach was more meaningful to our central question of LGN vs. MGN specification, and yielded a number of interesting candidate pathways that would not have been identified with the single gene approach (SAM) alone. Cytokine signaling pathways, such as the CD40 downregulated pathway and the IL-2 pathway, were implicated in neonatal LGN development, while novel transcriptional networks, including the *MeCP2* and *Hoxc8* pathways, were linked to the neonatal MGN. One intriguing result was the identification in P5 LGN of several pathways previously implicated in visual plasticity. TNF α is involved in homeostatic increases of synaptic

strength from non-deprived inputs to V1 after monocular deprivation (Kaneko et al., 2008), as well as in retinal ganglion cell degeneration in a mouse model of glaucoma (Nakazawa et al., 2006). Conversely, the mTOR pathway has been shown to positively regulate adult ganglion cell axon regeneration (Park et al., 2008) and the VEGF pathway to promote ganglion cell survival after injury (Kilic et al., 2006; Nishijima et al., 2007). The GSEA data newly implicates these processes in shaping the structure of emerging retinogeniculate circuits in the developing LGN.

The gene microarray approach has been a productive tool for elucidating complex processes of early neurodevelopment (Kawasaki et al., 2004; Leamey et al., 2008; Sun et al., 2005; Murray et al., 2007, 2008). The advantage of this technique is its capacity to identify previously unidentified candidates, such as *Zic4* and *Foxp2*, as well as functional pathways among the vast system of gene networks involved in regional specification. These enriched groups, representing the molecular identity of brain regions, provide the link between early patterning events and later functional processes of circuit formation and cellular differentiation.

Limitations of the microarray data include the fact that microarrays reflect transcript and not protein expression, which may be explored in the future with protein arrays. Our dissections pooled structural subdivisions, including dorsal and ventral subdivisions of the nuclei, as well as functional cell subpopulations, as indicated by growing evidence for specialized streams of visual information in the mouse (Huberman et al., 2008; Kim et al., 2008). Laser dissection or fluorescence activated cell sorting (FACS) techniques may be necessary in the future to characterize the genetic identity of these structural or functional subdivisions (Arlotta et al., 2005).

***Zic4* exhibits a novel role in retinogeniculate mapping**

Zic4 is a zinc-finger transcription factor with a role in cerebellar development, its heterozygous co-deletion with *Zic1* leading to cerebellar malformation in mice and Dandy-Walker malformation in humans (Grinberg et al., 2004). We provide the first report of *Zic4*'s role in visual pathway patterning. While loss of family member, *Zic2*, leads to the wholesale failure of retinogeniculate fibers to project ipsilaterally (Pak et al., 2004), *Zic4* loss leads to the disordering of appropriately targeted ipsilateral retinogeniculate fibers. Moreover, *Zic2* is not detectably expressed in LGd, highlighting a divergent role for *Zic4* in visual pathway patterning.

Increased clustering and disorganization of the ipsilateral terminal zone in *Zic4* null mice resembles, but does not mimic, the phenotype of the *ephrin-A2/3/5* null mouse (Pfeiffenberger et al., 2005). While both null mice exhibit increased ipsilateral clustering, dorsomedial expansion of the ipsilateral retinogeniculate projection in the *Zic4* null mouse is not present in the *ephrin-A2/3/5* null mouse, suggesting a unique role for *Zic4* that is distinct from that of the *ephrin-As*. Interestingly, this dorsomedial expansion is the complement of the dorsoventral expansion of ipsilateral fibers in the *Ten_m3* null mouse (Leamey et al., 2007) and whether these molecules interact to establish proper retinotopic organization of the ipsilateral eye warrants future investigation.

An open question is whether it is loss of *Zic4* in the projecting cells or in the target cells or both that leads to the mismapping of ipsilateral retinogeniculate fibers. Loss of the temporal high *Zic4* gradient in the retina might allow the ipsilateral axons

formerly enriched in *Zic4* to terminate more dorsomedially in the LGd. Alternatively, the loss of *Zic4* in dorsolateral geniculate target cells might downregulate a repulsive cue that permits the ipsilateral expansion. It is also unclear whether *Zic4* regulates the expression of downstream axon guidance cues or acts itself as a cue, as has been demonstrated for other transcriptional factors such as *En-2* (Brunet et al., 2005). *In vitro* assays testing the interaction of *Zic4* null retina with normal thalamus and vice versa would be useful in addressing this question. Additional *in vivo* work with region-specific mutants of *Zic4*, or *in utero* electroporation experiments in which retinal cells or thalamic cells are specifically targeted for *Zic4* knock-down or overexpression, would also be informative.

Foxp2 and activity-dependent regulation in the mammalian brain

Foxp2 is a transcriptional repressor, implicated in deficits of ultrasonic vocalizations in perinatal mice (Shu et al., 2005), orofacial dyspraxia and abnormalities in corticostriatal circuitry in humans with a heterozygous loss-of-function mutation (Vernes et al., 2006), and abnormalities in song learning of adult canaries after knock-down (Haesler et al., 2007). *Foxp2* expression is dynamically regulated with activity or conditions of learning in songbirds. In zebrafinches, *Foxp2* expression is upregulated in Area X during a period of vocal learning and downregulated during unidirected singing but not directed singing in adulthood (Teramitsu and White, 2006). In adult canaries, it is upregulated in Area X during seasons of song learning (Haesler et al., 2004).

We report here for the first time in mammals, that *Foxp2* protein is positively upregulated with auditory stimulation, suggesting an activity dependent role in synaptic

plasticity of the primary auditory pathway. It is not clear whether this function is exclusive to the auditory pathway, or exists in other sensory pathways. Although a role in axonal pathfinding was not explored in this study, *Foxp2* may additionally contribute to corticocollicular and/or geniculocortical mapping of the auditory pathway, as family member, *Foxp1*, has been shown to regulate motoneuron differentiation and pathfinding (Rousso et al. 2008). A role for *Foxp2* in early stages of auditory processing may contribute to higher level deficits of speech and language in humans.

Mechanisms of cross-modal plasticity in response to early injury

In the cortex, processes of areal specification are driven by both intrinsic factors, including positional and lineage-derived gene programs (Miyashita-Lin et al., 1999) and extrinsic factors, such as the pattern of activity, or frequency code, and identity of inputs (Dehay et al, 1993, 2001, Lukaszewicz et al., 2005). Our data show that, like cortical areas, the functional differentiation of thalamic nuclei is influenced by its specific inputs. A quarter of genes and a number of gene pathways, including the mTOR related pathway, that were upregulated in the rwMGN were also present in the group of genes and processes specifying the LGN, suggesting that some genetic programs of LGN and rwMGN development are derived from retinal input. Retinal axons potentially use a different frequency code from auditory afferents of the inferior colliculus and may also secrete different neurotransmitters, trophic factors, or synaptic modulators that contribute to LGN specification (Stevens et al, 2007). Because is unlikely that LGN-like patterns of gene expression are the “default state” of the MGN in the absence of IC input, we

propose that the frequency code and/or chemical signaling of retinal inputs are translated into specific patterns of LGN-like patterns of gene expression. Conversely, there may be constraints on how the MGN interprets these novel signals, and thus may respond with additional “plasticity-related” networks.

The molecular mechanism of ectopic retinal targeting to the deafferented MGN is not understood. It is possible that patterns of rwMGN gene expression include axon guidance pathways mediating retinal axon ingrowth. We searched for candidates by isolating genes with a known role in synapse formation and additionally screening a number of known axon guidance molecules. A promising candidate, the downregulated serotonin transporter, *Slc6a4*, has previously been shown to modulate eye-specific segregation of retinal axons in the LGd and mediate the formation of barrels in somatosensory cortex (Salichon et al., 2001; Upton et al., 1999, 2001). However, *Slc6a4* null mice were not rewired, suggesting either that its loss is not sufficient to induce visual rewiring or that the effects are compensated by other genes during development. Future experiments using *in utero* electroporation for more spatially and temporally specific gene modulation would provide a more rigorous test of *Slc6a4* contribution to retinal rewiring. It is possible that other genes alone or in addition to *Slc6a4* are required for rewiring or that the physical ablation of IC is necessary. Other intriguing candidates include the upregulated *Clqb*, a complement protein implicated in retinogeniculate synapse elimination (Stevens et al., 2007), upregulated *Zic4*, which was confirmed with *in situ* hybridization (Suppl. Fig. 6) and other screened axon guidance cues.

CONCLUSION

In summary, we report here newly identified, enriched groups of candidate genes for perinatal murine LGN and MGN specification. These candidates potentially reflect distinct differentiation programs set by differences in patterning cues and neural inputs and may contribute to the structural and functional maturation of the principal visual and auditory thalamic relay nuclei. From this screen, we identify for the first time a role for *Zic4* in ipsilateral retinotopic patterning to the thalamus and an activity-dependent regulation of *Foxp2* in response to auditory stimulation. Additional microarray data comparing visually rewired MGN and normal MGN suggest that abnormal visual inputs respecify the MGN with both LGN-like and novel patterns of gene expression. Our data identify a number of novel candidates involved in the molecular mechanisms linking early patterning events to the functional differentiation of the visual and auditory pathways.

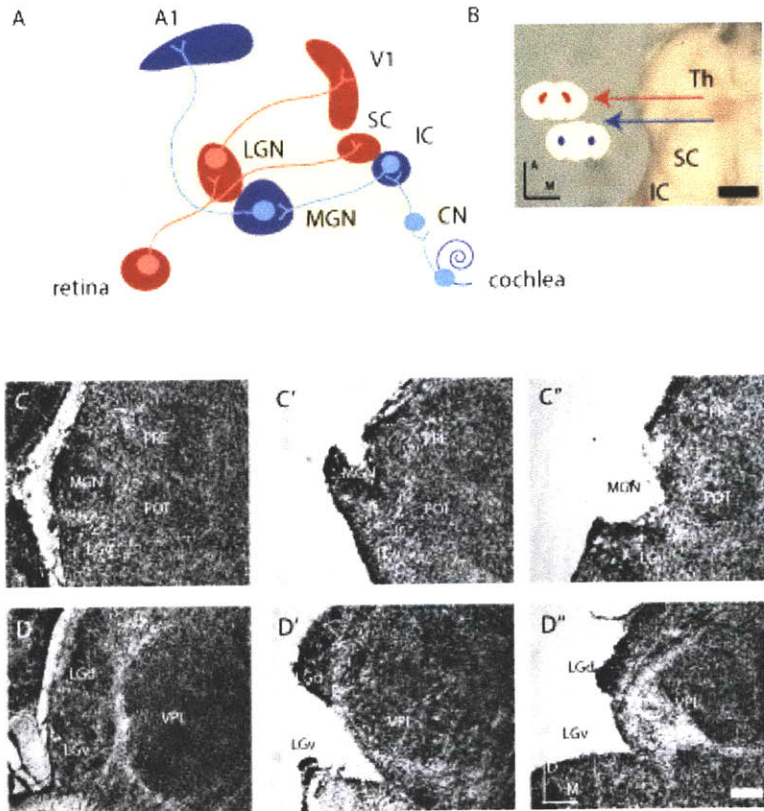


Figure 1. Primary visual and auditory sensory pathways to the cortex. (A) Retinal ganglion cells project to the lateral geniculate nucleus (LGN), which in turn projects to the primary visual cortex (V1). Auditory afferents from the cochlea terminate in the cochlear nucleus (CN) of the brainstem, which then innervates the inferior colliculus (IC). Cells from the IC project to the medial geniculate nucleus (MGN), which in turn projects to the primary auditory cortex (A1). (B) Dorsal view of the neonatal thalamus (the cortex has been peeled off), red arrow: LGN, blue arrow: MGN, Th, thalamus, SC, superior colliculus, IC, inferior colliculus, Scale Bar, 1 mm. Colored lines show coronal planes of section for Nissl stains and point to schematics of coronal sections featuring the MGN (blue) and LGN (red). Coronal sections of cresyl violet stains reveal the nuclear structure of the MGN (C) and LGN (D) at P0. Two examples of MGN (C',C'') and LGN (D',D'') dissected brain are representative of the tissue samples taken for microarray analysis. PRE: pretectal nucleus, POT: posterior thalamic nucleus, VPL: ventral posterior thalamic nucleus, lateral part, LGv: ventral subdivision of the LGN, D: dorsal, M: medial, Scale bar=150 μ m

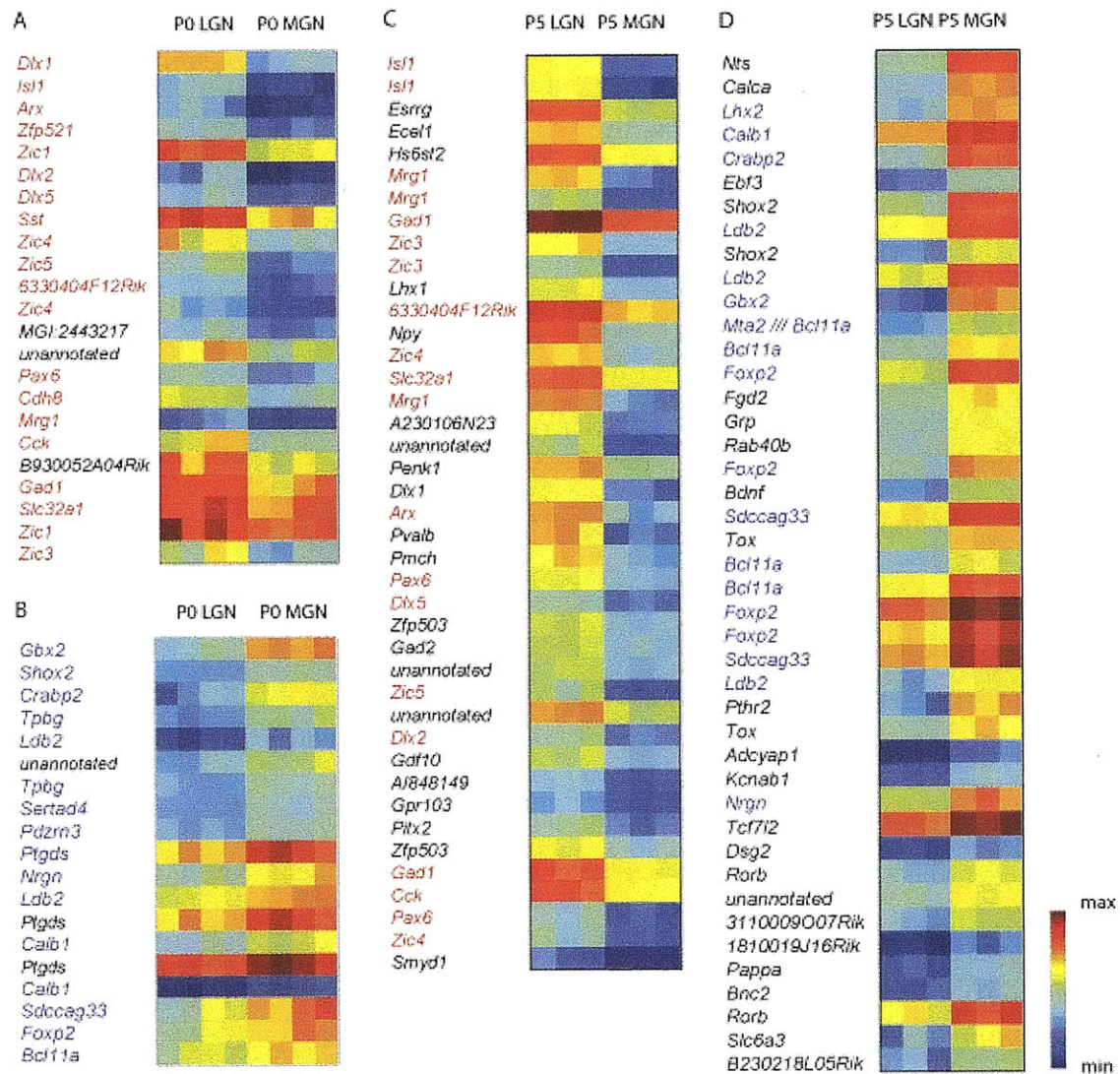


Figure 2. Significance Analysis of Microarrays (SAM) identifies LGN and MGN enriched groups at P0 and P5. (A) A group of 20 unique genes enriched in P0 LGN and (B) a group of 13 unique genes enriched in P0 MGN, determined in SAM using a fold change (FC) >2 and a delta value adjustment to 0.831 in order to yield a false discovery rate (FDR) < 0.01%. Seventeen/20 (85%) of the P0 LGN genes (red type) were present in the P5 LGN group using the same SAM criteria and 12/13 (92%) of the P0 MGN genes (blue type) were present in the P5 MGN group. Each P0 group has 4 replicates with n=15-20 each. (C) Thirty-one unique genes were enriched in P5 LGN with FC >3, delta =1.4 for FDR <0.01%. Thirteen/30 (43%) of these genes were present in the P0 LGN set (red type). (D) Thirty unique genes were enriched in P5 MGN with these criteria;10/30 (33.3%) were present in the P0 MGN set (blue type). Each P5 group has 3 replicates with n=15-20 each. All genes are ranked by SAM d-score. Colorbar, blue represents minimum intensity value within the gene group on the microarray, red represents maximum intensity.

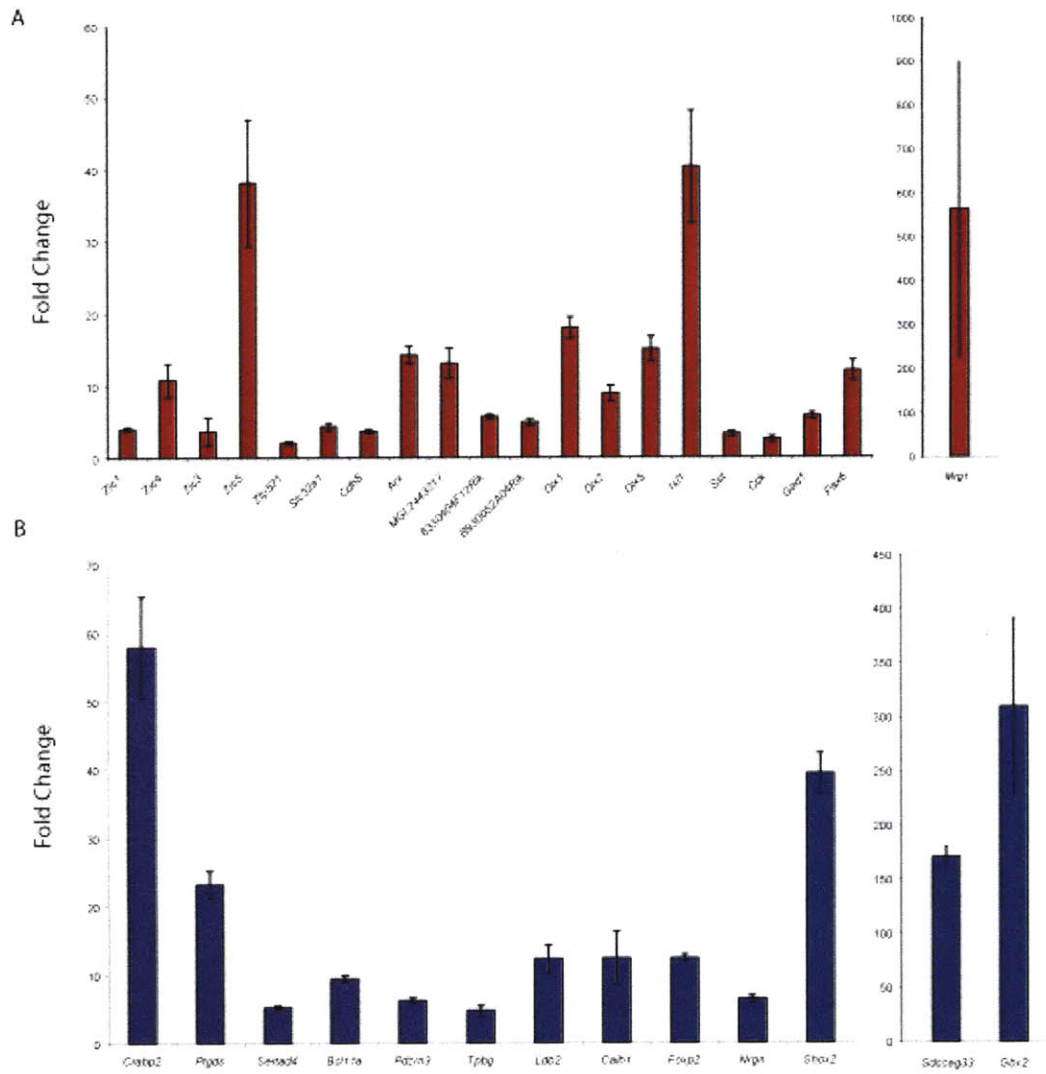


Figure 3. Quantitative RT-PCR of LGN and MGN specific genes confirms differential gene expression. (A) P0 LGN enriched genes are all significantly upregulated (20/20, $p < 0.05$, $FC > 2$ in LGN samples vs. MGN samples and (B) P0 MGN enriched genes are all significantly upregulated (13/13, $p < 0.05$, $FC > 4$) as well.

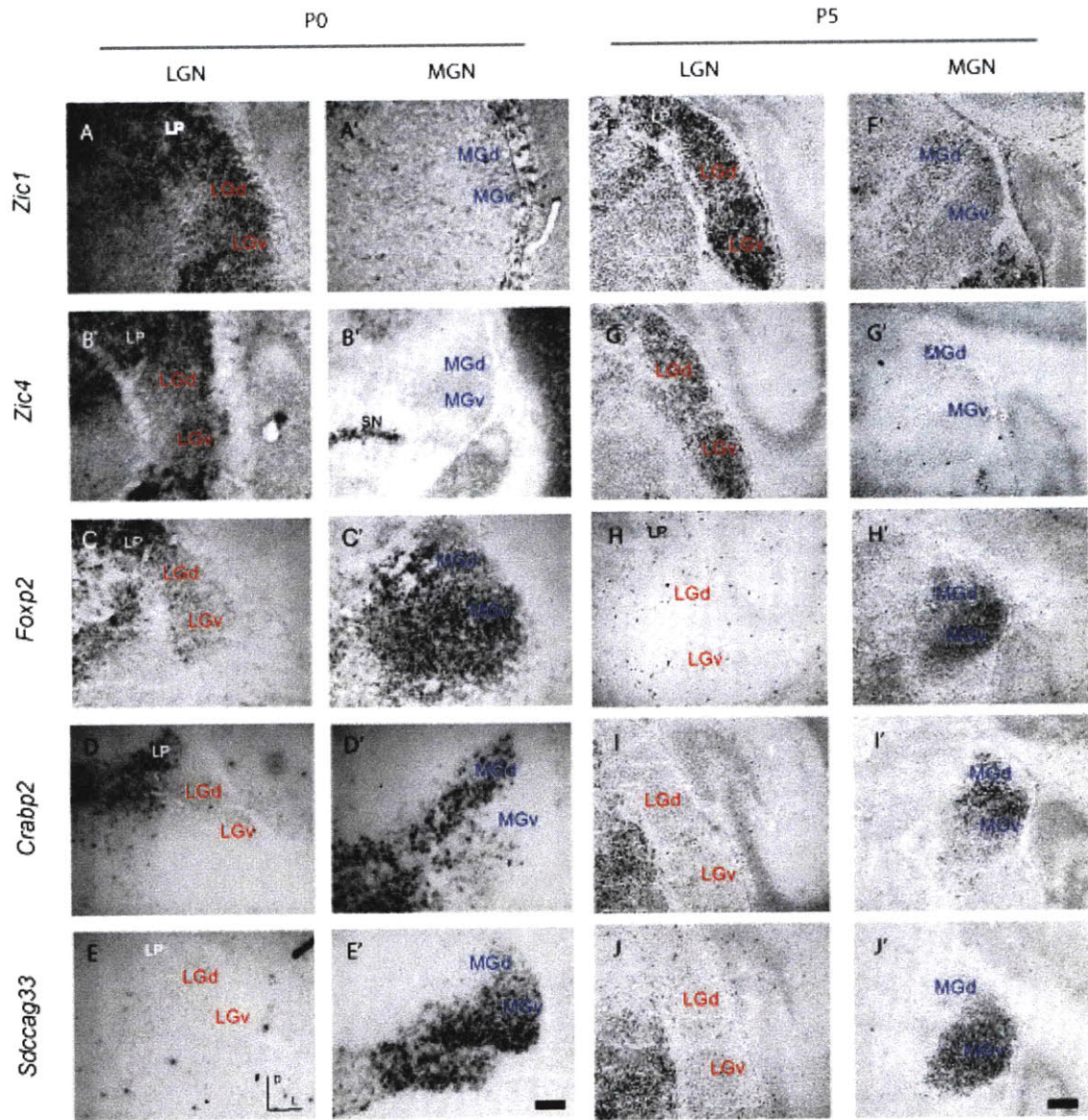


Figure 4. *In situ* hybridizations at P0 (A-E, A'-E') and P5 (F-J, F'-J') confirm the differential expression of LGN and MGN enriched genes. (A, A', F, F') *Zic1* and (B, B', G, G') *Zic4* are expressed in LGd (A,B,F,G) but not MGN (A',B', F',G'), while (C, C', H, H') *Foxp2*, (D, D', I, I') *Crabp2*, and (E, E', J, J') *Sdccag33* are expressed in MGN (C'-E', H'-J') but not in LGd (C-E, H-J). Sense probes were tested for all genes and yielded no signal (data not shown). LGd, dorsal lateral geniculate nucleus, MGd, dorsal body of the medial geniculate nucleus, MGv, ventral division of the medial geniculate nucleus, LP, lateral posterior thalamic nucleus, SN, substantia nigra, LGv, ventral lateral geniculate nucleus. Scale bar= 150 μ m for P0, 300 μ m for P5.

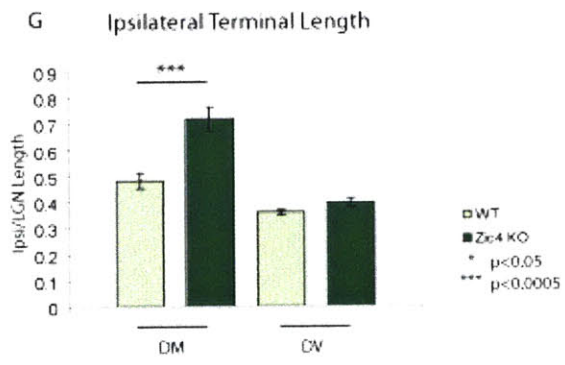
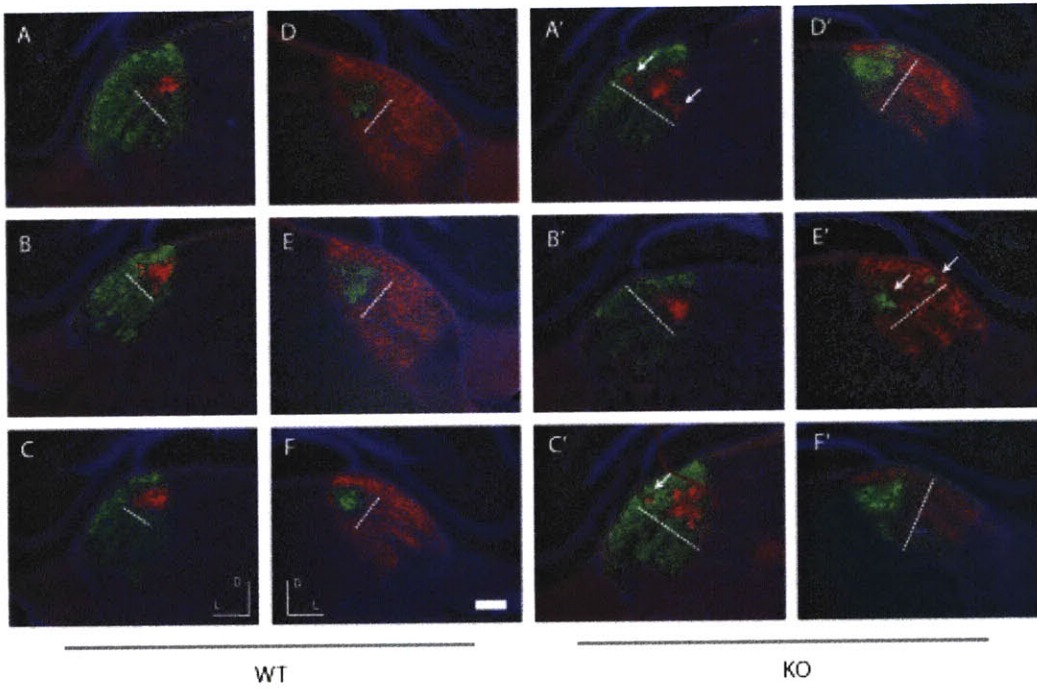


Figure 5. Ipsilateral projections are disrupted in the rostral LGd of *Zic4* KOs.

Representative samples of intraocular 488- and 594-CTB tracings to the LGd in control (left A-C, right D-F) and *Zic4* KO (left (A'-C', right D'-F')); dotted white line: length of ipsilateral zone along the dorsomedial axis; white arrows, multiple ipsilateral terminals in KO; D, dorsal, L, lateral, scale bar= 300 μ m. (G) Ipsilateral terminal length along the dorsomedial (DM) and dorsoventral (DV) axes, expressed as a fraction of the total LGd terminal length.

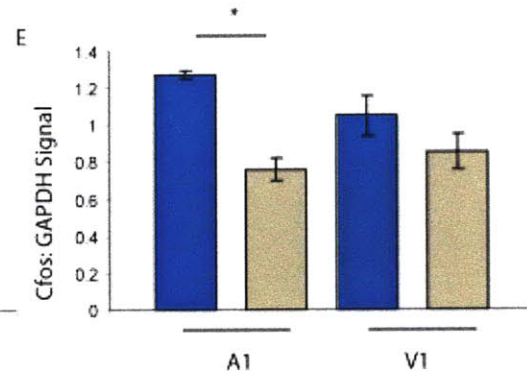
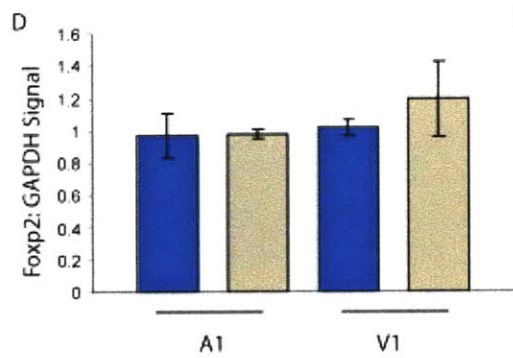
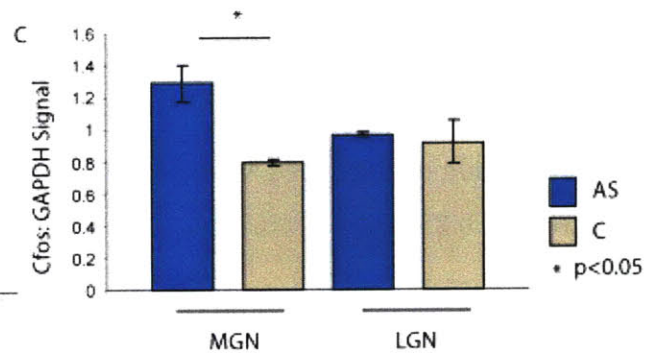
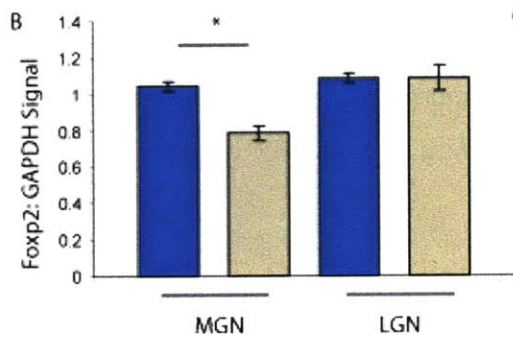
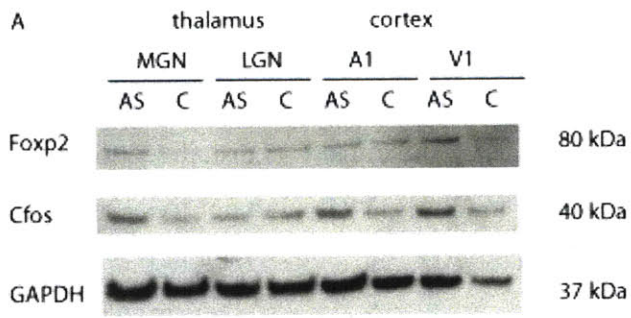


Figure 6. Activity-dependent expression of Foxp2 protein in the auditory thalamus. (A) Western blotting of Foxp2, cFos and GAPDH in the MGN, LGN, A1 and V1 of P18 mice exposed to 2 hours of ramped, high decibel white noise vs. no treatment. AS: auditory stimulation, C: control. Quantitated signal of Foxp2 (B) and cFos (C) normalized to GAPDH levels shows an increase in Foxp2 expression in the MGN, but not LGN of mice undergoing auditory stimulation. Foxp2 MGN: 1.04 ± 0.025 vs. 0.78 ± 0.037 , $p < 0.05$, $n = 4$ pooled for each group, technical replicate $n = 3$ for each group; cFos MGN: 1.29 ± 0.02 vs. 0.78 ± 0.02 , $p < 0.05$. In the cortex (D, E), Foxp2 levels do not change in response to auditory stimulation (Foxp2 A1: 0.967 ± 0.14 vs. 0.977 ± 0.03 , $p = 0.585$; Foxp2 V1: 1.01 ± 0.048 vs. 1.19 ± 0.232 , $p = 0.54$), while cFos levels increase in both A1 and to a lesser extent, V1, of stimulated mice (A1: 1.27 ± 0.025 vs. 0.76 ± 0.059 , $p < 0.05$; cFos V1: 1.05 ± 0.108 vs. 0.85 ± 0.096 , $p = 0.786$).

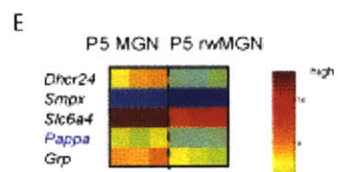
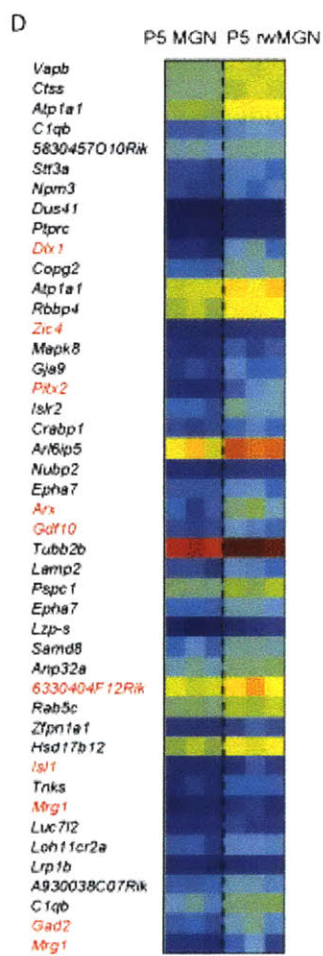
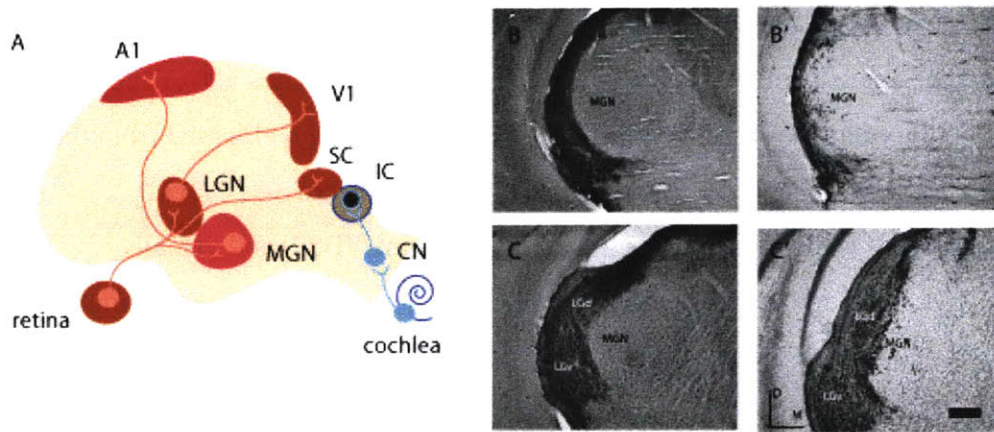
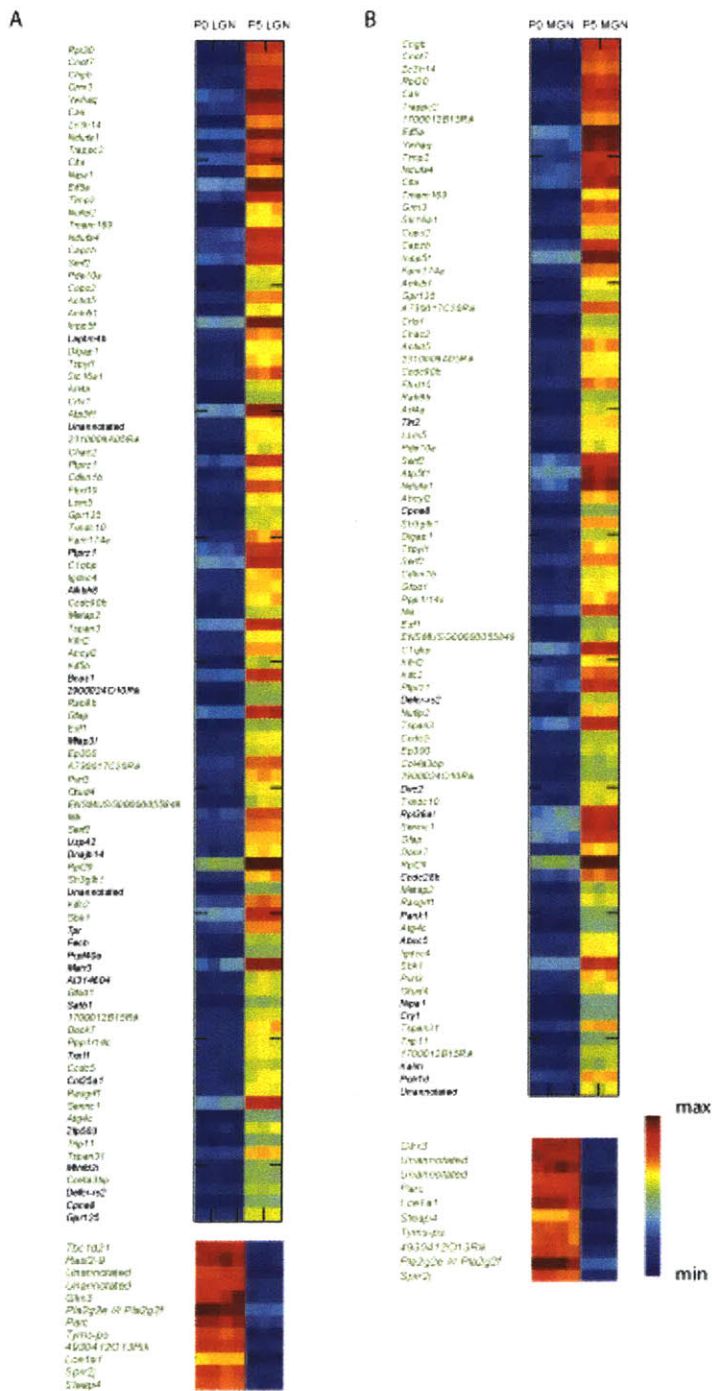
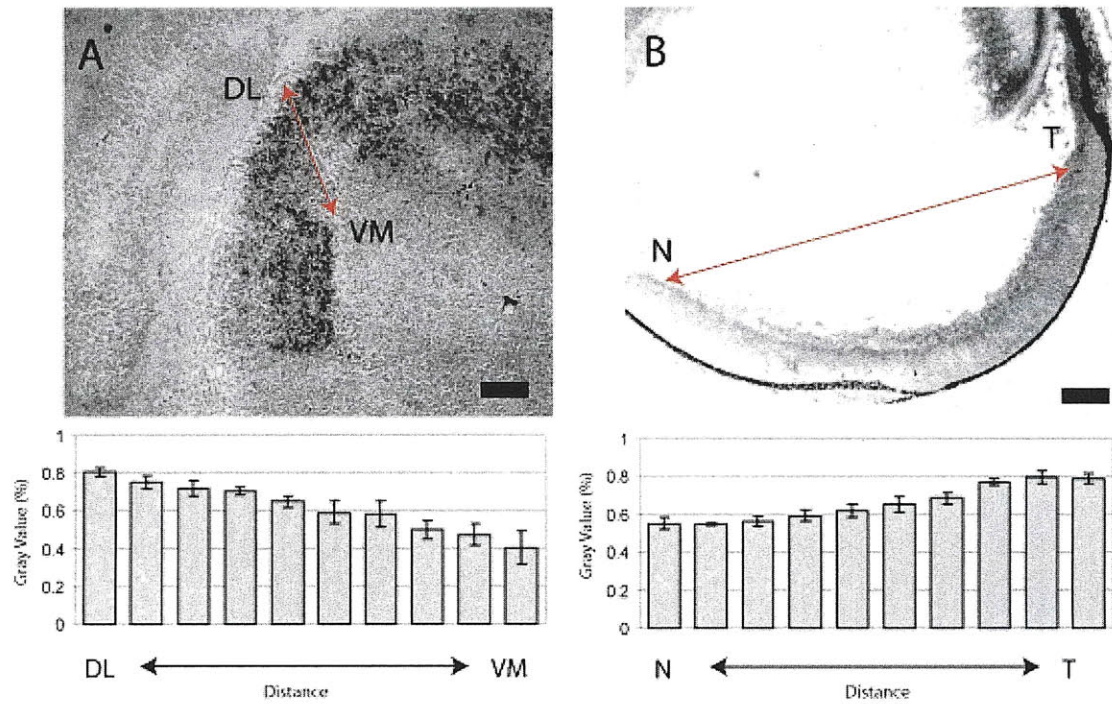


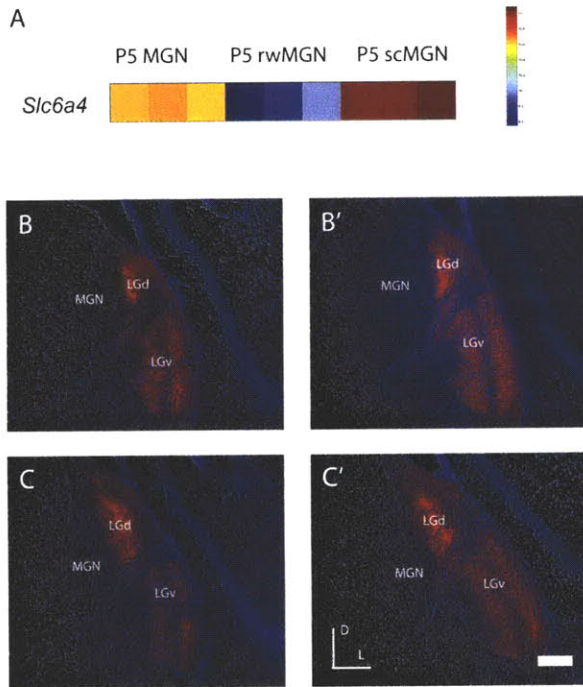
Figure 7. Significance Analysis of Microarrays (SAM) identifies both novel and LGN-like patterns of gene expression in visually rewired MGN (rwMGN) at P5. (A) Schematic of the rewired auditory pathway after IC ablation. MGN receives novel inputs from the retina, which drive the MGN and A1 to mediate visually driven responses. (B,C) Intraocular injections of CTB project to the thalamus in normal (B,C) and visually rewired (B',C') mice. Coronal sections demonstrate ectopic retinogeniculate terminals in the rewired MGN (B',C') but not the normal MGN (B,C). (D) 44 probe sets, corresponding to 41 unique genes, are enriched in the P5 rwMGN with a fold-change (FC) >1.5 and false discovery rate <3.37% (n=15-20 per replicate, 3 replicates per group, delta-value=0.666), and 10/41 (24.4%) of these enriched genes were present in the P5 LGN enriched set (red type). (E) Five probe sets, corresponding to 5 unique genes, were downregulated in the rwMGN and only one was a gene enriched in the P5 MGN (blue type). Each group has 3 replicates with n=15-20 each. All gene sets are ranked by SAM d-score. Colorbar, blue represents minimum intensity value within the gene set on the microarray, red represents maximum intensity.



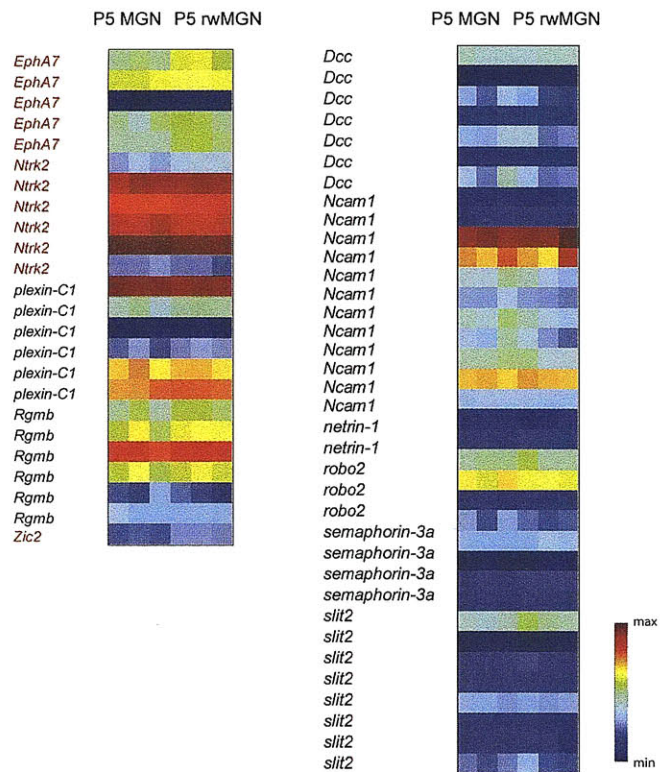
Supplemental Figure 1. Significance Analysis of Microarrays (SAM) identifies common differences in gene expression of LGN (A) and MGN (B) between P0 and P5. Seventy-nine percent (green type) of the top 115 probe sets of differentially expressed genes between P0 and P5 were the same in both LGN and MGN, suggesting that there are common and coincident pathways of maturation at the two ages.



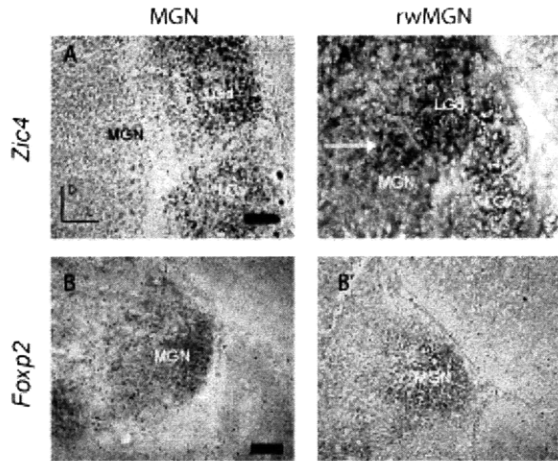
Supplemental Figure 3. *In situ* hybridization demonstrates graded *Zic4* expression in the perinatal LGd and retina. (A) *Zic4* is expressed in a high dorsomedial to low ventrolateral gradient in the perinatal LGd. DL, dorsolateral, VM, ventromedial, red line, axis of signal measurement, expressed as a percentage of the maximum signal intensity, scale bar= 150 μ m. (B) *Zic4* is expressed in a high temporal to low ventral gradient in perinatal retinal ganglion cells. T=temporal, N=nasal, red line, axis of signal measurement, expressed as a percentage of the maximum signal intensity, scale bar= 300 μ m.



Supplemental Figure 4. *Slc6a4* is significantly downregulated in rwMGN (A), but visual rewiring of retinal axons to the MGN is not seen in CTB retinogeniculate tracings of *Slc6a4* null mice (B,C), whose retinogeniculate anatomy is comparable to that of wild-type (B',C'). D, dorsal, L, lateral, scale bar= 300 μ m.



Supplemental Figure 5. Groups of known axonal guidance factors are upregulated and downregulated in the rwMGN relative to normal MGN at P5. Two upregulated genes, *EphA7* and *Ntrk2*, were also enriched in P5 LGN relative to normal MGN (red type).



Supplemental Figure 6. *In situ* hybridization confirms upregulation of *Zic4* in rwMGN (A') compared to control P5 MGN (A). D, dorsal, L, lateral, scale bar= 150 μ m. No change in *Foxp2* expression (B, B') was observed. Scale bar= 300 μ m.

Primers used for qRT-PCR

P0 LGN enriched group

	F primer	R primer
<i>Zic4</i>	TCTGGCTACGACTCGGCTAT	CATCATTGCTCACGTCTGT
<i>Slc32a1</i>	GGCGACTTCACTCTGGAGAA	ACAGTCCACGACCGGATAC
<i>Gad1</i>	GCAGGGGGAAGTGCATATAA	CAAATGGGAAGAAAATACAAGATG
<i>Zic1</i>	CCGAAAGCCAACTGTTTGTA	CTGTTAGGTCGACGTGGAGA
<i>5330404F12Rik</i>	CTCCAATCCCCTTCTTCTCC	GGCATGCATGTACCTCCTTT
<i>Zic5</i>	TGTTCAAGCAGAAATGGAGAGA	CAGCAGAGGACAGAGAAAGCA
<i>Zfp521</i>	ATCAATGGTAAAAACCAAGAC	ATATGGGCCGTATCCAGATG
<i>MGI_2443217</i>	GGGAAGCTCAGGTCTTTTCA	CACACGTTTTCCATCCACCT
<i>Cdh8</i>	TGTTTATGGTGATGCGCAGA	CTCCTACATGGCAGGTTTGC
<i>Arx</i>	GGCTTCGAAACCTTCAAGA	GAGCGTGACACTTCTCCACT
<i>B930052A04Rik</i>	CCCCAGGAATATAGAGTTTGC	CCCAGCTCCGCTACACTACA
<i>Pax5</i>	TGCTTCCCCTAGAAATCCTCAGA	GCTGGCCAAGAAAGAAACAA
<i>Dlx2</i>	TCCAGCTCTCCCAACTCTTC	AAATGAGGTATCCGCAAAG
<i>Isl1</i>	CTGGCAGTGAAGTAGCATCG	TCCCCACTTTCTCCAACAGG
<i>Dlx5</i>	CGGGACGCTTTATTAGATGG	CATCCCCGTATGAATTCCTTT
<i>Sst</i>	CCCAGACTCCGTCAGTTTCT	GCATCATTCTCTGTCTGGTTG
<i>Cck</i>	AAGTGACCGGACTACATGG	CTCATTCCACCTCCTCCAAG
<i>Mrg1</i>	CCCCAAGGAAGTTGAGCATA	TTGAAGGTGATCTCTCAAGCTG
<i>Zic3</i>	CCGGAATCGTCAGTTCTCTC	TTGTGCGTTAGTCAGCAAGC
<i>Dlx1</i>	AGAACACCTGGCCAAGAAGA	TAAAGCGACCTGGAATTGG

P0 MGN enriched group

	F primer	R primer
<i>Crabp2</i>	TGGATGGGAGACCCTGTAAG	CAGCTCTCCATCATTGGTCA
<i>Ptgds</i>	CCCAGACTCTGAAGGACGAG	CCAGCCCTCTGACTGACTTC
<i>Serfad4</i>	GCGGAACGTTATTTTGGAGA	TCCGAGTCCCCTGAGTACA
<i>Sdocag33</i>	CCTTCTGGCTGTATGCTTTCT	TGCAAGGGCAGGTAATTTTT
<i>Bcl11a</i>	CGCACAGAACACTCATGGAT	GAGCTTCCATCCGAAAACCTG
<i>Pdzrn3</i>	CACTTCGCTGAATGTGTTTCA	TGTGTCAAATCACCAACCAGA
<i>Tpbp</i>	TGACCTGAGATTTTTCGGTGT	AACAATCCAGTTTGTGGATCTC
<i>Ldb2</i>	GGTGACTTTCTGACAAGCTGAA	GCATACATTTCTCAGGGTCCA
<i>Caib1</i>	GGACTCTTTCCCCTCAAGAATGA	TTCCAAATACGTGCCGAAGT
<i>Foxp2</i>	CCAAATTGTTGGAATGCTGA	CAAGACTTGGCACAGCACAT
<i>Nrgn</i>	ACCTCCTAAACCTGGGGCTA	CAGGCAGGTATGGGATAGGA
<i>Gbx2</i>	GTGCCCAAAGGTAACAGGA	AAATCAACCGACTGCTCTGC
<i>Shox2</i>	CGCCCTTGGGACTAAAATTC	CTGTGGCGCTATCCACTTCT

Supplemental Table 1. Primer sequences used to measure relative levels of LGN and MGN enriched genes with qRT-PCR.

Primers used for *in situ* hybridization

P0 LGN enriched group

	F primer	R primer
<i>Zic1</i>	CCAAAAAGTCGTGCAACAAA	CTGTTGTGGGAGACACGATG
<i>Zic4</i>	CAAGAAAGGGAGGAGGAACC	CGACAAGCAGGAATGTCTCA

P0 MGN enriched group

	F primer	R primer
<i>Foxp2</i>	GGAATGCATTGCTGTGTGAT	TCCAGCAGAAGTGAGACACTG
<i>Crabp2</i>	AGATCGGGGAGGAATTTGAG	GTGGGAGGGTTCTGAGCTTC
<i>Sdccag33</i>	GCTGACCTGCCTATCTGGAC	AGACAGCTTCCGTCTCCAA

Supplemental Table 2. Primer sequences used to synthesize *in situ* hybridization probes.

Axon Guidance Factors Screened in P5 Microarray Data

<i>Bdnf</i>	<i>Frizzled-6</i>	<i>semaphorin-3b</i>
<i>beta 2 laminin</i>	<i>Frizzled-7</i>	<i>semaphorin-3c</i>
<i>cadherin-4</i>	<i>Frizzled-8</i>	<i>semaphorin-3d</i>
<i>collapsin response mediator protein-1</i>	<i>Frizzled-9</i>	<i>semaphorin-3e</i>
<i>contactin 2</i>	<i>Frzb</i>	<i>semaphorin-3f</i>
<i>Dcc</i>	<i>Isl2</i>	<i>semaphorin-4a</i>
<i>Dpysl5</i>	<i>L1CAM</i>	<i>semaphorin-4b</i>
<i>engrailed-2</i>	<i>laminin, alpha 1</i>	<i>semaphorin-4c</i>
<i>EphA1</i>	<i>laminin, beta 3</i>	<i>semaphorin-4d</i>
<i>EphA2</i>	<i>Ncam1</i>	<i>semaphorin-4f</i>
<i>EphA3</i>	<i>Ncam2</i>	<i>semaphorin-4g</i>
<i>EphA4</i>	<i>netrin-1</i>	<i>semaphorin-5a</i>
<i>EphA5</i>	<i>netrin-2 like</i>	<i>semaphorin-5b</i>
<i>EphA6</i>	<i>netrin-4</i>	<i>semaphorin-6a</i>
<i>EphA7</i>	<i>netrin-G1</i>	<i>semaphorin-6b</i>
<i>EphA8</i>	<i>netrin-G2</i>	<i>semaphorin-6c</i>
<i>EphB1</i>	<i>neuropilin-1</i>	<i>semaphorin-6d</i>
<i>EphB2</i>	<i>neuropilin-2</i>	<i>semaphorin-7a</i>
<i>EphB3</i>	<i>Ntf3</i>	<i>Sfrp1</i>
<i>EphB4</i>	<i>Ntf5</i>	<i>Sfrp2</i>
<i>EphB6</i>	<i>Ntrk1</i>	<i>Sfrp4</i>
<i>ephrin-A1</i>	<i>Ntrk2</i>	<i>Sfrp5</i>
<i>ephrin-A2</i>	<i>Ntrk3</i>	<i>Shh</i>
<i>ephrin-A3</i>	<i>Ntrk3</i>	<i>slit1</i>
<i>ephrin-A4</i>	<i>Plat</i>	<i>slit2</i>
<i>ephrin-A5</i>	<i>plexin-A1</i>	<i>slit3</i>
<i>ephrin-B1</i>	<i>plexin-A2</i>	<i>Slitrk1</i>
<i>ephrin-B2</i>	<i>plexin-A3</i>	<i>Slitrk2</i>
<i>ephrin-B3</i>	<i>plexin-A4</i>	<i>Slitrk3</i>
<i>Fgf2</i>	<i>plexin-B1</i>	<i>Slitrk4</i>
<i>Fgfr1</i>	<i>plexin-B2</i>	<i>Slitrk5</i>
<i>Fgfr2</i>	<i>plexin-B3</i>	<i>Slitrk6</i>
<i>Fgfr3</i>	<i>plexin-C1</i>	<i>Unc5b</i>
<i>Fgfr4</i>	<i>Rgma</i>	<i>Unc5c</i>
<i>Frizzled-1</i>	<i>Rgmb</i>	<i>Wnt4</i>
<i>Frizzled-10</i>	<i>robo1</i>	<i>Wnt5a</i>
<i>Frizzled-2</i>	<i>robo2</i>	<i>Wnt5b</i>
<i>Frizzled-3</i>	<i>robo3</i>	<i>Zic2</i>
<i>Frizzled-4</i>	<i>Ryk receptor</i>	
<i>Frizzled-5</i>	<i>semaphorin-3a</i>	

Supplemental Table 3. List of known axonal guidance factors used to screen P5 gene microarray data.

Top 20 Enriched Gene Sets for P0 LGN

NAME	SIZE	ES	NES	NOM p-val	FDR q-val	FWER p-val
TSADAC_HYPOMETH_OVCA_UP	35	0.46	1.64971	0	1	0.527
BCNU_GLIOMA_NOMGMT_48HRS_UP	18	0.48	1.60866	0	1	0.646
BASSO_GERMINAL_CENTER_CD40_DN	57	0.502	1.60289	0	0.75607	0.674
HDACI_COLON_BUT2HRS_UP	56	0.393	1.5928	0	0.646825	0.721
HSA00650_BUTANOATE_METABOLISM	41	0.483	1.58615	0	0.553943	0.732
HSA00252_ALANINE_AND_ASPARTATE_METABOLISM	30	0.553	1.5828	0	0.482242	0.732
SHIPP_DLBCL_CURED_DN	31	0.494	1.54377	0	0.646394	0.869
NADLER_OBESITY_HYPERGLYCEMIA	43	0.425	1.54327	0	0.569843	0.869
LEE_TCELLS6_UP	19	0.548	1.53387	0.046	0.567148	0.885
RORIE_ES_PNET_UP	21	0.619	1.52695	0	0.544126	0.913
CARDIACEGFPATHWAY	17	0.528	1.52451	0.0782779	0.514666	0.924
HSA04070_PHOSPHATIDYLINOSITOL_SIGNALING_SYSTEM	58	0.377	1.50148	0	0.601181	0.951
KANNAN_P53_UP	32	0.462	1.48528	0	0.67504	0.972
HSA00562_INOSITOL_PHOSPHATE_METABOLISM	39	0.396	1.47474	0	0.695055	0.985
ALANINE_AND_ASPARTATE_METABOLISM	19	0.607	1.46867	0.0673469	0.701018	0.985
TGZ_ADIP_UP	15	0.518	1.45668	0.0220441	0.746246	0.985
IL2RBPATHWAY	34	0.423	1.44937	0.0180723	0.768476	1
WONG_IFNA_HCC_RESISTANT_VS_SENSITIVE_DN	26	0.515	1.44652	0.027668	0.746061	1
IDX_TSA_UP_CLUSTER1	24	0.542	1.44469	0	0.718328	1

Supplemental Table 4. Ranked list of top 20 enriched gene set pathways for P0 LGN.

Top 20 Enriched Gene Sets for P0 MGN

NAME	SIZE	ES	NES	NOM p-val	FDR q-val	FWER p-val
HSA05010_ALZHEIMERS_DISEASE	25	-0.568611	-1.966606	0	0.02	0
TSA_HEPATOMA_CANCER_UP	37	-0.627499	-1.880277	0	0.066727	0.099
LEE_MYC_E2F1_UP	47	-0.60601	-1.837335	0	0.057243	0.117
ET743_HELA_UP	53	-0.546914	-1.82482	0	0.053958	0.135
ADI1P_DIFF_CLUSTER1	53	-0.537132	-1.820337	0	0.051987	0.135
PASSERINI_GROWTH	32	-0.600852	-1.796972	0	0.05517	0.162
5FU_RESIST_GASTRIC_DN	15	-0.65135	-1.778482	0	0.057444	0.203
IRITANI_ADPROX_VASC	134	-0.450606	-1.767829	0	0.054215	0.216
HSA00530_AMINOSUGARS_METABOLISM	25	-0.462984	-1.755907	0	0.054678	0.228
APPEL_IMATINIB_UP	31	-0.541586	-1.752958	0.01636	0.057212	0.246
GATA3PATHWAY	15	-0.665047	-1.749634	0	0.057462	0.264
RETT_UP	32	-0.467294	-1.746837	0	0.056349	0.264
TPA_RESIST_EARLY_UP	26	-0.586174	-1.743355	0	0.057579	0.288
NADLER_OBESITY_UP	54	-0.466435	-1.743135	0	0.054894	0.288
CMV_HCMV_TIMECOURSE_24HRS_DN	36	-0.556577	-1.717328	0	0.059403	0.347
LEI_HOXC8_DN	17	-0.769249	-1.708973	0	0.064676	0.37
POMEROY_DESMOPLASIC_VS_CLASSIC_MD_DN	36	-0.505099	-1.706428	0	0.062674	0.37
HOFMANN_MDS_CD34_LOW_AND_HIGH_RISK	36	-0.475666	-1.692606	0	0.07756	0.418
VEGF_MMMEC_12HRS_UP	27	-0.655342	-1.691136	0	0.075201	0.418

Supplemental Table 5. Ranked list of top 20 enriched gene set pathways for P0 MGN.

Top 20 Enriched Gene Sets for P5 LGN

NAME	SIZE	ES	NES	NOM p-val	FDR q-val	FWER p-val
ELECTRON_TRANSPORT_CHAIN	91	0.438	1.64472	0	1	0.548
HSA00020_CITRATE_CYCLE	24	0.573	1.62466	0	1	0.592
FLECHNER_KIDNEY_TRANSPLANT_WELL_PBL_DN	38	0.453	1.60248	0	1	0.795
GLYCOGEN_METABOLISM	32	0.427	1.57331	0	1	0.795
P53GENES_ALL	15	0.631	1.56594	0	1	0.795
MITOCHONDRIAL_FATTY_ACID_BETAOXIDATION	15	0.682	1.5561	0	1	0.795
GAMMA_ESR_WS_UNREG	25	0.601	1.54163	0	1	0.795
HDACI_COLON_SUL24HRS_DN	106	0.445	1.53118	0	1	0.795
TNFALPHA_30MIN_UP	39	0.438	1.5293	0	1	0.846
PTDINSPATHWAY	21	0.353	1.52894	0	0.929417	0.846
MMS_HUMAN_LYMPH_HIGH_24HRS_UP	18	0.637	1.52864	0	0.848925	0.846
NADLER_OBESITY_DN	35	0.512	1.52189	0	0.814216	0.846
ADIP_VS_FIBRO_UP	33	0.394	1.51873	0	0.794207	0.846
MTORPATHWAY	23	0.416	1.51345	0	0.776668	0.904
CITRATE_CYCLE_TCA_CYCLE	17	0.615	1.50404	0	0.772756	0.904
HSA00071_FATTY_ACID_METABOLISM	40	0.503	1.50038	0	0.758804	0.904
VEGFPATHWAY	25	0.428	1.49734	0	0.745856	0.904
LEE_TCELLS3_UP	82	0.605	1.49232	0	0.747395	0.904
PRMT5_KD_DN	23	0.647	1.48966	0	0.745433	0.962

Supplemental Table 6. Ranked list of top 20 enriched gene set pathways for P5 LGN.

Top 20 Enriched Gene Sets for P5 MGN

NAME	SIZE	ES	NES	NOM p-val	FDR q-val	FWER p-val
WNTPATHWAY	25	-0.601527	-1.545217	0	1	0.788
HSA05040_HUNTINGTONS_DISEASE	26	-0.638401	-1.505897	0	1	0.942
HIPPOCAMPUS_DEVELOPMENT_POSTNATAL	43	-0.48833	-1.504516	0	1	0.942
ALZHEIMERS_INCIPIENT_DN	131	-0.343693	-1.498745	0	0.869916	0.942
AGUIRRE_PANCREAS_CHR6	28	-0.387935	-1.476847	0	0.874879	0.942
POMEROY_DESMOPLASIC_VS_CLASSIC_MD_DN	37	-0.414736	-1.47151	0	0.776732	0.942
NFATPATHWAY	50	-0.386005	-1.468295	0	0.698806	0.942
HPV31_DN	40	-0.479486	-1.466462	0	0.630065	0.942
HOX_GENES	50	-0.546701	-1.45455	0	0.668062	0.942
HSA04740_OLFACTORY_TRANSDUCTION	25	-0.577244	-1.445114	0	0.648444	0.942
LEE_ACOX1_DN	58	-0.443804	-1.430049	0	0.735662	1
HSA00600_SPHINGOLIPID_METABOLISM	31	-0.426271	-1.421491	0	0.728617	1
UVC_XPCS_8HR_UP	54	-0.464254	-1.416488	0	0.707508	1
SMOOTH_MUSCLE_CONTRACTION	139	0.381882	-1.416345	0	0.662184	1
UVC_XPCS_ALL_UP	56	-0.455418	-1.410368	0	0.64961	1
HSA04310_WNT_SIGNALING_PATHWAY	137	-0.319562	-1.403979	0	0.650524	1
HSA03050_PROTEASOME	22	-0.422831	-1.388926	0.179688	0.721593	1
CCR3PATHWAY	21	-0.511738	-1.370046	0.102204	0.816168	1
REGULATION_ACTIN_CYTOSKELETON_RHO_GTPASES	34	-0.339351	-1.361423	0.088235	0.829013	1

Supplemental Table 7. Ranked list of top 20 enriched gene set pathways for P5 MGN.

Top 20 Enriched Gene Sets for P5 rwMGN

NAME	SIZE	ES	NES	NOM p-val	FDR q-val	FWER p-val
PENG_Glutamine_DN	234	-0.348	-1.89017	0	0.078602	0.038
PENG_Rapamycin_DN	174	-0.3986	-1.80589	0	0.118384	0.127
Cell_Cycle_Checkpoint	24	-0.5459	-1.80372	0	0.105124	0.127
Ubiquitin_Mediated_Proteolysis	23	-0.5257	-1.79752	0	0.087843	0.127
Chauhan_2ME2	45	-0.5007	-1.79333	0	0.077474	0.127
TARTE_Plasma_Blastic	277	-0.3999	-1.76983	0	0.09605	0.181
Idx_TSA_Up_Clusters5	90	-0.4158	-1.7558	0	0.097836	0.232
TNFR1Pathway	27	-0.4988	-1.7489	0	0.104989	0.232
HSC_IntermediateProgenitors_Adult	119	-0.4347	-1.73001	0	0.12862	0.383
PENG_Leucine_DN	132	-0.3471	-1.71881	0	0.150467	0.48
Flechner_Kidney_Transplant_Well_PBL_Up	132	-0.3504	-1.70401	0	0.186593	0.521
Idx_TSA_DN_Cluster2	61	-0.5142	-1.69278	0	0.202667	0.521
HSC_IntermediateProgenitors_Shared	110	-0.431	-1.67929	0	0.201708	0.521
PRMT5_KD_Up	169	-0.4402	-1.67701	0	0.192915	0.521
Small_Ligand_GPCRS	16	-0.6811	-1.67404	0	0.187552	0.521
HSA00650_Butanoate_Metabolism	42	-0.5113	-1.67164	0	0.196124	0.57
Basso_Regulatory_Hubs	122	-0.3755	-1.67059	0	0.186705	0.57
Lizuka_L0_SM_L1	16	-0.6014	-1.66747	0	0.178332	0.57
ET743_Sarcoma_Up	60	-0.5624	-1.66682	0	0.170841	0.57

Supplemental Table 8. Ranked list of top 20 enriched gene set pathways for P5 rwMGN.

Top 20 Downregulated Gene Sets for P5 rwMGN

NAME	SIZE	ES	NES	NOM p-val	FDR q-val	FWER p-val
NFKBPATHWAY	23	0.51477	1.525717	0	1	0.91
ASTIER_FN_DIFF	52	0.27873	1.503993	0	1	0.946
ASTIER_BCELL	51	0.26972	1.481648	0	1	0.946
FALT_BCLL_UP	37	0.39972	1.332901	0	1	1
CMV_HCMV_TIMECOURSE_14HRS_DN	34	0.33759	1.320187	0.110883	1	1
HSA04930_TYPE_II_DIABETES_MELLITUS	41	0.38516	1.311868	0.1	1	1
HSA04742_TASTE_TRANSDUCTION	26	0.40352	1.278951	0.104938	1	1
HSA04310_WNT_SIGNALING_PATHWAY	137	0.23798	1.25605	0	1	1
CELLCYCLEPATHWAY	21	0.30326	1.251048	0.10119	1	1
HUMAN_TISSUE_PANCREAS	31	0.41914	1.209177	0.227642	1	1
NOUZOVA_CPG_METHLTD	48	0.26657	1.197118	0	1	1
VERNELL_PRB_CLSTR2	17	0.42241	1.162737	0.17773	1	1
TAKEDA_NUP8_HOXA9_6H_DN	35	0.38585	1.141964	0.336016	1	1
HSA05217_BASAL_CELL_CARCINOMA	54	0.34107	1.136774	0.323108	1	1
CANCERDRUGS_PROBCELL_UP	19	0.3686	1.11091	0.206897	1	1
ST_JNK_MAPK_PATHWAY	38	0.31233	1.095413	0.186235	1	1
UVC_HIGH_ALL_UP	16	0.3942	1.095124	0.40873	1	1
STANELLE_E2F1_UP	25	0.30069	1.094072	0.322	1	1
BADPATHWAY	20	0.35335	1.093088	0.30042	1	1

Supplemental Table 9. Ranked list of top 20 downregulated gene set pathways for P5 rwMGN.

CHAPTER 3

***Zic4* and *Ten_m3* Exert Complementary Effects on Retinotopic Map Formation and Position of the Visual Cortex**

SUMMARY

The proper formation of the retinotopic map in primary visual cortex (V1) is critical to a coherent internal representation of visual space. Visual acuity and survival behaviors rely on the integrity of this map, which is susceptible to both genetic and experience-dependent abnormalities during development. The connection between early patterning genes and the organization of neural circuits in the visual pathway is not well understood. We report a role for two such patterning molecules, the transcriptional regulators, *Zic4* and *Ten_m3*, in shaping the structure of the retinotopic map in the lateral geniculate nucleus (LGN) and V1. *Zic4* and *Ten_m3* are expressed in similar gradients in the retina, visual thalamus and V1, but they produce complementary loss-of-function phenotypes. *Zic4* loss leads to a dorsomedial spread of ipsilateral retinogeniculate fibers, while *Ten_m3* loss leads to a dorsoventral spread. The binocular zone of V1 is decreased in size in *Zic4* null mice while it is increased in size in *Ten_m3* null mice, and both exhibit decreased cortical drive in the binocular zone, evidence for an eye-specific mismatch leading to increased intracortical suppression. Furthermore, the position of V1 is shifted laterally in *Zic4* mutants while it is shifted medially in *Ten_m3* mutants. *Ten_m3/Zic4* double null mice show a partial rescue in the retinothalamic projections of

the ipsilateral eye, while cortical map structure and position is restored to normal, indicating that these two genes exert a bidirectional effect on mechanisms of retinotopic map formation.

INTRODUCTION

In the mammalian brain, information from sensory stimuli is relayed through primary sensory pathways, whose circuits are organized structurally to respond to and process a variety of stimulus features (reviewed in Sur and Rubenstein, 2005). In the visual pathway, the most fundamental of these features is a topographic representation of visual space (reviewed in White and Fitzpatrick, 2007). Locations in space reflect light onto the surface of the retina, which transmits this input to the lateral geniculate nucleus (LGN) of the thalamus, with the dorsal subdivision of the LGN in turn projecting to the primary visual cortex (V1) (reviewed in Sur and Leamey, 2001). In order to perceive the relative position of objects in the outside world, the retinal sheet must maintain the order of its projections to the LGN, which then must preserve this order up to V1 (reviewed in Huberman et al, 2008). Stereoscopic vision, or depth perception, also requires that inputs to the two eyes from the same stimulus in regions of binocular space be aligned (Mitchell et al., 1984).

Sperry's theory that complementary gradients of attractive and repulsive receptor-ligand pairs could parsimoniously instruct the formation of retinotopic maps was confirmed by the discovery of intrinsic gradients of ephrinA-EphA receptor signaling and their necessity for proper organization of the visual pathway (Huberman, 2007; Pfeiffenberger et al, 2006, 2005; Huberman et al, 2005; Cang et al, 2005a, 2008; Brown et al, 2000; Feldheim et al, 1998). Activity-dependent processes of synaptic refinement have also been shown to influence the quality of retinotopic maps (Huberman et al, 2006; Cang et al, 2005b). Nonetheless, additional cues likely contribute to retinotopic

development and the link between early patterning events and map formation is not completely understood.

Novel roles in the organization of retinogeniculate fibers were identified for two transcriptional regulators, *Zic4* and *Ten_m3*, after their discovery in two microarray studies screening for candidates enriched in the visual pathway relative to other sensory regions (Leamey et al, 2007a; Horng et al, in submission, 2009). *Zic4* encodes a zinc-finger transcription factor belonging to a family of patterning genes with diverse roles in early developmental events (Ishigoro et al, 2005; reviewed in Aruga et al, 2004; Grinberg and Millen, 2005; Fig. 1A). *Zic4* and *Zic1* are critical for proper cerebellar development (Grinberg et al, 2004), while loss of *Zic2* can lead to holoprosencephaly and *Zic3* to situs inversus (Warr et al, 2008; Gebbia et al, 2007). *Zic4* is expressed in gradients throughout the forebrain and specifically in regions of the visual pathway. Loss of *Zic4* in mice leads to a mismapping of ipsilateral retinogeniculate fibers along the dorsomedial axis, a phenotype similar to but distinct from that of the *ephrin-A2,3,5* triple null mutant (Huberman et al, 2005; Pfeiffenberger et al, 2005, 2006). In this study, we used in vivo optical imaging of intrinsic signals to characterize the retinotopic structure of V1 in *Zic4* null mice order to examine the effect of *Zic4* loss on the cortical map. We found a decrease in the size of the binocular zone, or ipsilaterally driven region, of V1, although no change in the total size of V1 or map scatter was detected. Strength of the binocularly driven map was decreased in the ipsilaterally driven region, suggesting an eye-specific mismatch and consequent intracortical suppression. Finally, the areal position of V1 was shifted laterally in the *Zic4* null mouse, reminiscent of the dual effects of ephrin-A loss on V1 positioning and intra-areal structure (Cang et al, 2005a).

Ten_m3 codes for a type II homophilic transmembrane receptor present on the surface of developing axons (Levine et al, 1994; Fig. 1B). It belongs to the *Ten_m/Odz* family of pair rule genes implicated in the embryonic segmentation of *Drosophila* (Oohashi et al., 1999, Baumgartner et al., 1994; Levine et al., 1994). Binding of the extracellular domain of *Ten_m1* and *2* leads to cleavage of the intracellular domain, which translocates to the nucleus and acts as a transcriptional cofactor and regulator (Bagutti et al., 2003; Nunes et al., 2005). *Ten_m3* is also expressed in gradients throughout the developing visual pathway and its loss leads to mismapping of ipsilateral retinogeniculate fibers along the dorsoventral axis, a phenotype complementary to that of the *Zic4* mutant (Leamey et al, 2007a,b). *In vitro* experiments have shown that *Ten_m2* and *Zic1* exert mutually repressive effects on common downstream transcriptional targets (Bagutti et al., 2003, Fig. 1C). Sequence homology among the *Ten_m* and *Zic* family members raises the possibility that *Ten_m3* and *Zic4* may interact in a similar way. In order to further examine the *Ten_m3* loss of function phenotype on cortical retinotopic structure and compare it to that of *Zic4*, we performed cortical optical imaging experiments on *Ten_m3* null mice, and found further evidence for complementary mapping deficits between the two genes: an increase in the size of the binocular zone, with no change in total V1 size or map scatter; a similar decrease in magnitude of the binocular zone, and a medial shift of V1. In addition, we found increased segregation of ipsilaterally and contralaterally driven regions in the *Ten_m3* mutant, confirming recent findings on the presence of de-novo ocular dominance domains (Leamey et al., in submission, 2009).

In order to test whether *Ten_m3* and *Zic4* interact functionally, we crossed the two mutants and performed retinogeniculate tracing and cortical optical imaging experiments on the combination mutant. In the retinogeniculate projection, we found a restoration of the dorsomedial spread previously reported for the *Zic4* mutant mice but a persistence of the dorsoventral spread of the *Ten_m3* mutant mice. Ipsilateral terminals were also more clustered and appeared less homogenous than those in the *Ten_m3* null mouse. Cortical measurements however were restored to normal, suggesting a restoration of cortical map structure by opposing interactions of *Zic4* and *Ten_m3*. We propose a model in which *Zic4* and *Ten_m3* exert opposing effects on binocular map formation in the visual pathway.

METHODS

Animals

Zic4 null mice were generated and maintained on a 129/SvIMJ background (Grinberg and Millen, 2004) and were viable and fertile. *Ten_m3* null mice were generated on a C57/Bl6 background and maintained on a 129/SvEv background (Leamey et al, 2007) and were viable and fertile. Double mutants were generated by crossing single mutants and were viable and fertile. All experimental measures on single null mice were conducted along with matched littermate controls of the same background. Wild-type data from *Zic4* and *Ten_m3* backgrounds were then compared using a student t-test and found to be no different in all measures. In addition, *Ten_m3* null mice on their

native background were found to be no different in all measures to *Ten_{m3}* null mice on the crossed background. *Zic4* null mice on the crossed background were not tested. Data from all four groups were then analyzed with one-way ANOVA tests, and when applicable, followed by a Tukey's honestly significant difference (HSD) test. All experiments were approved by MIT's IACUC and performed in compliance with by NIH and NHMRC guidelines.

***In Situ* Hybridization**

500-600 bp digoxigenin (DIG)-labeled antisense and sense riboprobes were synthesized from sample cDNA using a T7 reverse transcriptase in vitro kit with DIG labeled ribonucleotides (Invitrogen). Riboprobes were purified on Micro Bio-spin Columns (Biorad) and quantified by UV spectrophotometry. Brains were flash frozen in isopentane, stored at -80° C and sectioned at a thickness of 18 microns at -20° C on a cryostat. Sections were processed using the *in situ* hybridization protocol of Braissant et al.(1998).

Retinogeniculate CTB Tracings

Retinogeniculate projections were traced using intraocular injections of Alexa fluor 488- and 594-conjugated cholera toxin-B (CTB, Invitrogen Molecular Probes). Wild-type, *Zic4* null, *Tenm3* null, and *Tenm3/Zic4* null mice (P28-48) were injected using

a 5ul Hamilton syringe with 1-2ul of 488-CTB and 594-CTB in each eye. Mice were allowed to recover for 48 hours to complete tracing and sacrificed.

Retinogeniculate tracings were imaged from 50 μm brain sections using a Zeiss Axioskop 2 microscope. LGN images were divided into anterior, middle and posterior groups. For each animal, 3 sections from the anterior group were imaged and analyzed (n=3, each group). Axiovision LE Rel. 4.4 software was used to measure the dorsomedial and ventrolateral length of both the total LGN and ipsilateral projection zone, as well as to count the number of ipsilateral clusters in each section.

Intrinsic Signal Optical Imaging and Analysis

Animals at age P28-P35 from *Zic4* +/+, *Tenm3* +/+, *Zic4* -/-, *Tenm3* -/- and *Tenm3*-/-;*Zic4*-/- groups were anesthetized with 10% urethane (1.5 mg/g i.p.) and 1% chlorprothixene (0.2 mg/animal, i.p.). After exposure of the skull in the area over V1 and placement of the animal in a custom-made stereotactic frame, the region of interest was covered with a 1.5% agarose solution and glass coverslip. The cortical surface was illuminated with a tungsten halogen light source and imaged with a custom built system with a CCD camera (Cascade 512B, Roper Scientific). Green light (550 nm) was used to obtain a reference image of the cortical vasculature at the surface, while red light (630) was used to acquire intrinsic hemodynamic signals after focusing 300-500 μm below the cortical surface. In a 62 x 72° region of visual space, a drifting horizontal or vertical white bar (9 s/cycle) over a uniformly gray background was presented to both eyes, as well as to the contralateral and ipsilateral eye alone (stimulus to the other eye was

blocked with a masking cover) (Rao et al, 1997 Bonhoeffer and Grinvald, 1991). Images of V1 were captured at 15 frames/s for a stimulus session of 25 min.

A temporal high pass filter (135 frames) was used to remove slow noise components. A temporal Fast Fourier Transform (FFT) component at the stimulus frequency (9 s^{-1}) was calculated pixel by pixel from the set of images (Kalatsky and Stryker, 2003). To calculate the magnitude of response, the amplitude of the FFT component normalized to that of background in the absence of visual stimuli was measured and the average of the top 2000 pixels in the map was obtained. Retinotopic maps were generated from the phase of the FFT of the response time series at the stimulus frequency. To measure the size of cortical area of stimulation, the magnitude map was filtered by thresholding at a level of 40% of the peak response and number of pixels measured within a defined area of interest. To measure map quality, scatter values were obtained calculating the average difference in phase value between each pixel in the retinotopic maps and its surrounding 25 pixels (Cang et al, 2005a,b,c, Smith and Trachtenberg, 2007). Ocular dominance values were calculated using the ocular dominance index (ODI), which takes the difference in magnitude of the contralateral and ipsilateral stimulated maps divided by the sum of the magnitudes; a value of -1 represents predominant ipsilateral drive while a value of +1 represents predominant contralateral drive. Position of V1 was measured by aligning the retinotopic phase map within the imaged region of interest with an image of the surface cortical vasculature.

RESULTS

***Zic4* is expressed in gradients of the developing visual pathway**

In accordance with Sperry's chemoaffinity hypothesis (Sperry, 1963), a receptor-ligand system, the EphA receptors and ephrin-A ligands, is expressed in gradients of the retina, LGN and visual cortex and contributes to topographic mapping of the visual pathway (Feldheim et al, 1998; Huberman et al, 2005, Cang et al, 2005a; Pfeiffenberger et al, 2005, 2006). Using *in situ* hybridization, we tested whether *Zic4*, a transcription factor whose loss leads to deficits in retinogeniculate mapping distinct from that of the ephrin-As (Horng et al, in submission, 2009; Huberman et al, 2005), is also expressed in gradients of the developing visual pathway (Fig. 2A). In the neonatal retina, *Zic4* is enriched in the temporal region of the ganglion cell layer, which provides the ipsilateral retinal projections to the dLGN (Herrera et al, 2003; Pak et al, 2004) and is consistent with its role in mapping of ipsilateral retinogeniculate terminals (Horng et al, in submission, 2009; Fig 2B). We found that *Zic4* was indeed expressed in gradients throughout the embryonic and postnatal LGN (from E15.5 to P16) that were high in the dorsolateral region and low in the ventromedial region of the dorsal LGN (LGd) (Fig. 2C-E). Interestingly, expression declined after P16, a time by which the strength and retinotopic organization of the V1 map has reached its adult form (Fig. 2F, Smith and Trachtenberg, 2006). In the developing cortex at E18.5, *Zic4* is expressed in the posterior cortex (Fig. 2H-J), but not in the anterior cortex (Fig. 2K,L). Within the posterior cortex, *Zic4* expression is low medially (Fig. 2H) and high laterally within the ventricular zone and layer V (Fig 2 I, J), exhibiting a high lateral to low medial gradient in V1 (Fig. 2H, black arrows).

Ten_m3, a homophilic binding receptor with an intracellular transcriptional modulator domain whose loss of function produces a unique retinogeniculate mapping defect complementary to that of *Zic4*, is expressed in gradients of the visual pathway that are similar to those of *Zic4*. Described previously (Leamey, 2007a,b), expression is enriched in the ventral retina, high in the dorsomedial LGd and posterior-lateral cortex.

***Zic4* and *Ten_m3* exert complementary effects on the organization of ipsilateral retinogeniculate projections**

Using intraocular injections of fluorophore tagged cholera toxin-B, we confirmed the complementary effects of *Zic4* and *Ten_m3* loss on the targeting of ipsilateral retinogeniculate projections, and tested whether combination mutants would show an additive or compensated phenotype. As previously described, *Zic4* loss was found to produce an expansion and trend of increase in clustering of ipsilateral retinogeniculate terminals along the dorsomedial axis of the LGd, while *Ten_m3* loss produced a dorsoventral expansion (Fig. 3A,B). Loss of both *Zic4* and *Ten_m3* led to a full rescue of the dorsomedial expansion seen in *Zic4* mutants, as measured by the ratio of the axial length of the ipsilateral projection to the length of the total LGd ($72.07 \pm 0.047\%$ *Zic4* KO vs. $50.67 \pm 0.043\%$ WT, $F_{3,35}=5.34$, $p<0.05$, one-way ANOVA, Tukey's HSD test, $n=3$ each group; $52.95 \pm 0.038\%$ DKO: nonsignificant vs. WT and $43.5 \pm 0.025\%$ *Ten_m3* KO: nonsignificant vs. WT; Fig. 3A green line) and a persistence (with a nonsignificant trend of partial rescue) in the dorsoventral expansion seen in *Ten_m3* mutants ($83.46 \pm 0.023\%$ *Ten_m3* KO vs. $40.51 \pm 0.014\%$ WT, $F_{3,32}=51.6$, $p<0.01$; 74.61

± 0.033 % DKO vs. WT, $p < 0.01$; 43.59 ± 0.013 *Zic4* KO vs. WT: nonsignificant; $n=3$ each group, Fig 3A, B, yellow line). An increase in clustering of the ipsilateral terminals was present in the *Ten_m3/Zic4* combination mutant (mean no. of clusters=2.2 vs. 1.2, DKO vs. WT, $p < 0.01$; 1.6 *Zic4* KO: nonsignificant vs. WT; 1.4 *Ten_m3* KO: nonsignificant vs. WT; $n=3$ each group, Fig. 3C), suggesting that loss of *Ten_m3* and *Zic4* together produces a qualitative combination of deficits that is less quantitatively severe than those produced by either mutation alone.

Binocular zone size is altered in opposite directions in *Zic4* and *Ten_m3* null mutants, while total V1 size remains intact

Given their role on axis-specific mapping of ipsilateral retinogeniculate projections and their additional expression in V1, we next tested whether *Zic4* and *Ten_m3* loss altered the structure of cortical retinotopic maps using optical imaging of intrinsic hemodynamic signals in response to a bar drifting in both elevation and azimuth axes. In both *Zic4* and *Ten_m3* mutants, the total size of V1 was unchanged from that of age-matched littermate controls (4976 ± 260 vs. 4834 ± 192 pixels, *Zic4* KO vs WT, $p=0.691$, t-test, $n=10$ KO, $n=7$ WT; 3850 ± 292 vs. 3975 ± 263 pixels, *Ten_m3* KO vs WT, $p=0.754$, $n=8$ KO, $n=8$ WT; 1 pixel= $18 \mu\text{m} \times 18 \mu\text{m}$). However, the size of the ipsilaterally stimulated region, which corresponds to the binocular zone of V1, was altered in opposite directions in the *Zic4* and *Ten_m3* mutants. In *Zic4* null mice, the binocular zone, as measured as a fraction of the total V1 size, was decreased (0.53 ± 0.03 vs. 0.65 ± 0.02 , *Zic4* KO vs. WT, $F_{3,43}=15.59$, $p < 0.05$, one-way ANOVA, Tukey's HSD

test, n=10 *Zic4* KO, n=15 WT, Fig. 4A,B), while it was increased in *Ten_m3* null mice (0.84 ± 0.05 : *Ten_m3* KO, $p < 0.01$, n=8 KO, n=15 WT, Fig. 4A,B). In the *Ten_m3* mutant, the expansion of the binocular zone was characterized by strip-like regions invading the more medial regions of V1 (Fig 4A, arrow in *Ten_m3* KO panel; see also below). There was no difference in the size of the contralaterally stimulated region between either mutant line and matched wild-type controls (data not shown).

In order to test whether loss of *Zic4* and *Ten_m3* would restore respective changes in the binocular zone size, measurements were made in *Ten_m3/Zic4* combination mutants. In the double knock-out, binocular zone size was restored to normal (0.70 ± 0.04 : *Ten_m3/Zic4* DKO, nonsignificant vs. WT, n=7 KO, n=15 WT, Fig. 4A, B).

Retinotopic organization and total cortical drive is unchanged in *Zic4* and *Ten_m3* null mutants, while binocular drive is selectively weaker in the binocular zone of *Zic4* and *Ten_m3* null mutants

The quality of retinotopic maps acquired through intrinsic signal optical imaging in V1 is typically assessed using phase scatter measurements to quantify the topographic precision of retinotopy, as well as the amplitude of signal to represent the strength of cortical drive (Kalatsky and Stryker, 2005; Cang et al, 2005c; Smith and Trachtenberg, 2006). In order to measure retinotopic precision in *Zic4* and *Ten_m3* mutants, we analyzed phase scatter, a measurement of average difference in phase value for each pixel and its surrounding 25 pixels, in binocularly, contralaterally and ipsilaterally driven maps. Scatter values in all maps for both mutants were no different from age matched

littermate controls (data not shown), suggesting that the general precision of retinotopic organization was either largely unchanged or undetectable by this technique despite alterations in thalamocortical mapping of ipsilateral inputs.

Measurements of signal amplitude were also made for the total area of binocularly, contralaterally and ipsilaterally driven maps in order to quantify the total strength of cortical drive. For both *Zic4* and *Ten_m3* mutant mice, magnitudes of signal for binocular, contralateral and ipsilateral maps were no different from those of controls (data not shown). However, within the binocular zone of azimuth maps, the magnitude of the binocularly driven map was decreased in both the *Zic4* null ($11.89 \pm 1.36\%$ vs. $28 \pm 3.6\%$, *Zic4* KO vs WT, $p < 0.05$, $F_{3,23} = 11.15$, one-way ANOVA, Tukey's HSD test, $n = 7$ *Zic4* KO, $n = 10$ WT, Fig. 5A,B), and *Ten_m3* null mouse ($6.2 \pm 2.2\%$, *Ten_m3* KO, $p < 0.01$, $n = 3$ *Ten_m3* KO, Fig. 5A,B), indicating that binocular cortical drive is suppressed in regions receiving both contralateral and ipsilateral input. This finding is consistent with the retinotopic mismatch between contralateral and ipsilateral projections (compare the azimuth map within the ipsilateral and contralateral projection zones in *Zic4* and *Ten_m3* mutant mice, Fig. 5A), and the induction of intracortical suppression previously reported as arising from an interocular mismatch (Sengpiel, 2006, 1995; Sengpiel and Vorobyov 2005; Wong et al, 2005, Tyschen et al, 2004; White et al, 2001). In elevation maps, this suppression was present in the *Ten_m3* null mouse ($23.25 \pm 6.76\%$ vs. $43.6 \pm 5.34\%$, *Ten_m3* KO vs. WT, $p < 0.01$, $F_{3,23} = 2.28$, one-way ANOVA, Tukey's HSD test, $n = 4$ *Ten_m3* KO, $n = 10$ WT, Fig. 6A,B), and was not statistically significant in the *Zic4* null mouse ($33.4 \pm 6.07\%$, *Zic4* KO, nonsignificant, $n = 5$ *Zic4* KO,

Fig. 6A,B), indicating that eye-specific mismatch is more severe along the azimuth dimension for the *Zic4* null mouse.

In the *Ten_m3/Zic4* double null mouse, this cortical suppression was not statistically significant in either the azimuth or elevation maps, reflecting normal levels of binocular drive in the binocular zone of V1 (azimuth: $32.4 \pm 5.00\%$, *Ten_m3/Zic4* DKO, nonsignificant, n=5 DKO; elevation: $32 \pm 1.64\%$, *Ten_m3/Zic4* DKO, nonsignificant, n=5 KO, Fig. 5A,B; Fig. 6A,B). These results suggest that combining *Ten_m3* and *Zic4* loss alleviates the eye-specific mismatch caused by each mutation alone.

***Ten_m3* null mutants exhibit increased segregation of eye specific domains in V1**

The organization of eye-specific input is shaped by activity-dependent processes and can be drastically reorganized with novel patterns of input (Constantine Patton and Law, 1978; Sur et al, 1998; Gordon and Stryker, 1996; Cang et al, 2005b, Pfeiffenberger et al, 2005, 2006; Hooks and Chen, 2006). In order to test whether the balance of ipsilateral and contralateral representation in V1 was altered in *Zic4* and *Ten_m3* null mice, given a mismatch in ipsilateral and contralateral inputs, we calculated the ocular dominance index (ODI) in the binocular region of V1. ODI is an averaged measure of relative ipsilateral and contralateral drive, calculated by taking the difference in contralateral and ipsilateral magnitude divided by the sum for each pixel. Values close to -1 indicate strong ipsilateral drive while values close to +1 represent strong contralateral drive. While the *Zic4* null mouse showed no difference in ODI compared to control for both azimuth and elevation maps (azimuth: 0.31 ± 0.026 vs. 0.34 ± 0.043 , *Zic4* KO vs.

WT, nonsignificant, $F_{3, 18}=7.38$, $p<0.05$, one-way ANOVA, Tukey's HSD test, $n=4$ *Zic4* KO, $n=8$ WT; elevation: 0.11 ± 0.057 vs. 0.16 ± 0.056 , *Zic4* KO vs WT, nonsignificant, $n=5$ *Zic4* KO, $n=10$ WT Fig 7A, B), the *Ten_m3* null mouse exhibited a marked ipsilateral shift in ODI within the binocular zone of its azimuth maps and a (not statistically significant) trend of ipsilateral shift in the elevation maps (azimuth: 0.048 ± 0.035 , *Ten_m3* KO, $p<0.01$, $n=3$ *Ten_m3* KO; elevation: 0.049 ± 0.08 , *Ten_m3* KO, nonsignificant, $n=4$ *Ten_m3* KO, Fig 7A, B). The medial expansion of these ipsilaterally dominated regions intertwined with more contralaterally driven regions resembles the ocular dominance columns present in higher carnivores, such as ferrets and primates (reviewed in Sur and Leamey, 2001; White and Fitzpatrick, 2005; Fig. 7A, white arrows). Such medially expanded ipsilaterally dominated regions interdigitated with contralaterally dominated regions are seen in every *Ten_m3* null animal (see, for example, ipsilateral regions marked by arrow in Figs. 4A, 5A and 6A). The presence of these domains in the *Ten_m3* mutant but not *Zic4* mutant suggests that eye-specific mismatch may contribute to but not be sufficient for the creation of these domains, and that the medial expansion of inputs may be necessary for effective segregation of cortical inputs.

In the *Ten_m3/Zic4* combination mutant, the ipsilateral shift in ODI was not present (azimuth: 0.17 ± 0.08 , *Ten_m3/Zic4* DKO, nonsignificant, $n=4$ DKO; elevation: 0.26 ± 0.02 , *Ten_m3/Zic4* DKO, nonsignificant, $n=5$ DKO, Fig 7A, B), supporting our previous findings that the loss of both genes reduces the severity in mapping deficits of either mutation alone.

***Zic4* and *Ten_m3* exert complementary effects on the position of V1 on the medial-lateral axis of the cortex**

The EphA-ephrinA system has shown to influence intracortical mapping as well as the positioning of V1 on the medial-lateral axis of the cortical sheet (Cang et al, 2005a, 2008). In order to test whether *Zic4* and *Ten_m3* affect the position of V1 on the cortical surface, we measured the distance of the binocularly stimulated map of V1 from the midline suture (Fig. 8A-D), as a ratio of that distance over the distance from the midline to the lateral edge of the cortex (as a control for brain size). We found that *Zic4* mutants exhibited a lateral shift in V1 compared to age-matched littermate controls (0.68 ± 0.01 vs. 0.62 ± 0.01 , *Zic4* KO vs WT, $p < 0.01$, $F_{3, 46} = 17.08$, $p < 0.05$, one-way ANOVA, Tukey's HSD test, $n = 11$ *Zic4* KO, $n = 18$ WT, Fig. 8E), *Ten_m3* mutants exhibited a medial shift (0.57 ± 0.01 , *Ten_m3* KO vs WT, $p < 0.05$, $n = 10$ *Ten_m3* KO, Fig. 8C), and *Ten_m3/Zic4* combination mutants showed no difference in position (0.60 ± 0.01 , *Ten_m3/Zic4* DKO vs. WT: nonsignificant, $n = 8$ KO, Fig. 8D). Distance from the lambda suture, or interaural suture, was no different from controls for any of the groups, specifying the medial-lateral axis as that on which these two genes influence position.

DISCUSSION

During development, regional patterns of gene expression set the blueprint for the functional differentiation of brain areas (Rakic, 1998; O'Leary, 1989; Job and Tan, 2003). Throughout the forebrain, localized gradients of signaling molecules determine

both the gross positioning of these regions and the internal structure of their circuits (Shimogori et al, 2004; Sur and Rubenstein, 2005). In the visual pathway, the EphA receptors and ephrin-A ligands are expressed in complementary gradients on projecting axons and cell bodies, respectively (Feldheim, 1998). Pairing of receptor and ligand induces a range of attractive and repulsive effects depending on the levels of signaling within the gradient (Hansen et al, 2004). In this way, the relative order of projections representing a retinotopic array of information is preserved.

The connection between early developmental patterning and later effectors of circuit formation is an active area of investigation. In this study, we examined the role of two early patterning genes, *Zic4* and *Ten_m3*, in the establishment of retinotopic maps of the LGd and V1. Previously reports established deficits in ipsilateral retinogeniculate patterning along different axes in *Zic4* and *Ten_m3* null mice (Horng et al, in submission, 2009; Leamey et al., 2007b), and these alterations were distinct from those observed in *ephrin-A2/3/5* triple knock out mice (Huberman et al, 2005; Pfeiffenberger et al., 2005), suggesting a unique mechanism of action in retinotopic mapping. We characterized the structure of cortical retinotopic maps in *Zic4* and *Ten_m3* null mice and found complementary effects on the representation of ipsilateral inputs, as well as the position of V1. Furthermore, combining the mutations led to a rescue of the cortical phenotypes seen with each mutation alone, suggesting that *Zic4* and *Ten_m3* modulate a common effector mechanism of retinotopic map formation.

***Zic4* and *Ten_m3* expression gradients and mapping of the ipsilateral visual pathway**

Zic4 and *Ten_m3* exhibit similar patterns of gene expression in the retina, LGd and V1. As transcriptional regulators, we hypothesized that they might modulate early events in the topographic organization of the visual pathway. Their enrichment in the ventrotemporal retina, like *Zic2*, which positively regulates *EphB1* receptors and is necessary for repulsion of ipsilateral retinogeniculate fibers from the optic chiasm (Pak et al, 2004; Lee et al, 2008; Garcia-Frigola et al, 2008), suggested an important role in the ipsilateral retinogeniculate projection. Data showing alterations in ipsilateral retinogeniculate projections along the dorsomedial and dorsoventral axes of the LGd for *Zic4* and *Ten_m3* null mice, respectively, identified a unique and novel role for these two genes and confirmed a strong effect on the ipsilateral retina. Contralateral retinogeniculate projections, which originate from the dorsal and nasotemporal quadrants of the retina, appeared grossly normal, although focal tracings are necessary to characterize precisely their topographic organization.

In the LGd, *Zic4* and *Ten_m3* are expressed in a high dorsolateral to low ventromedial gradient. This pattern is subtly distinct from that of the EphA receptors, most prominently *EphA7* and *EphA4*, which show a high dorsomedial to low ventrolateral gradient (Suppl. Fig. 1). *Ten_m3* appears to be more strongly expressed and extend more medially than *Zic4* (Suppl. Fig. 1). Expression of *Zic4* and *Ten_m3* in the thalamus predicts a role in modulating both ipsilateral and contralateral inputs to the cortex, and the positioning changes we observe in the two mutants likely reflect mapping deficits on the complete array of thalamocortical axons (Fig. 10).

Finally, the high lateral to low medial cortical gradient of *Zic4* and *Ten_m3* may mediate processes of corticothalamic mapping not explored in this study, although we cannot rule out a possible contribution to thalamocortical mapping, as well. In sum, we correlate the strong expression of *Zic4* and *Ten_m3* in the ipsilateral retinogeniculate pathway with a predominantly ipsilateral loss-of-function phenotype. The ipsilateral mapping errors to the thalamus are likely then perpetuated to the cortex, where we observe deficits in the ipsilateral representation and signs of an eye-specific mismatch (Fig. 10). The thalamic expression of *Zic4* and *Ten_m3* encompasses both ipsilateral and contralateral zones and probably contributes to the cortical targeting of both inputs. While we report mapping deficits predominantly in the ipsilateral thalamocortical projection, finer scale experiments involving focal anatomical tracing, single unit recording or two-photon calcium imaging may be necessary to more closely characterize changes in retinotopic mapping for both the ipsilateral and contralateral inputs.

Role of *Zic4* and *Ten_m3* in shaping the structure of visual cortical maps

In the *ephrin-A* triple null mice, large scale deficits in cortical drive and map scatter were reported (Cang et al, 2005a, 2008), confirming the major role of ephrin-A-EphA signaling in retinotopic organization of V1. In our study, we observe novel and unique cortical mapping deficits in *Zic4* and *Ten_m3* null mice. While total cortical drive and map scatter were unchanged in both mutants, potentially reflecting the insensitivity of our assay to detect subtle changes in retinotopic organization, alterations in the size of

the ipsilaterally driven region of V1 and indications of eye-specific mismatch were found.

In *Zic4* mutants, a decrease in the size of the ipsilaterally driven region may be a result of the dorsomedial expansion of the ipsilateral retinogeniculate projection (Fig. 10B). Along this axis, ipsilateral retinogeniculate inputs innervate regions normally receiving contralateral inputs representing the binocular region of space. In the cortex, these contralateral inputs map along with their corresponding ipsilateral representations in the binocular zone (Fig. 9A). Any topographic mismatch between the novel ipsilaterally driven thalamocortical inputs from these regions and the normal ipsilateral inputs might lead to cortical suppression and an apparent decrease in the size of the binocular zone (Fig. 9B). In *Ten_m3* mutants, an increase in the size of the ipsilaterally driven region likely originates from the dorsoventral expansion of the ipsilateral retinogeniculate projection (Fig. 9C). Along this axis, the ipsilateral retinogeniculate inputs innervate regions normally receiving contralateral inputs representing the monocular region of visual space. In the cortex, ipsilateral stimulation then activates both the normal binocular zone and more medial regions of V1 that are typically devoted to the contralateral eye (Fig. 9C). In the combination *Ten_m3/Zic4* mutant, a less severe, but combined retinogeniculate phenotype weakens the respective changes seen in the single mutants and restores the size of the ipsilaterally driven region (Fig. 9D).

In the *Zic4* and *Ten_m3* mutants, binocular cortical drive within the ipsilaterally driven region was reduced. We propose that this suppression is due to mismatches in retinotopic representation between the ipsilateral and contralateral inputs (Sengpiel and Vorobyov, 2005). This effect was seen more strongly in the azimuth maps, suggesting

that downstream mechanisms of retinotopic mapping more strongly regulate this axis. Axis-specific defects in scatter along the azimuth dimension of mice lacking the *ephrin-As* and retinal waves support the existence of additional and distinct mapping cues involved in organizing the elevation dimension (Cang et al, 2008). In the combination *Ten_m3/Zic4* mutant, binocular cortical drive suppression was relieved indicating that eye-specific mismatch was improved. The decrease in severity of mismapping of the ipsilateral retinogeniculate projections in the combination mutant may underlie this rescue. Additional compensation in thalamocortical projections or activity dependent refinements of eye-specific mapping may also contribute to the restoration in the double null mouse.

The identification of increased eye-specific segregation in the *Ten_m3* null mouse confirms the surprising finding of anatomical experiments demonstrating novel ocular dominance domains in V1 of this mutant (Merlin and Leamey, personal communication). We posit that the decorrelated and expanded patterns of ipsilateral input into the medial V1 leads to Hebbian mechanisms of eye-specific segregation and the de novo creation of ocular dominance regions. Experiments in which an ectopic third eye is induced to innervate the superior colliculus and create additional ocular dominance stripes demonstrate that the structure of neural circuits may change to accommodate novel input (Constantine-Patton and Law, 1978). Similarly, the reorganization of intracortical inhibitory networks in response to abnormal cross-modal patterns of activity further illustrates the plasticity of cortical network structure (Sur et al., 1988). Interestingly, increased eye-specific segregation was not seen in the *Zic4* null mouse which also exhibited an eye-specific mismatch, suggesting that the size of the area of mismatch is

necessary for inducing the creation of ocular dominance columns. The presence of ocular dominance segregation was not reported in the *ephrin-A* triple null mice, and it would be fruitful to examine the extent of eye-specific mismatch in these mice and whether it drives the formation of ocular dominance stripes.

Interaction of *Zic4* and *Ten_m3* and a Rescue of Ipsilateral Map Structure, Eye Specific Matching, and Positional Shifts

In this study, we found that changes in the structure and position of V1 caused by *Zic4* and *Ten_m3* loss were rescued by the combined loss of both genes, suggesting that they modulate a common downstream pathway in opposite directions. *In vitro* work on related *Zic* and *Ten_m* family members demonstrate that their transcriptional effects are mutually repressed by one another, making such a bidirectional modulation plausible. The high dorsolateral to low ventromedial gradients of *Zic4* and *Ten_m3* resemble the high dorsomedial to low ventrolateral gradient of *EphA* receptor expression in the LGd (Suppl. Fig. 1). Because *Ten_m3/Zic4* combination mutants show a compensated phenotype, the *EphA* receptors may be a common downstream target. With preliminary *in situ* hybridization and ephrinA5-AP probing experiments (Suppl. Fig 2), we were unable to detect changes in *EphA7* or total EphA receptor expression in our mutant lines, although others have found evidence for decreased EphA receptor expression in *Ten_m3* null mice (Glendining and Leamey, personal communication). Correlative techniques, such as qRT-PCR or microarray analysis, and direct biochemical tests for transcriptional modulators and their target DNA sequences, such as the chip-ChIP assay, will be useful

in providing evidence for modulation of EphA receptor expression by *Zic4* or *Ten_m3*. In addition, it would be informative to compare the visual pathway phenotype of *Zic4* and *Ten_m3* to that of the *EphA7* null mouse, whose deficits in somatosensory and retinocollicular, though not eye-specific, mapping have previously been studied (Miller et al., 2006; Rashid et al., 2005).

Alternatively or additionally, effects on retinotopic mapping could be mediated by separate effectors that have antagonistic interactions. Also, direct actions of *Zic4* and *Ten_m3* protein are possible. It is conceivable that *Zic4*, like another transcription factor, *En-2*, in the superior colliculus (Brunet et al., 2005), acts as a secreted axon guidance cue or promotes the release of a secreted cue for retinal axons. A repulsive action of this cue on axons could explain the dorsomedial expansion of ipsilateral retinogeniculate projections and the lateral positional shift of the thalamocortical drive to V1 after *Zic4* deletion. Chemoattractant effects of homophilic *Ten_m3* binding could potentially explain the dorsoventral expansion of ipsilateral retinogeniculate fibers after *Ten_m3* loss as well as the medial positional shift of V1. Further experiments investigating the cellular actions of *Zic4* and *Ten_m3* will distinguish between a direct or regulatory role of these two genes on retinotopic mapping. In addition, it is an open question whether the effects of *Zic4* and *Ten_m3* are mediated through their effect on projecting axons, target cell bodies or both. *In vitro* assays testing the interaction between projection cells and targets from normal and mutant animals, as well as *in vivo* experiments using region-specific mutations or *in utero* electroporation, will be useful for addressing this issue.

CONCLUSION

Novel and unique deficits in retinotopic mapping are present in the visual pathway of *Zic4* and *Ten_m3* null mice, identifying a role for these two transcriptional regulators in pathways of topographic organization, specifically the coordination of eye-specific inputs to the LGd and V1. A combination of these two mutations leads to the rescue of their respective mapping deficits, demonstrating for the first time a bidirectional regulation of mapping mechanisms. Linking early patterning genes with later processes of circuit formation will improve our understanding of neurodevelopmental programs of regionalization and functional differentiation. In addition, further elucidating the mechanisms of eye-specific mapping will shed light on how visual processing centers respond structurally and functionally to a mismatch in inputs, as in strabismic amblyopia.

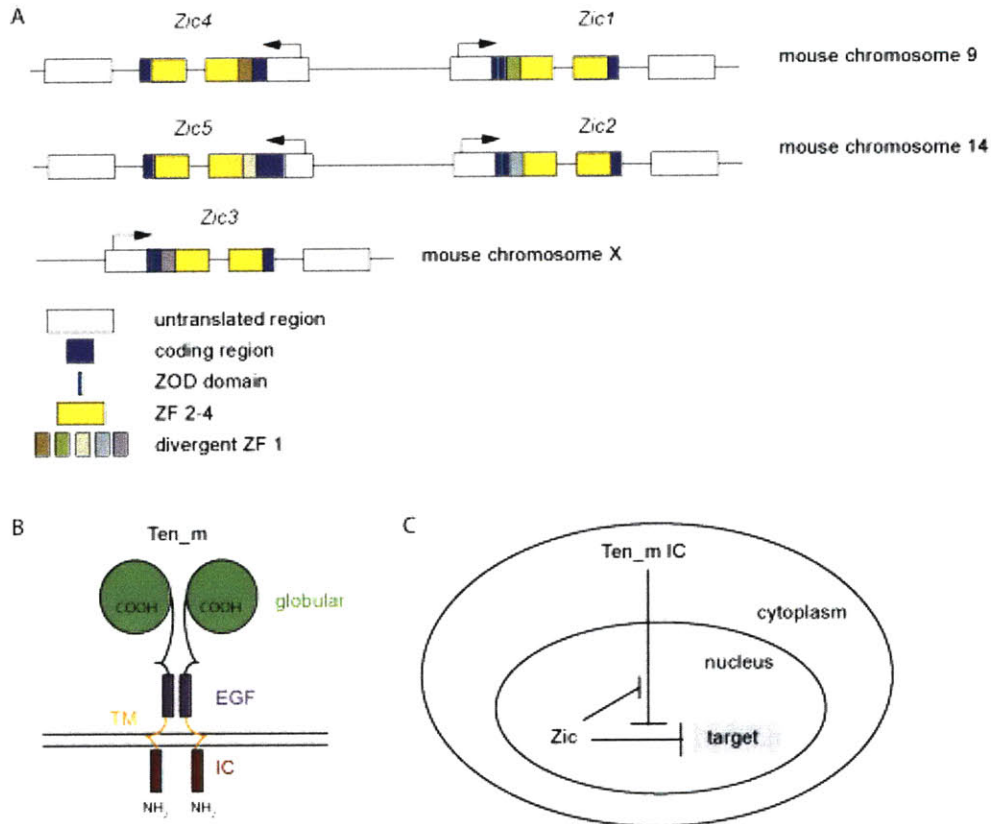


Figure 1. Structure and interaction of *Zic* and *Ten_m* family members. (A) *Zic4* is one of five members of a transcription factor family containing four zinc-finger (ZF) DNA binding domains. ZF-1 is divergent for each family member, likely conferring transcriptional specificity, and *Zic4* does not have the *Zic* and *Drosophila* Odd-paired domain (ZOD) present in *Zic1-3*, suggesting a more recent divergence from the family. Figure adapted from Aruga, 2004. (B) The protein structure of the four mammalian *Ten_m* homologues includes an extracellular globular domain, linker epidermal growth factor (EGF) like repeats, transmembrane (TM) domain, and intracellular (IC) domain. Adapted from Feng et al., 2002. (C) Extracellular binding of *Ten_m* leads to the cleavage of the IC domain, which translocates to the nucleus and modulates gene transcription. In vitro experiments have shown that *Ten_m2* and *Zic1* exert mutually repressive effects on a common downstream gene transcription pathway (Bagutti et al, 2004).

Figure 2. *In situ* hybridization of *Zic4* shows graded expression patterns in the developing visual pathway. (A) Solid lines on the schema of a lateral view of the brain identify the position of coronal sections through the retina, LGd, and visual cortex along the anterior (a)-posterior (p) axis. Dotted lines indicate the region of coronal section along the dorsal-ventral axis. (B) At P0 in the retina, *Zic4* is expressed in the ganglion cell layer in a high temporal to low nasal gradient, scale bar=300 μ m, N=nasal, T=temporal. (C-F) At E15.5 through P16, *Zic4* expression is present in a high dorsolateral to low ventromedial gradient of the LGd, scale bar=150 μ m, D=dorsal, L=lateral. (G) By P28, *Zic4* expression in the thalamus is downregulated, suggesting a less prominent role in the mature visual pathway. (H-J) In the posterior cortex at P18.5, *Zic4* is expressed in the ventricular zone and layer V in a high lateral to low medial gradient. In H, black arrows bracket the developing V1, which includes a graded region of *Zic4* expression, scale bar=300 μ m, D=dorsal, L=medial.

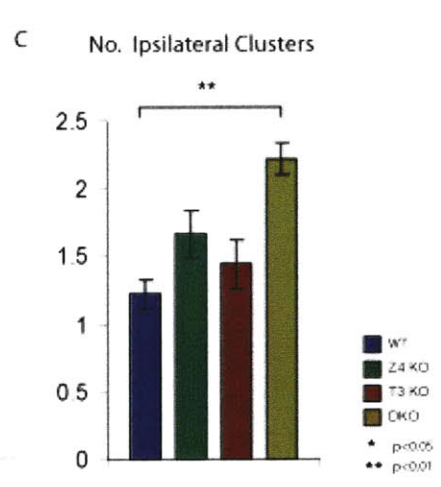
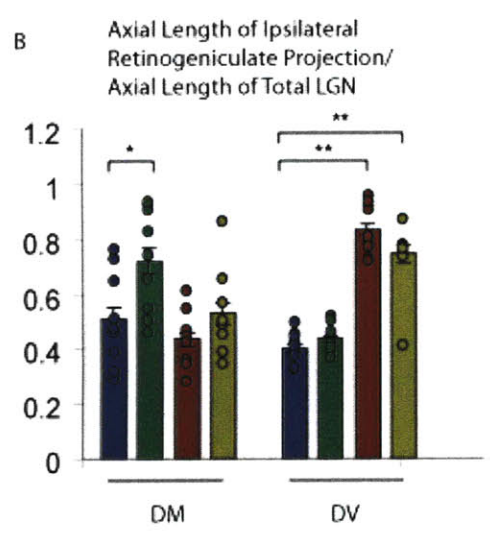
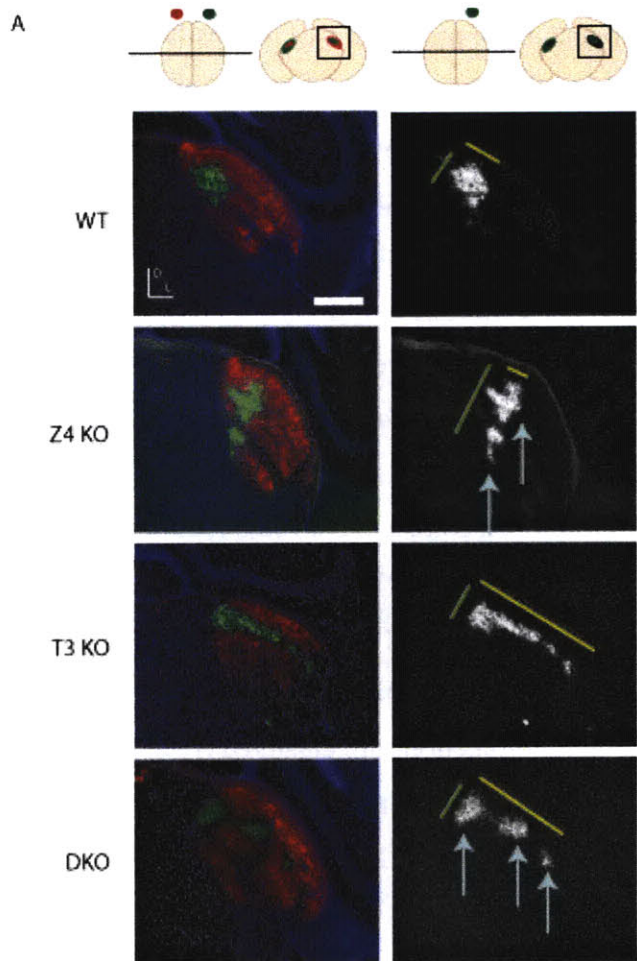


Figure 3. *Zic4* and *Ten_m3* influence retinogeniculate projections of the ipsilateral eye along opposite axes. (A) Inset schema shows a bird's eye view of the brain with red and green tracers injected into the left and right eyes, respectively. The black line shows the coronal plane of section with an adjacent coronal section displaying patterns of contralateral and ipsilateral termination in the dLGN. The left column shows coronal sections through the dLGN of wild-type (WT), *Zic4* knock-out (Z4 KO), *Ten_m3* knock-out (T3 KO) and *Ten_m3/Zic4* double knock-out (DKO) mice. Red (contralateral) and green (ipsilateral) retinogeniculate tracer are shown with blue nuclear DAPI staining. The right column shows the same section with the ipsilateral tracer only in grayscale. In the wild-type, ipsilateral projections are confined to a compact, core-like region in the dorsal center of the dLGN. In the *Zic4* null mouse, they are expanded along the dorsomedial axis (green line) and disorganized into clusters (blue arrows), while in the *Ten_m3* null mouse, they are spread dorsoventrally (yellow line) in one central stripe. In the *Tenm_3/Zic4* combination mutant, ipsilateral projections are clustered (blue arrows in A; B) but display a normal dorsomedial spread (B), and a dorsoventral expansion is still present (yellow line in A, B). Scale bar=300 μ m, D=dorsal, L=lateral. Error bars represent SEM.

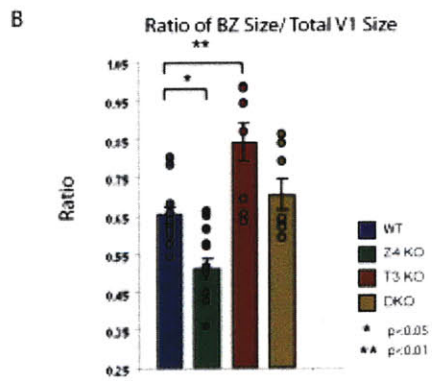
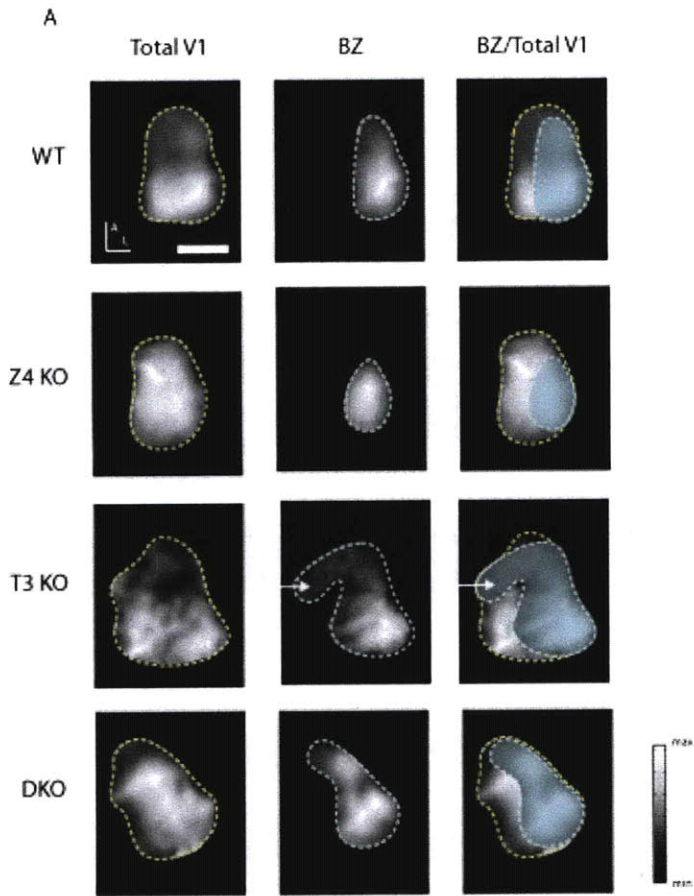


Figure 4. Size of the V1 binocular zone is decreased in *Zic4* and increased in *Ten_m3* mutants and restored in combination mutants. (A) The total area of V1 was no different among the groups, but the binocular zone/total V1 size ratio was smaller in *Zic4* null mice ($p<0.05$), while it was larger in *Ten_m3* null mice ($p<0.01$), and no different in combination mutants (See text for details). Scale bar=500 μm , A=anterior, L=lateral. Grayscale bar shows fractional change in reflection in grayscale. Area displayed is a visual approximation of the response amplitude of the activated region thresholded to a level of 40% of the peak response. Arrow in *Ten_m3* KO panel denotes region that corresponds to expanded ipsilateral zone and an ocular dominance stripe; see also Fig. 7. (B) Histogram displays changes in binocular zone size caused by *Zic4* and *Ten_m3* mutations and the restoration produced by a double mutation. Error bars represent SEM.

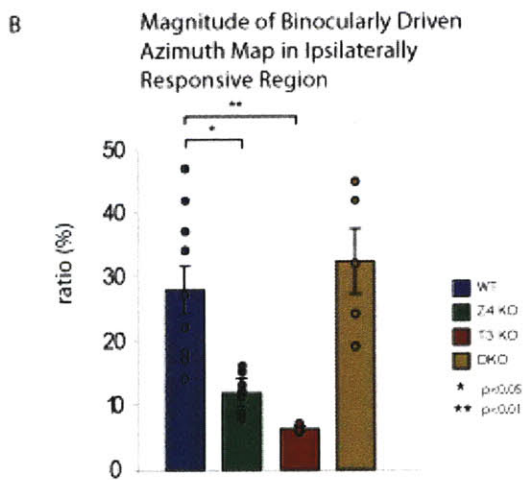
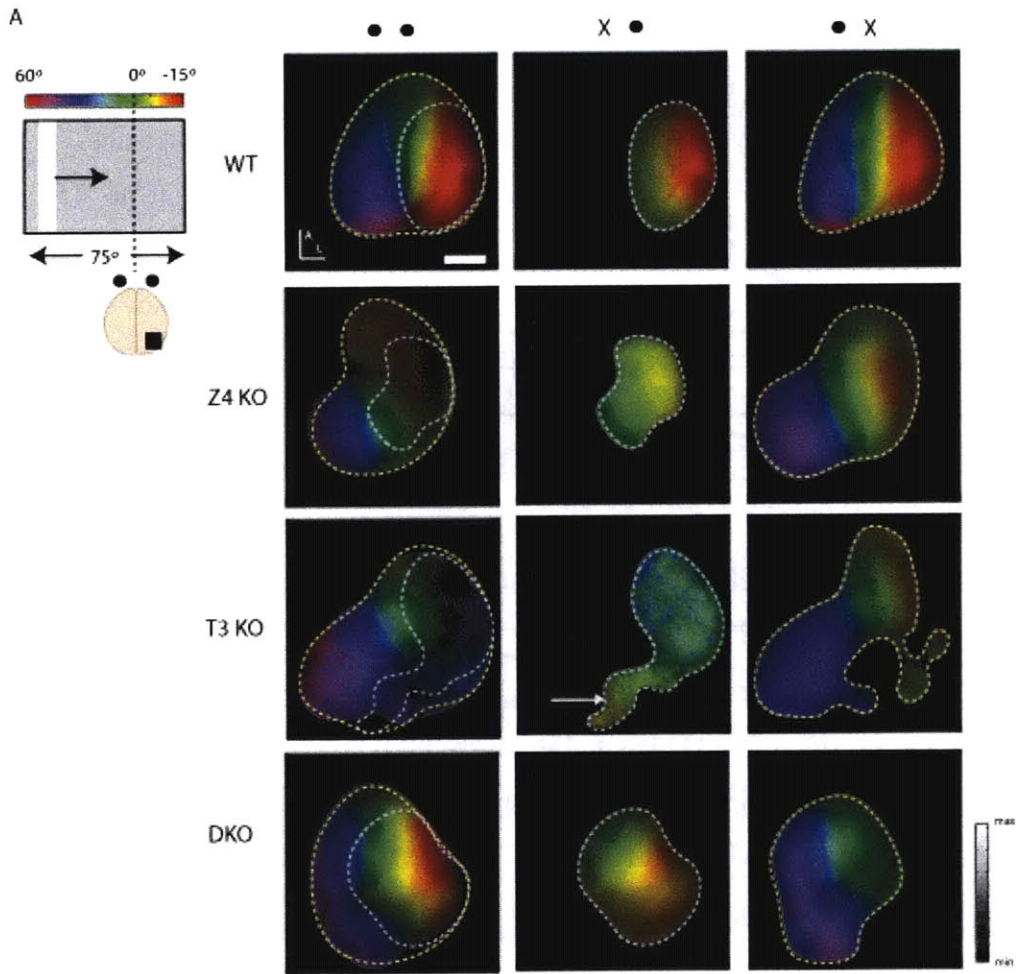


Figure 5. *Zic4* and *Ten_m3* loss result in a suppression of response amplitude in the binocular zone of the binocularly driven azimuth map. (A) Inset schema depicts the stimulus monitor presenting a drifting bar along the azimuth axis (spanning 60° to -15° representing the contralateral and binocular visual field, as coded by the colorbar). The black box shows the region of intrinsic signal optical imaging over a dorsal view of the cortex. The first column presents the binocularly driven maps (outlined in dotted yellow), with the binocular zone outlined for reference (dotted gray). The second column displays the ipsilaterally driven maps, which corresponds to the binocular zone (outlined in dotted gray), and the third column displays the contralaterally driven maps (outlined in dotted yellow). Compared to wild type and the double mutant, which exhibit normal azimuth maps, *Zic4* and *Ten_m3* null mice show a smaller and larger binocular zone, respectively, within which the response magnitude of the binocularly driven map is decreased. This suppression of cortical signal is consistent with a retinotopic mismatch in ipsilateral and contralateral inputs. Scale bar=500 μm, A=anterior, L=lateral. Grayscale bar shows fractional change in reflection in grayscale. Area displayed is a visual approximation of the response amplitude of the activated region thresholded to a level of 40% of the peak response. Arrow in *Ten_m3* KO panel denotes region that corresponds to expanded ipsilateral zone and an ocular dominance stripe; see also Fig. 7. (B) Histogram displays the decrease in response magnitude, expressed as fractional change in reflection in grayscale, for *Zic4* and *Ten_m3* null mice of the binocularly driven azimuth map in the binocular zone and the restoration of normal magnitude in the *Tenm_3/Zic4* combination mutant (See text for details). Error bars represent SEM.

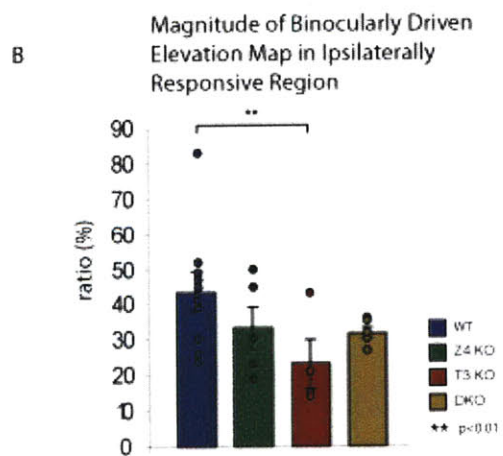
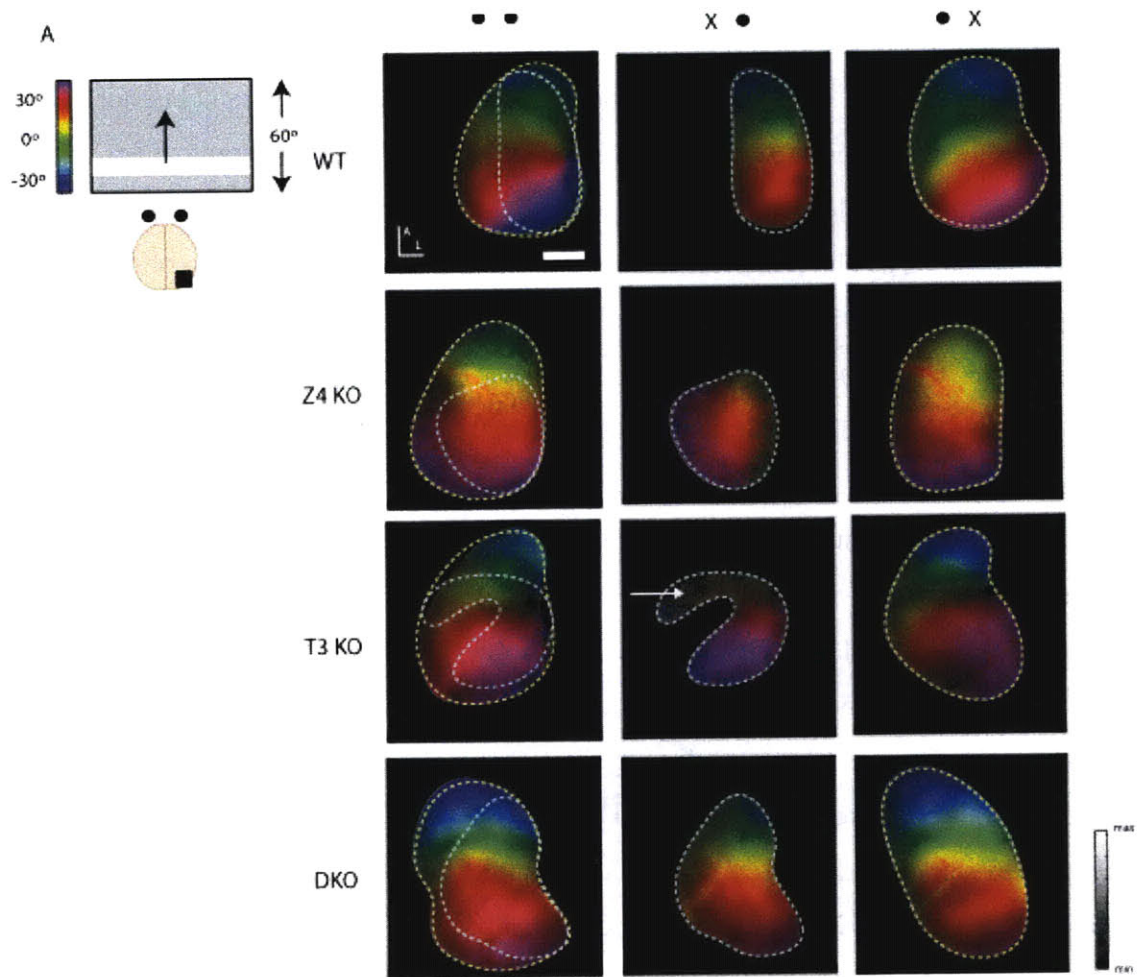


Figure 6. In the binocular zone of the binocularly driven elevation map, *Ten_m3* loss results in a suppression of response amplitude, while *Zic4* loss shows a trend but not statistically significant decrease. (A) Inset schema depicts the stimulus monitor presenting a drifting bar along the elevation axis (spanning 30° to -30° of the visual field, coded by the colorbar). The black box shows the region of imaging with the columns presenting the binocularly driven (dotted yellow), ipsilaterally driven (dotted gray), and contralaterally driven maps (dotted yellow), as in Figure 5. Along the elevation axis, only *Ten_m3* loss produced a detectable suppression in binocular drive within the binocular zone, while *Zic4* loss showed a suppressive trend and *Tenm_3/Zic4* was normal. Scale bar=500 μm, A=anterior, L=lateral. Grayscale bar shows fractional change in reflection in grayscale. Area displayed is a visual approximation of the response amplitude of the activated region thresholded to a level of 40% of the peak response. Arrow in *Ten_m3* KO panel denotes region that corresponds to expanded ipsilateral zone and an ocular dominance stripe; see also Fig. 7. (B) Histogram displays the decrease in response magnitude, expressed as fractional change in reflection in grayscale, for *Ten_m3* null mice of the binocularly driven elevation map in the binocular zone, a statistically insignificant decrease for *Zic4* null mice, and the restoration of normal magnitude in the *Tenm_3/Zic4* combination mutant (See text for details). Error bars represent SEM.

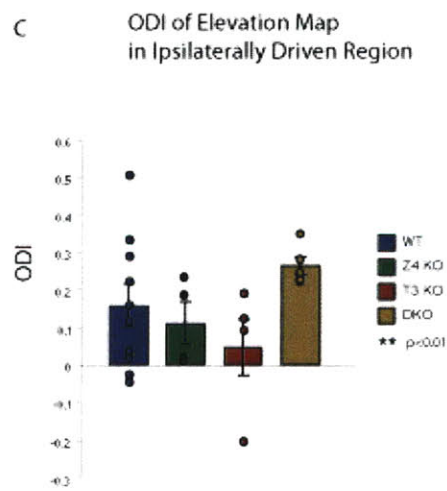
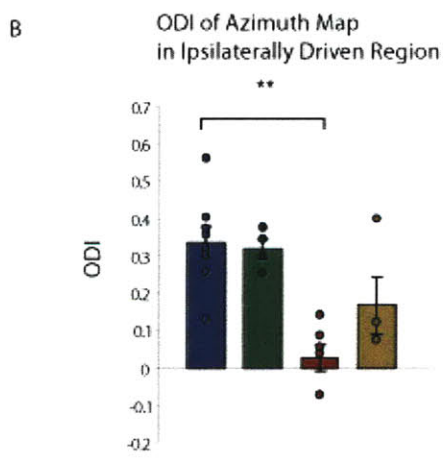
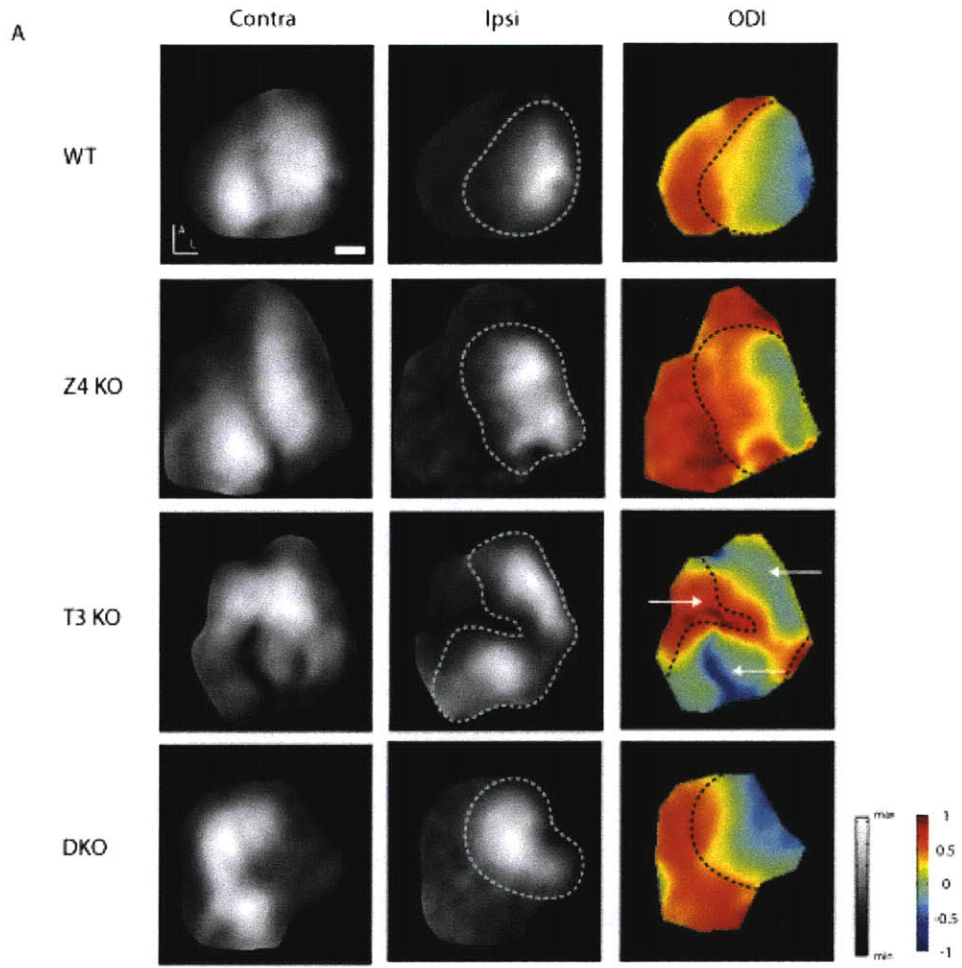


Figure 7. *Ten_m3* null mice display increased segregation of eye-specific domains in V1. (A) Contralateral and ipsilateral driven maps are displayed in columns 1 and 2, respectively with a map of ocular dominance index (ODI) values in column 3. ODI is a measure of the relative eye-specific drive of each pixel and is calculated by the difference in response magnitudes from the contralateral and ipsilateral driven maps divided by the sum of the magnitudes. *Ten_m3* null mice exhibit segregated regions (white arrows) of strong ipsilateral (blue) and contralateral (red) drive, and the ipsilateral regions extend more medially than the typical binocular zone of the wild-type. Scale bar=500 μm , A=anterior, L=lateral. Grayscale bar shows fractional change in reflection in grayscale. Area displayed is a visual approximation of the response amplitude of the activated region thresholded to a level of 40% of the peak response. Colorbar represents the ODI value; Blue (-1) indicates predominate ipsilateral drive while red (+1) represents predominant contralateral drive. (B) In the azimuth maps, the average ODI value of the ipsilaterally driven region is decreased in the *Ten_m3* null mouse (indicating more ipsilateral drive) and unchanged in the *Zic4* and *Tenm_3/Zic4* null mice. (C) In the elevation maps, the average ODI value of the ipsilaterally driven region shows no difference among the groups. Error bars represent SEM.

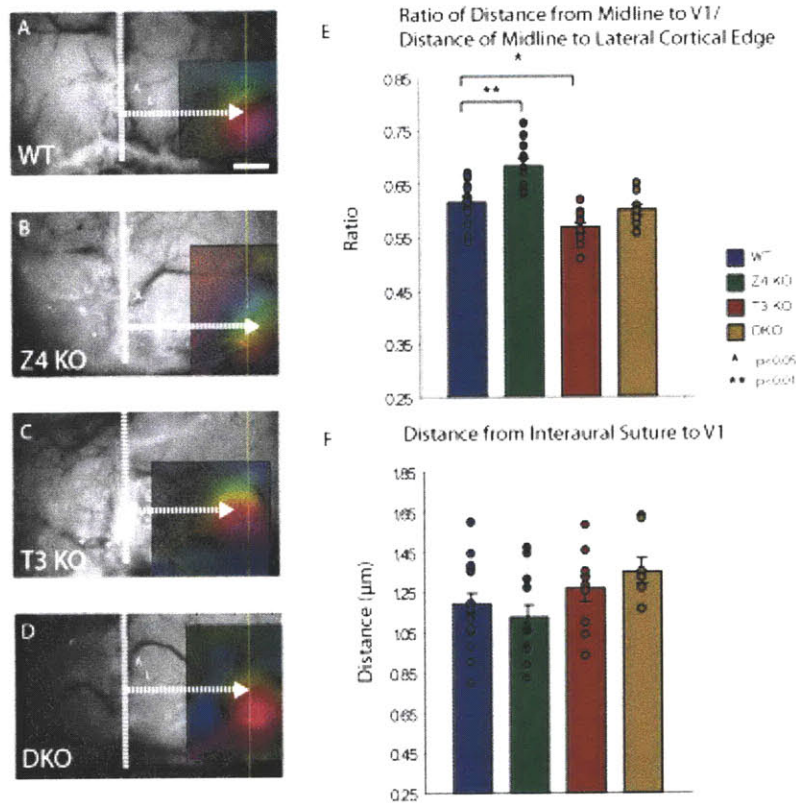


Figure 8. Position of V1 is shifted laterally in *Zic4* null mice, medially in *Ten_m3* null mice and restored to normal in combination mutants. (A) The position of V1 was measured along the medial-lateral axis as a ratio of the distance of V1 from the midline suture over the distance of the midline suture to the lateral edge of the cortex. In the wild-type animal, V1 shows a ratio of 0.62 ± 0.01 (yellow dotted line for reference), while in the *Zic4* null mouse (B), it is shifted laterally (0.68 ± 0.01 vs. 0.62 ± 0.01 , *Zic4* KO vs WT, $p < 0.01$, $F_{3,46} = 17.08$, $p < 0.01$, one-way ANOVA, Tukey's HSD test, $n = 11$ *Zic4* KO, $n = 18$ WT). (C) In the *Ten_m3* mutant, it is shifted medially (0.57 ± 0.01 , *Ten_m3* KO vs WT, $p < 0.05$, $n = 10$ *Ten_m3* KO), and in *Ten_m3/Zic4* combination mutants (D), restored to normal (0.60 ± 0.01 , *Ten_m3/Zic4* DKO vs. WT: nonsignificant, $n = 8$ DKO). V1 images correspond to elevation phase maps aligned to a blood vessel map of the cortical surface. Scale bar = 1.5mm. A=Anterior, L=Lateral. (E) Histogram of V1 position along the medial-lateral axis of the four groups. Error bars represent SEM. (F) Histogram showing no shifts in V1 position along the anterior-posterior axis, as measured by the distance of V1 from the lambda, or interaural suture.

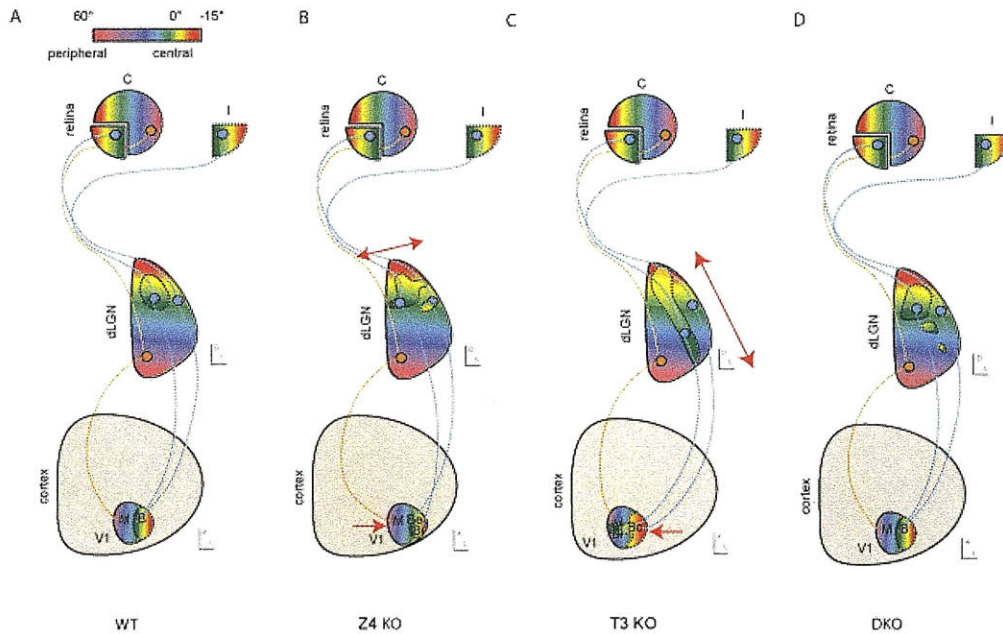
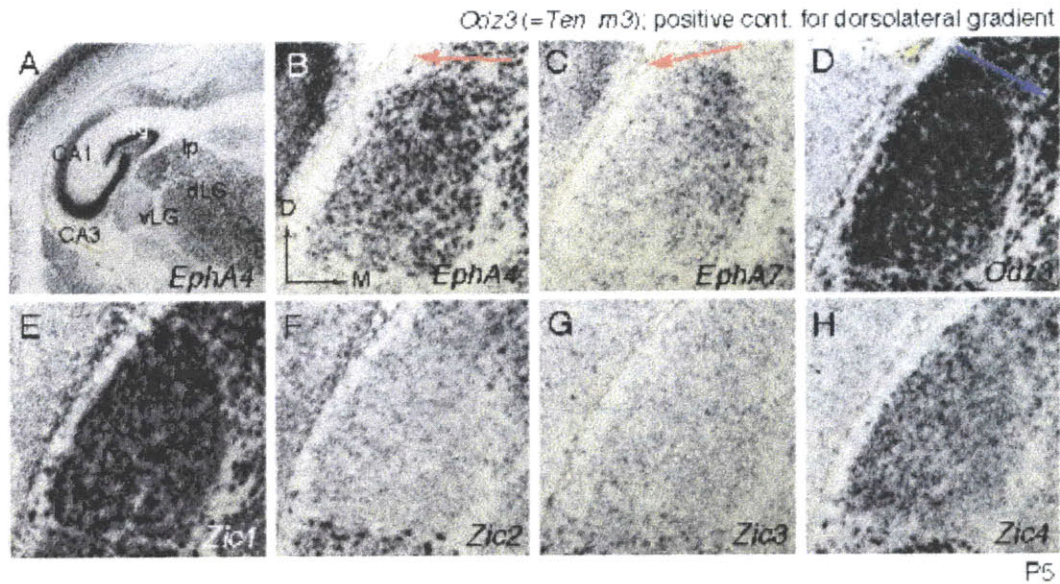
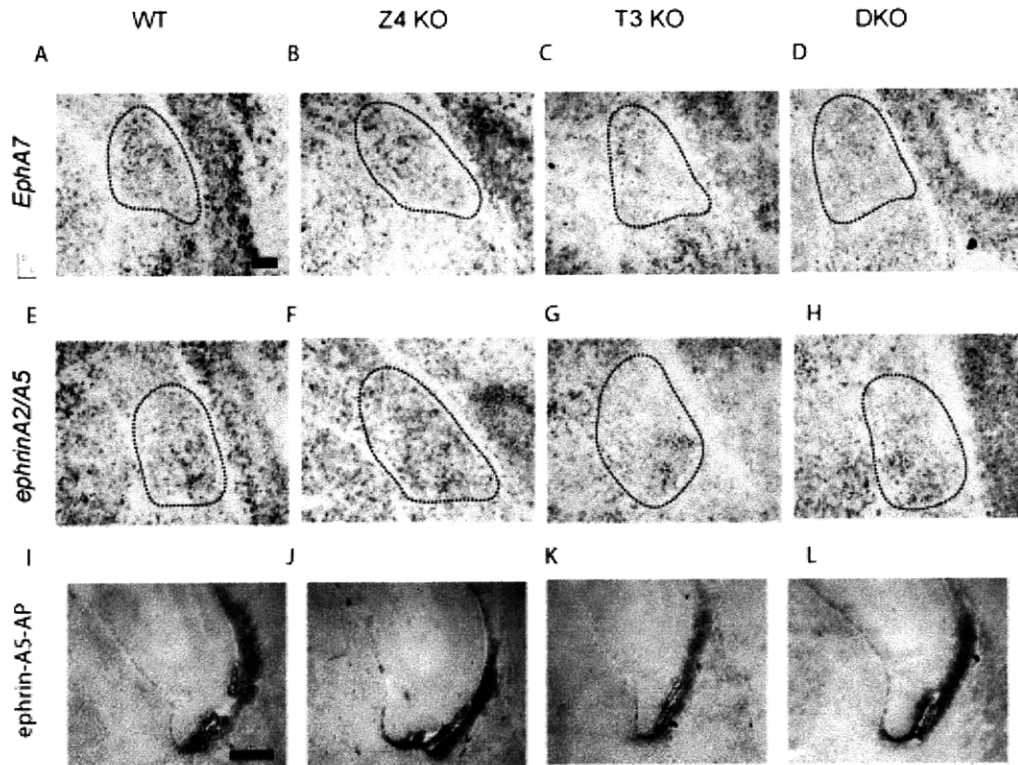


Figure 9. A summary of complementary retinogeniculate and cortical map phenotypes in the *Zic4* null and *Ten_m3* null mice and the restoration of normal mapping in the combination mutant. (A) In the wild-type, an azimuthal map (colorbar) in the binocular region of visual space is reflected onto the contralateral (C) and ipsilateral (I) retina (blue cells) and projected to the dorsal dLGN and binocular (B, dotted line) region of V1. Objects in the peripheral visual field get reflected onto the contralateral eye (orange cell), represented in the ventral dLGN and monocular zone (M) of V1. A=Anterior, D=dorsal, M=medial, L=lateral. (B) In the *Zic4* null mouse, ipsilateral retinogeniculate fibers spread their terminals along the dorsomedial axis (red arrow). This leads to a mistargeting of corresponding contralateral and ipsilateral inputs (blue cells) and subsequent mismatch of cells representing these points to different regions of the binocular V1 (Bc, Bi), producing a response suppression of that zone when driven by both eyes. The apparent binocular zone is decreased in size, possibly due to mismapped ipsilateral inputs and increased intracortical suppression during ipsilateral stimulation. V1 is also shifted laterally (red arrow). (C) In the *Ten_m3* null mouse, ipsilateral retinal axons extend into a dorsoventral stripe (red arrow), again producing a mistargeting of corresponding contralateral and ipsilateral inputs (blue cells) and mismatch within the binocular region

of V1 (Bc, Bi), which again causes response suppression. The binocular zone is increased in size (dotted line) because of the ventral spread of ipsilateral input into the dLGN, which drives geniculocortical cells projecting to the medial, typically monocular, region of V1. V1 is shifted medially (red arrow). (D) In the *Ten_m3/Zic4* combination mutant, the ipsilateral retinogeniculate projection is still abnormally expanded ventrally and exhibits clusters but is less severe compared to the *Zic4* and *Ten_m3* mutants. The binocular zone size, response magnitude and V1 position are no different from control, suggesting that the relative topography of contralateral and ipsilateral inputs is largely restored.



Supplemental Figure 1. *In situ* hybridization shows expression gradients of *EphA* receptors, *Ten_m3* and *Zic* family genes in the dLGN. (A) *EphA4* is localized to the dLGN, (B) *EphA4* and (C) *EphA7* exhibit high dorsomedial to low ventrolateral expression gradients, while (D) *Ten_m3* (aka. *Odz3*) is expressed in a high dorsolateral to low ventromedial gradient. (E) *Zic1* is expressed strongly in the same pattern, while (F) *Zic2* and (G) *Zic3* are not clearly detectable in the dLGN. (H) *Zic4* is expressed in a high dorsolateral to low ventromedial gradient. Figure and data courtesy of Takashi Inoue.



Supplementary Figure 2. Preliminary experiments using *in situ* hybridization and AP-fusion ephrinA5 probing failed to detect changes in *EphA7*, *ephrinA2/A5* and total EphA expression in the thalamus of *Zic4* (A,E,J), *Ten_m3* (B,F,K) and combination mutants (D,H,L) in comparison to wild type (A). More subtle changes in *EphA/ephrin-A* expression may occur and require more sensitive measurement techniques, such as qRT-PCR. (A-D) The dorsolateral gradient of *EphA7* is present in *Zic4* null mice, *Ten_m3* null mice and *Ten_m3/Zic4* combination mutants. Scale bar=300 μ m, D=dorsal, L=medial. (E-H) The ventromedial gradient of *ephrin-A2* and *A5* (probed together) is present in the four groups. Scale bar=300 μ m (I-L) Assayed using an AP-fusion ephrinA5 probe, total EphA protein expressed on axonal tracts of the internal capsule showed no major differences in the four groups. Scale bar=500 μ m.

CHAPTER 4

SUMMARY AND CONCLUSIONS

In the first chapter, a brief overview of visual pathway development and its context in early developmental processes of regionalization and functional differentiation was provided. The central thrust of this work has been to identify and pursue the role of *Zic4*, a novel patterning gene, in processes of topographic visual circuit formation.

Chapter two formulates this line of inquiry with a microarray screen designed to isolate candidates enriched in the developing LGN and MGN that are potentially involved in orchestrating sensory-specific differentiation events. Out of that screen, two candidates were studied: *Zic4*, a member of a zinc finger transcription factor family with graded expression in the retina, LGN and V1, and *Foxp2*, a transcriptional repressor with a known role in human speech and language development. Experiments using *Zic4* null mice demonstrated that *Zic4* is necessary for proper ipsilateral retinogeniculate patterning, and an acoustic stimulation paradigm was used to demonstrate for the first time in mammals that *Foxp2* is positively regulated by activity in the MGN. Additional experiments on the “rewired” mouse model revealed that cross-modal inputs to the MGN altered its patterns of gene expression to resemble LGN in addition to conferring novel plasticity related patterns of gene expression.

In chapter three, the role of *Zic4* on retinotopic patterning was further explored by examining the structure and function of cortical maps in *Zic4* null mice using intrinsic signal optical imaging. The cortical phenotype of *Ten_m3* null mice was also

characterized, and the interaction between the two genes was explored by analyzing the combination mutants. We found complementary deficits for the two mutants in ipsilateral retinotopic mapping in both the thalamus and the cortex, suggesting that these two genes contribute to mechanisms of retinotopic map formation and the coordination of eye-specific inputs along the visual pathway. This provides the first account of a bidirectional modulation of retinotopic mapping during development. Moreover, a rescue of those phenotypes in the combination mutant indicates that *Zic4* and *Ten_m3* interact in opposite directions on downstream effectors.

In sum, this thesis provides an in depth investigation of the role of two patterning molecules of the visual pathway, *Zic4* and *Ten_m3*, in retinotopic map formation, specifically the matching of eye-specific inputs to the thalamus and visual cortex. This work contributes to our growing understanding of the molecular programs specifying functional pathway development, as well as mechanisms of neural circuit formation important to visual stimulus processing and the production of binocular vision.

REFERENCES

- Arlotta P, Molyneaux BJ, Chen J, Inoue J, Kominami R, Macklis JD. (2005) Neuronal subtype-specific genes that control corticospinal motor neuron development in vivo. *Neuron*. 45(2):207-21.
- Aruga J (2004) The role of *Zic* genes in neural development. *Mol Cell Neurosci* 26:205-221.
- Bagutti C, Forro G, Ferralli J, Rubin B, Chiquet-Ehrismann R (2003) The intracellular domain of teneurin-2 has a nuclear function and represses *zic-1*-mediated transcription. *J Cell Sci* 116:2957-2966.
- Baumgartner S, Martin D, Hagios C, Chiquet-Ehrismann R (1994) *Tenm*, a *Drosophila* gene related to tenascin, is a new pair-rule gene. *Embo J* 13:3728-3740.
- Bengel D, Murphy DL, Andrews AM, Wichems CH, Feltner D, Heils A, Mössner R, Westphal H, Lesch KP. (1998) Altered brain serotonin homeostasis and locomotor insensitivity to 3, 4-methylenedioxymethamphetamine ("Ecstasy") in serotonin transporter-deficient mice. *Mol Pharmacol*. 53(4):649-55.
- Bolstad BM, Irizarry RA, Astrand M, Speed TP. (2003) A comparison of normalization methods for high density oligonucleotide array data based on variance and bias. *Bioinformatics*. 19(2):185-93.
- Bonhoeffer T, Grinvald A (1991) Iso-orientation domains in cat visual cortex are arranged in pinwheel-like patterns. *Nature* 353:429-431.
- Bonnin A, Torii M, Wang L, Rakic P, Levitt P. (2007) Serotonin modulates the response of embryonic thalamocortical axons to netrin-1. *Nat Neurosci*. 10(5):588-97.
- Braissant O., Wahli W. (1998) A simplified in situ hybridization protocol using non-radioactively labelled probes to detect abundant and rare mRNAs on tissue sections. *Biochemica* 1, pp. 10-16, 1998.
- Braun, M. M., Etheridge, A., Bernard, A., Robertson, C. P. and Roelink, H. (2003). Wnt signaling is required at distinct stages of development for the induction of the posterior forebrain. *Development* 130,5579 -5589.
- Brown A, Yates PA, Burrola P, Ortuno D, Vaidya A, Jessell TM, Pfaff SL, O'Leary DD, Lemke G (2000) Topographic mapping from the retina to the midbrain is controlled by relative but not absolute levels of EphA receptor signaling. *Cell* 102:77-88.
- Brunet I, Weint C, Piper M, Trembleau A, Volovitch M, Harris W, Prochiantz A, Holt C. (2005) The transcription factor *Engrailed-2* guides retinal axons. *Nature*. 438(7064):94-8.

- Cang J, Niell CM, Liu X, Pfeiffenberger C, Feldheim DA, Stryker MP. (2008) Selective disruption of one Cartesian axis of cortical maps and receptive fields by deficiency in ephrin-As and structured activity. *Neuron*. 57(4):511-23.
- Cang J, Kaneko M, Yamada J, Woods G, Stryker MP, Feldheim DA (2005a) Ephrin-as guide the formation of functional maps in the visual cortex. *Neuron* 48:577-589.
- Cang J, Rentería RC, Kaneko M, Liu X, Copenhagen DR, Stryker MP. (2005b) Development of precise maps in visual cortex requires patterned spontaneous activity in the retina. *Neuron*. 48(5):797-809.
- Cang J, Kalatsky VA, Löwel S, Stryker MP. (2005) Optical imaging of the intrinsic signal as a measure of cortical plasticity in the mouse. *Vis Neurosci*. 22(5):685-91.
- Constantine-Paton M, Law MI. (1978) Eye-specific termination bands in tecta of three-eyed frogs. *Science*. 202(4368):639-41.
- Dehay C, Savatier P, Cortay V, Kennedy H. (2001) Cell-cycle kinetics of neocortical precursors are influenced by embryonic thalamic axons. *J Neurosci*. 21(1):201-14.
- Dehay C, Giroud P, Berland M, Smart I, Kennedy H. (1993) Modulation of the cell cycle contributes to the parcellation of the primate visual cortex. *Nature*. 366(6454):464-6.
- Feldheim DA, Vanderhaeghen P, Hansen MJ, Frisen J, Lu Q, Barbacid M, Flanagan JG (1998) Topographic guidance labels in a sensory projection to the forebrain. *Neuron* 21:1303-1313.
- Feng K, Zhou XH, Oohashi T, Morgelin M, Lustig A, Hirakawa S, Ninomiya Y, Engel J, Rauch U, Fassler R (2002) All four members of the Ten-m/Odz family of transmembrane proteins form dimers. *J Biol Chem* 277:26128-26135.
- Figdor MC, Stern CD. (1993) Segmental organization of embryonic diencephalon. *Nature*. 363(6430):630-4.
- Flanagan, J.G., et al. (2000). Alkaline phosphatase fusions of ligands or receptors as in situ probes for staining of cells, tissues and embryos. *Methods in Enzymology* 327, 17-35.
- García-Frigola C, Carreres MI, Vegar C, Mason C, Herrera E. (2008) Zic2 promotes axonal divergence at the optic chiasm midline by EphB1-dependent and -independent mechanisms. *Development*. 135(10):1833-41.
- Gaston-Massuet C, Henderson DJ, Greene ND, Copp AJ. (2005) Zic4, a zinc-finger transcription factor, is expressed in the developing mouse nervous system. *Dev Dyn*. 233(3):1110-5.

- Gebbia M, Ferrero GB, Pilia G, Bassi MT, Aylsworth A, Penman-Splitt M, Bird LM, Bamforth JS, Burn J, Schlessinger D, Nelson DL, Casey B. (1997) X-linked situs abnormalities result from mutations in ZIC3. *Nat Genet.* 17(3):305-8.
- Gordon JA, Stryker MP. (1996) Experience-dependent plasticity of binocular responses in the primary visual cortex of the mouse. *J Neurosci.* 16(10):3274-86.
- Grinberg I, Northrup H, Ardinger H, Prasad C, Dobyns WB, Millen KJ (2004) Heterozygous deletion of the linked genes ZIC1 and ZIC4 is involved in Dandy-Walker malformation. *Nat Genet* 36:1053-1055.
- Grinberg I, Millen KJ. (2005) The ZIC gene family in development and disease. *Clin Genet.* Apr;67(4):290-6.
- Grove EA, Fukuchi-Shimogori T. (2003) Generating the cerebral cortical area map. *Annu Rev Neurosci.* 26:355-80.
- Guido W. (2008) Refinement of the retinogeniculate pathway. *J Physiol.* 586(Pt 18):4357-62.
- Haesler S, Wada K, Nshdejan A, Morrisey EE, Lints T, Jarvis ED, Scharff C. (2004) FoxP2 expression in avian vocal learners and non-learners. *J Neurosci.* 24(13):3164-75.
- Haesler S, Rochefort C, Georgi B, Licznarski P, Osten P, Scharff C. (2007) Incomplete and inaccurate vocal imitation after knockdown of FoxP2 in songbird basal ganglia nucleus Area X. *PLoS Biol.* 5(12):e321.
- Hansen MJ, Dallal GE, Flanagan JG. (2004) Retinal axon response to ephrin-as shows a graded, concentration-dependent transition from growth promotion to inhibition. *Neuron.* 42(5):717-30.
- Harrington SC, Simari RD, Conover CA. (2007) Genetic deletion of pregnancy-associated plasma protein-A is associated with resistance to atherosclerotic lesion development in apolipoprotein E-deficient mice challenged with a high-fat diet. *Circ Res.* 100(12):1696-702.
- Herrera E, Brown L, Aruga J, Rachel RA, Dolen G, Mikoshiba K, Brown S, Mason CA. (2003) Zic2 patterns binocular vision by specifying the uncrossed retinal projection. *Cell.* 114(5):545-57.
- Hooks BM, Chen C. (2006) Distinct roles for spontaneous and visual activity in remodeling of the retinogeniculate synapse. *Neuron.* 52(2):281-91.
- Huberman AD, Manu M, Koch SM, Susman MW, Lutz AB, Ullian EM, Baccus SA, Barres BA. (2008) Architecture and activity-mediated refinement of axonal projections

from a mosaic of genetically identified retinal ganglion cells. *Neuron*. Aug 14;59(3):425-38.

Huberman AD. (2007) Mechanisms of eye-specific visual circuit development. *Curr Opin Neurobiol*. 17(1):73-80.

Huberman AD, Speer CM, Chapman B. (2006) Spontaneous retinal activity mediates development of ocular dominance columns and binocular receptive fields in v1. *Neuron*. 52(2):247-54.

Huberman AD, Murray KD, Warland DK, Feldheim DA, Chapman B. (2005) Ephrin-As mediate targeting of eye-specific projections to the lateral geniculate nucleus. *Nat Neurosci*. 8(8):1013-21.

Huberman AD, Feller MB, Chapman B. (2008) Mechanisms underlying development of visual maps and receptive fields. *Annu Rev Neurosci*. 31:479-509.

Irizarry RA, Bolstad BM, Collin F, Cope LM, Hobbs B, Speed TP. (2003) Summaries of Affymetrix GeneChip probe level data. *Nucleic Acids Res*. 31(4):e15.

Ishiguro A, Inoue T, Mikoshiba K, Aruga J. (2004) Molecular properties of Zic4 and Zic5 proteins: functional diversity within Zic family. *Biochem Biophys Res Commun*. 324(1):302-7.

Job, C. and Tan, S. (2003) Constructing the mammalian neocortex: the role of intrinsic factors. *Dev Biol* 257, 221-232.

Jones, EG. (2007). *The Thalamus*. Second Ed. Plenum, New York.

Jones EG, Rubenstein JL. (2004) Expression of regulatory genes during differentiation of thalamic nuclei in mouse and monkey. *J Comp Neurol*. 477(1):55-80.

Kalatsky VA, Stryker MP. (2003) New paradigm for optical imaging: temporally encoded maps of intrinsic signal. *Neuron*. 38(4):529-45.

Kaneko M, Stellwagen D, Malenka RC, Stryker MP. (2008) Tumor necrosis factor- α mediates one component of competitive, experience-dependent plasticity in developing visual cortex. *Neuron*. 58(5):673-80.

Kataoka A, Shimogori T. (2008) Fgf8 controls regional identity in the developing thalamus. *Development*. 135(17):2873-81.

Kawasaki H, Crowley JC, Livesey FJ, Katz LC. (2004) Molecular organization of the ferret visual thalamus. *J Neurosci*. 24(44):9962-70.

Kiecker C, Lumsden A. (2005) Compartments and their boundaries in vertebrate brain development. *Nat Rev Neurosci*. 6(7):553-64.

Kiecker C, Lumsden A. (2004) Hedgehog signaling from the ZLI regulates diencephalic regional identity. *Nat Neurosci.* 7(11):1242-9.

Kilic U, Kilic E, Järve A, Guo Z, Spudich A, Bieber K, Barzena U, Bassetti CL, Marti HH, Hermann DM. (2006) Human vascular endothelial growth factor protects axotomized retinal ganglion cells in vivo by activating ERK-1/2 and Akt pathways. *J Neurosci.* 26(48):12439-46.

Kim IJ, Zhang Y, Yamagata M, Meister M, Sanes JR. (2008) Molecular identification of a retinal cell type that responds to upward motion. *Nature.* 452(7186):478-82.

Kitamura K, Miura H, Yanazawa M, Miyashita T, Kato K. (1997) Expression patterns of Brx1 (Rieg gene), Sonic hedgehog, Nkx2.2, Dlx1 and Arx during zona limitans intrathalamica and embryonic ventral lateral geniculate nuclear formation. *Mech Dev.* 67(1):83-96

Leamey CA, Glendining KA, Kreiman G, Kang ND, Wang KH, Fassler R, Sawatari A, Tonegawa S, Sur M (2007a) Differential Gene Expression between Sensory Neocortical Areas: Potential Roles for Ten_m3 and Bcl6 in Patterning Visual and Somatosensory Pathways. *Cereb Cortex.*

Leamey CA, Merlin S, Lattouf P, Sawatari A, Zhou X, Demel N, Glendining KA, Oohashi T, Sur M, Fassler R (2007b) Ten_m3 regulates eye-specific patterning in the mammalian visual pathway and is required for binocular vision. *PLoS Biology* 5:e241.

Levine A, Bashan-Ahrend A, Budai-Hadrian O, Gartenberg D, Menasherow S, Wides R (1994) Odd Oz: a novel Drosophila pair rule gene. *Cell* 77:587-598.

Lim Y, Golden JA. (2007) Patterning the developing diencephalon. *Brain Res Rev.* 53(1):17-26.

Lukaszewicz A, Savatier P, Cortay V, Giroud P, Huissoud C, Berland M, Kennedy H, Dehay C. (2005) G1 phase regulation, area-specific cell cycle control, and cytoarchitectonics in the primate cortex. *Neuron.* 47(3):353-64.

Lyckman AW, Horng S, Leamey CA, Tropea D, Watakabe A, Van Wart A, McCurry C, Yamamori T, Sur M. (2008) Gene expression patterns in visual cortex during the critical period: synaptic stabilization and reversal by visual deprivation. *Proc Natl Acad Sci U S A.* 105(27):9409-14.

Lyckman AW, Jhaveri S, Feldheim DA, Vanderhaeghen P, Flanagan JG, Sur M. (2001) Enhanced plasticity of retinothalamic projections in an ephrin-A2/A5 double mutant. *J Neurosci.* 21(19):7684-90.

Miller K, Kolk SM, Donoghue MJ. (2006) EphA7-ephrin-A5 signaling in mouse somatosensory cortex: developmental restriction of molecular domains and postnatal maintenance of functional compartments. *J Comp Neurol.* 496(5):627-42.

Mitchell DE, Ruck M, Kaye MG, Kirby S (1984) Immediate and long-term effects on visual acuity of surgically induced strabismus in kittens. *Exp Brain Res* 55:420-430

Murray KD, Choudary PV, Jones EG. (2007) Nucleus- and cell-specific gene expression in monkey thalamus. *Proc Natl Acad Sci U S A.*104(6):1989-94.

Lee R, Petros TJ, Mason CA. (2008) Zic2 regulates retinal ganglion cell axon avoidance of ephrinB2 through inducing expression of the guidance receptor EphB1. *J Neurosci.* 28(23):5910-9.

Nakagawa Y, O'Leary DD. (2001) Combinatorial expression patterns of LIM-homeodomain and other regulatory genes parcellate developing thalamus. *J Neurosci.* 21(8):2711-25.

Nakagawa, Y. and O'Leary, D.D. (2002) Patterning centers, regulatory genes and extrinsic mechanisms controlling arealization of the neocortex. *Curr Opin Neurobiol.* 12(1):14-25.

Nakazawa T, Nakazawa C, Matsubara A, Noda K, Hisatomi T, She H, Michaud N, Hafezi-Moghadam A, Miller JW, Benowitz LI. (2006) Tumor necrosis factor- α mediates oligodendrocyte death and delayed retinal ganglion cell loss in a mouse model of glaucoma. *J Neurosci.* 26(49):12633-41.

Newton JR, Ellsworth C, Miyakawa T, Tonegawa S, Sur M (2004) Acceleration of visually cued conditioned fear through the auditory pathway. *Nat Neurosci.* 7(9):968-73.

Nishijima K, Ng YS, Zhong L, Bradley J, Schubert W, Jo N, Akita J, Samuelsson SJ, Robinson GS, Adamis AP, Shima DT. (2007) Vascular endothelial growth factor-A is a survival factor for retinal neurons and a critical neuroprotectant during the adaptive response to ischemic injury. *Am J Pathol.* 171(1):53-67.

Nunes SM, Ferralli J, Choi K, Brown-Luedi M, Minet AD, Chiquet-Ehrismann R (2005) The intracellular domain of teneurin-1 interacts with MBD1 and CAP/ponsin resulting in subcellular codistribution and translocation to the nuclear matrix. *Exp Cell Res* 305:122-132

O'Leary DD. (1989) Do cortical areas emerge from a protocortex? *Trends Neurosci.* 12(10):400-6.

Oohashi T, Zhou XH, Feng K, Richter B, Morgelin M, Perez MT, Su WD, Chiquet-Ehrismann R, Rauch U, Fassler R (1999) Mouse ten-m/Odz is a new family of dimeric type II transmembrane proteins expressed in many tissues. *J Cell Biol* 145:563-577.

Pak W, Hindges R, Lim YS, Pfaff SL, O'Leary DD (2004) Magnitude of binocular vision controlled by islet-2 repression of a genetic program that specifies laterality of retinal axon pathfinding. *Cell* 119:567-578.

Park KK, Liu K, Hu Y, Smith PD, Wang C, Cai B, Xu B, Connolly L, Kramvis I, Sahin M, He. (2008) Promoting axon regeneration in the adult CNS by modulation of the PTEN/mTOR pathway. *Science*. 322(5903):963-6.

Pfeiffenberger C, Yamada J, Feldheim DA (2006) Ephrin-As and patterned retinal activity act together in the development of topographic maps in the primary visual system. *J Neurosci* 26:12873-12884.

Pfeiffenberger C, Cutforth T, Woods G, Yamada J, Renteria RC, Copenhagen DR, Flanagan JG, Feldheim DA (2005) Ephrin-As and neural activity are required for eye-specific patterning during retinogeniculate mapping. *Nat Neurosci* 8:1022-1027.

Rakic P. (1988) Specification of cerebral cortical areas. *Science* 242, 170-176.

Ragsdale CW, Grove EA. (2001) Patterning the mammalian cerebral cortex. *Curr Opin Neurobiol.* 11(1):50-8.

Rao SC, Toth LJ, Sur M (1997) Optically imaged maps of orientation preference in primary visual cortex of cats and ferrets. *J Comp Neurol* 387:358-370

Rashid T, Upton AL, Blentic A, Ciossek T, Knöll B, Thompson ID, Drescher U. (2005) Opposing gradients of ephrin-As and EphA7 in the superior colliculus are essential for topographic mapping in the mammalian visual system. *Neuron*. 47(1):57-69.

Rouso DL, Gaber ZB, Wellik D, Morrisey EE, Novitch BG. (2008) Coordinated actions of the forkhead protein Foxp1 and Hox proteins in the columnar organization of spinal motor neurons. *Neuron*. 59(2):226-40.

Salichon N, Gaspar P, Upton AL, Picaud S, Hanoun N, Hamon M, De Maeyer E, Murphy DL, Mossner R, Lesch KP, Hen R, Seif I. (2001) Excessive activation of serotonin (5-HT) 1B receptors disrupts the formation of sensory maps in monoamine oxidase a and 5-HT transporter knock-out mice. *J Neurosci*. 21(3):884-96.

Schneider, G.E. (1973) Early lesions of superior colliculus: factors affecting the formation of abnormal retinal projections. *Brain Behav. Evol.*, 8: 73-109.

Sengpiel F, Vorobyov V (2005) Intracortical origins of interocular suppression in the visual cortex. *J Neurosci* 25:6394-6400.

Sengpiel F, Blakemore C, Harrad R (1995) Interocular suppression in the primary visual cortex: a possible neural basis of binocular rivalry. *Vision Res* 35:179-195.

Sengpiel F, Jirjann KU, Vorobyov V, Eysel UT (2006) Strabismic suppression is mediated by inhibitory interactions in the primary visual cortex. *Cereb Cortex* 16:1750-1758.

Sharma J., Agelucci A. And Sur, M. (2000) Induction of visual orientation modules in auditory cortex. *Nature* 404, 841-847.

Shimogori T, Banuchi V, Ng HY, Strauss JB, Grove EA. (2004) Embryonic signaling centers expressing BMP, WNT and FGF proteins interact to pattern the cerebral cortex. *Development*. 131(22):5639-47.

Shimogori T, Banuchi V, Ng HY, Strauss JB, Grove EA. (2004) Embryonic signaling centers expressing BMP, WNT and FGF proteins interact to pattern the cerebral cortex. *Development*. 131(22):5639-47.

Shu W, Cho JY, Jiang Y, Zhang M, Weisz D, Elder GA, Schmeidler J, De Gasperi R, Sosa MA, Rabidou D, Santucci AC, Perl D, Morrisey E, Buxbaum JD. (2005) Altered ultrasonic vocalization in mice with a disruption in the *Foxp2* gene. *Proc Natl Acad Sci U S A*. 102(27):9643-8.

Smith SL, Trachtenberg JT (2007) Experience-dependent binocular competition in the visual cortex begins at eye opening. *Nat Neurosci* 10:370-375.

Sperry RW (1963) Chemoaffinity in the Orderly Growth of Nerve Fiber Patterns and Connections. *Proc Natl Acad Sci U S A* 50:703-710.

Stevens B, Allen NJ, Vazquez LE, Howell GR, Christopherson KS, Nouri N, Micheva KD, Mehalow AK, Huberman AD, Stafford B, Sher A, Litke AM, Lambris JD, Smith SJ, John SW, Barres BA. (2007) The classical complement cascade mediates CNS synapse elimination. *Cell*. 131(6):1164-78.

Sun T, Patoine C, Abu-Khalil A, Visvader J, Sum E, Cherry TJ, Orkin SH, Geschwind DH, Walsh CA. (2005) Early asymmetry of gene transcription in embryonic human left and right cerebral cortex. *Science*. 308(5729):1794-8.

Sur M and Leamey CA. (2001) Development and plasticity of cortical areas and networks. *Nat Rev Neurosci*. 2(4):251-62.

Sur, M. and Rubenstein J.L.R. (2005) Patterning and plasticity of the cerebral cortex. *Science* 310, 805-810.

Sur, M., Garraghty, P.E. and Roe, A.W. (1988) Experimentally induced visual projectionis into auditory thalamus and cortex. *Science* 242, 1437-1441.

Szabó NE, Zhao T, Zhou X, Alvarez-Bolado G. (2009) The role of Sonic hedgehog of neural origin in thalamic differentiation in the mouse. *J Neurosci*. 29(8):2453-66.

- Teramitsu I, White SA. (2006) FoxP2 regulation during undirected singing in adult songbirds. *J Neurosci.* 26(28):7390-4.
- Tilford CA, Siemers NO. (2009) Gene set enrichment analysis. *Methods Mol Biol.*;563:99-121.
- Tusher VG, Tibshirani R, Chu G. (2001) Significance analysis of microarrays applied to the ionizing radiation response. *Proc Natl Acad Sci U S A.* 98(9):5116-21.
- Tuttle R, Braisted JE, Richards LJ, O'Leary DD. (1998) Retinal axon guidance by region-specific cues in diencephalons. *Development.* 125(5):791-801
- Tychsen L, Wong AM, Burkhalter A (2004) Paucity of horizontal connections for binocular vision in V1 of naturally strabismic macaques: Cytochrome oxidase compartment specificity. *J Comp Neurol* 474:261-275.
- Upton AL, Ravary A, Salichon N, Moessner R, Lesch KP, Hen R, Seif I, Gaspar P. (2002) Lack of 5-HT(1B) receptor and of serotonin transporter have different effects on the segregation of retinal axons in the lateral geniculate nucleus compared to the superior colliculus. *Neuroscience.*;111(3):597-610.
- Upton AL, Salichon N, Lebrand C, Ravary A, Blakely R, Seif I, Gaspar P. (1999) Excess of serotonin (5-HT) alters the segregation of ipsilateral and contralateral retinal projections in monoamine oxidase A knock-out mice: possible role of 5-HT uptake in retinal ganglion cells during development. *J Neurosci.*19(16):7007-24.
- Vargha-Khadem F, Gadian DG, Copp A, Mishkin M. (2005) FOXP2 and the neuroanatomy of speech and language. *Nat Rev Neurosci.* 6(2):131-8. Review.
- Vernes SC, Nicod J, Elahi FM, Coventry JA, Kenny N, Coupe AM, Bird LE, Davies KE, Fisher SE. (2006) Functional genetic analysis of mutations implicated in a human speech and language disorder. *Hum Mol Genet.* 15(21):3154-67.
- Von Melchner L, Pallas SL, Sur M. (2000) Visual behaviour mediated by retinal projections directed to the auditory pathway. *Nature.* 404(6780):871-6.
- Vue TY, Aaker J, Taniguchi A, Kazemzadeh C, Skidmore JM, Martin DM, Martin JF, Treier M, Nakagawa Y. (2007) Characterization of progenitor domains in the developing mouse thalamus. *J Comp Neurol.* 505(1):73-91.
- Vue TY, Bluske K, Alishahi A, Yang LL, Koyano-Nakagawa N, Novitch B, Nakagawa Y. (2009) Sonic hedgehog signaling controls thalamic progenitor identity and nuclei specification in mice. *J Neurosci.* 29(14):4484-97.

Warr N, Powles-Glover N, Chappell A, Robson J, Norris D, Arkell RM. (2008) Zic2-associated holoprosencephaly is caused by a transient defect in the organizer region during gastrulation. *Hum Mol Genet.* 17(19):2986-96.

White LE, Fitzpatrick D. (2007) Vision and cortical map development. *Neuron.* 56(2):327-38.

White LE, Bosking WH, Fitzpatrick D (2001) Consistent mapping of orientation preference across irregular functional domains in ferret visual cortex. *Vis Neurosci* 18:65-76.

Wong AM, Burkhalter A, Tychsen L (2005) Suppression of metabolic activity caused by infantile strabismus and strabismic amblyopia in striate visual cortex of macaque monkeys. *J Aapos* 9:37-47.

Zhou, C. J., Pinson, K. I. and Pleasure, S. J. (2004). Severe defects in dorsal thalamic development in low-density lipoprotein receptor-related protein-6 mutants. *J. Neurosci.* 24,7632 -7639.